NTNU

Norwegian University of
Science and Technology

# Effects of Seeding on the Crystallization Behaviour and Filtration Abilities of an Aromatic Amine

**Åsmund Linga**

Chemical Engineering and Biotechnology
Submission date: June 2017
Supervisor: Jens-Petter Andreassen, IKP
Co-supervisor: Xiaoguang Ma, IKP
Torfinn Haaland, GE Healthcare Lindesnes

Norwegian University of Science and Technology
Department of Chemical Engineering

# Abstract

One of the intermediates in the production of X-ray contrast agents at GE Healthcare Lindesnes, commonly referred to as an *aromatic amine*, is subject to a crystallization. Crystallization parameters such as size, size distribution and morphology have a strong impact on the subsequent filtration step in the production, where aromatic amine crystals are separated from the mother liquor. *Seeding* is a technique that allows for control of important crystal properties. The focus of this study is how variation of seeding parameters affects the crystallization behaviour of the aromatic amine, and how this can be connected to filtration abilities.

In this work, crystallization experiments have been carried out in a batch reactor followed by Nutsche filtration tests. Concentration of solute aromatic amine and chord lengths of particles have been measured through UV spectrophotometry and FBRM respectively. Samples of final crystals and filter cakes were analyzed in SEM. In general, experiments were performed in a synthetic solution based on composition data from the production.

Three seeding materials form the basis of this work; *untreated*, *wet-milled* and *dry-milled* seeds respectively. All materials have been applied at varying seeding ratios: 0.3, 1.7 and 3.3 g seeds/100 g final crystals. Extent of crystal growth was assumed independent of seeding ratio for untreated seeding. Growth on seed particles was most evident for dry-milled seeding. Secondary nucleation was most predominant for wet-milled seeding and was assumed proportional to seeding ratio for all applied materials.

A slurry addition of dry-milled seeds resulted in a slightly better filtration performance than a dry addition. Wet-milled seeding yielded a better filtration performance than untreated seeding at all tested seeding ratios. In terms of total surface area of seeds, a critical point was found at $\sim$1 $m^2$ seeds/100 g final crystals, where average specific cake resistance was reduced significantly.

Untreated seeding was performed at varying degrees of supersaturation. Seeding at a medium supersaturation indicated a high rate of secondary nucleation when no further HCl was added. A twofold increase in size of new-born crystals could be observed when seeding at a high supersaturation compared to a medium supersaturation. A transition from a synthetic to a process solution caused slightly improved filtration performances.

# Sammendrag

Et intermediat i produksjonen av kontrastvæskemidler ved GE Healthcare Lindesnes, kjent som et *aromatisk amin*, gjennomgår en krystallisering. Krystallisasjonsparametre som størrelse, størrelsesfordeling og morfologi har stor betydning for det påfølgende filtreringssteget i produksjonen, hvor aromatiske aminkrystaller separeres fra moderluten. *Poding* er en teknikk som muliggjør regulering av viktige krystallegenskaper. Fokuset i denne oppgaven er hvordan endring av podeparametre påvirkerer krystallisasjonsforløpet til det aromatiske aminet, og hvordan dette påvirker stoffets filtreringsegenskaper.

Krystalliseringsforsøk har blitt utført i en batchreaktor etterfulgt av filteringstester. Konsentrasjon av løst aromatisk amin og kordelengder av partikler har blitt målt ved hjelp av henholdsvis UV-spektrofotometri og FBRM. Prøver av endelige krystaller og filterkaker har blitt undersøkt i SEM. Forsøkene ble generelt sett utført i en tillaget løsning basert på komposisjonsdata fra produksjonen.

Tre podestoff danner grunnlaget for det eksperimentelle arbeidet - henholdsvis *ubehandlede*, *våtmøllede* og *tørrmøllede* poder. De tre podetypene har blitt testet ved ulike podeforhold; 0.3, 1.7 og 3.3 g poder/endelige krystaller. Omfang av krystallvekst kan antas å være uavhengig av podeforholdet ved bruk av ubehandlede poder. Vekst på poder var mest tydelig ved bruk av tørrmøllet podestoff. Sekundærnukleering var tydeligst ved bruk av våtmøllet podestoff, og raten kan antas å være proporsjonal med podeforholdet for alle podestoffene.

Slurrytilsats av tørrmøllet podestoff resulterte i en noe bedre filtrerbarhet enn tørr tilsats. Våtmøllet poding ga en bedre filtrering enn ubehandlet poding ved alle testede podeforhold. I form av totalt overflateareal av podestoffet kunne et kritisk punkt antas ved $\sim$1 $m^2$ poder/100 g endelige krystaller, hvor gjennomsnittlig spesifikk kakemotstand ble merkbart redusert.

Ubehandlet poding ble utført ved varierende grad av overmetning. Poding ved middels overmetning indikerte en høy sekundærnukleeringsrate når ingen videre tilsats av HCl ble utført. En størrelsesfordobling av nydannede krystaller kunne observeres når poding ble utført ved en høy overmetning i tilfellet med ingen videre tilsats av HCl. Krystaller fra en reell prosessløsning filtrerte noe bedre enn krystaller fra en tillagd løsning.

# Preface

This Master's Thesis, written spring 2017, is a result of a co-operation between NTNU, Department of Chemical Engineering and GE Healthcare Lindesnes. All experimental work has been carried out at NTNU as a part of the crystallization research group. Professor Jens-Petter Andreassen (NTNU) has been the supervisor for this thesis, in addition to Post.Doc. Xiaoguang Ma (NTNU) and Dr. Torfinn Haaland (GE Healthcare) as co-supervisors.

I would like to thank Jens-Petter Andreassen for his education, theoretical contribution and his constructive criticism, which has helped me a lot in the work of this thesis. Xiaoguang Ma has been very helpful with regards to his theoretical feedback and by always giving me a helping hand when facing technical problems. Torfinn Haaland has shown great enthusiasm throughout this work, and has contributed with motivational feedback and necessary information whenever I needed it.

Arne Askildsen from GE Healthcare Lindesnes has been a resource in the process of gathering information from industry in the experimental planning. Mikael Hammer and Ina Beate Jenssen have also helped me a lot with regards to technical equipment and important experimental procedures.

Thanks to all students in my reading room and other parts of the K4 building for long, entertaining lunch breaks. Also a special thanks to Marta Westad Hauge for showing more patience and endurance than me in general.

I hereby declare that this is an independent work according to the exam regulations of the Norwegian University of Science and Technology.

Trondheim, 15.06.2017

.....

Åsmund Linga

# Nomenclature

## Uppercase latin letters

| | | |
|---|---|---|
| $A$ | pre-exponential factor | $1/s\ m^3$ |
| $A$ | area of filter medium | $cm^2$ |
| $A_{BET}$ | total BET surface area | $m^2/g$ |
| $B$ | secondary nucleation rate | $1/s\ m^3$ |
| $C$ | concentration | wt.% |
| $C^*$ | solubility concentration | wt.% |
| $C^{(1)}$ | concentration in basis solution | wt.% |
| $C^{(2)}$ | concentration in synthetic solution | wt.% |
| $D_f$ | maximum theoretical final particle diameter | µm |
| $D_{f,\ real}$ | estimated final particle diameter | µm |
| $D_{nuclei}$ | estimated final particle diameter for assumed nuclei | µm |
| $D_s$ | seed particle diameter | µm |
| $D_{s,\ real}$ | estimated seed particle diameter | µm |
| $D_{small}$ | estimated final particle diameter for small crystals | µm |
| $G$ | growth rate | µm/s |
| $J$ | (primary) nucleation rate | $1/s\ m^3$ |
| $L$ | characteristic crystal length | µm |
| $M_T$ | magma density of present solids | $g/cm^3$ |
| $M_w$ | molecular weight | g/mol |
| $N_f$ | total number of final particles | – |
| $N_s$ | total number of seed particles | – |
| $R$ | universal gas constant | J/mol K |
| $R$ | molar excess ratio | – |
| $S$ | supersaturation | – |
| $T$ | temperature | °C |
| $T_{boil}$ | boiling point | °C |
| $V$ | filtrate volume | mL |
| $V_f$ | volume of a single final particle | $µm^3$ |
| $V_{f,\ tot}$ | total volume of final particles | $µm^3$ |
| $V_s$ | volume of a single seed particle | $µm^3$ |

## Lowercase latin letters

| | | |
|---|---|---|
| $a$ | activity | – |
| $a_{BET}$ | specific BET surface area | $m^2/g$ |
| $b$ | dependency on supersaturation index for B | – |
| $c_s$ | effective solids concentration | $g/cm^3$ |
| $g$ | dependency on supersaturation index for G | – |
| $h$ | height of filter cake | cm |
| $j$ | crystal-crystal/crystal-impeller (etc.) interaction index | – |
| $k$ | collision energy index | – |
| $k$ | Boltzmann constant | J/K |
| $k_g$ | growth rate constant | µm/s |
| $k_N$ | secondary nucleation rate constant | $s/m^3$ |
| $m$ | mass | g |
| $m^*$ | mass of solution required to reach saturation | g |
| $m^{(0)}$ | mass of solution added in initial portion | g |
| $m_{tot}^{(1)}$ | mass of basis solution | g |
| $m_{tot}^{(2)}$ | mass of synthetic solution | g |
| $m^{exc}$ | mass of solution required to neutralize excess base/acid | g |
| $m_{f,\,tot}$ | mass of final particles | g |
| $m^{rest}$ | mass of solution not added in the initial portion | g |
| $m_s$ | mass of seeds | g |
| $m^{sat}$ | mass of solution required to reach saturation | g |
| $m_{sol}$ | mass of solids (dry filter cake) | g |
| $m_{susp}$ | mass of filtered suspension | g |
| $m^{tot}$ | mass of solution | g |
| $m_{tot}$ | mass of initially dissolved compound in crystallizing solution | g |
| $p$ | pressure | bar(G) |
| $r$ | (spherical) crystal radius | µm |
| $r_c$ | critical size for nucleus stability | µm |
| $t$ | time | min |
| $t_g$ | time for nucleus to grow into a detectable size | min |
| $t_{ind}$ | induction time | min |
| $t_l$ | latent time | min |
| $t_n$ | nucleation time | min |

## Greek symbols

| | | |
|---|---|---|
| $\alpha_{ave}$ | average specific cake resistance | cm/g |
| $\beta$ | filter medium resistance | 1/cm |
| $\gamma$ | interfacial tension | J/cm |
| $\gamma_c$ | activity coefficient | – |
| $\epsilon$ | agitator speed | rpm |
| $\varepsilon$ | cake porosity | – |
| $\eta$ | dynamic viscosity | mPa s |
| $\mu$ | chemical potential | J/mol |
| $\mu_c$ | chemical potential of a solute in the bulk of a crystal phase | J/mol |
| $\mu_s$ | chemical potential of a solute in solution | J/mol |
| $\xi$ | extent of crystal growth | – |
| $\rho_s$ | density of final particles | g/cm$^3$ |
| $\rho_l$ | density of filtered suspension | g/cm$^3$ |
| $\rho_s$ | density of seeds or dry filter cake | g/cm$^3$ |
| $\sigma$ | relative supersaturation | – |
| $\upsilon$ | molecular volume | cm$^3$/mol |
| $\phi$ | seeding ratio | – |
| $\chi$ | weight fraction of pure compound in diluted solution | – |
| $\omega$ | fraction of total required HCl added prior to seeding | – |

## Abbreviations

| | |
|---|---|
| AA | aromatic amine |
| BET | Brunauer, Emmet, Teller |
| CLD | chord length distribution |
| CV | coefficient of variation |
| DF | dilution factor |
| FBRM | focused beam reflectance measurement |
| MeOH | methanol |
| MR | magnetic resonance |
| NaAc | sodium acetate |
| SEM | scanning electron microscopy |
| UV | ultraviolet |
| wt.% | weight percentage |

# Contents

**Abstract** **I**

**Sammendrag** **II**

**Preface** **III**

**Nomenclature** **IV**

**1 Introduction** **1**
1.1 Objective . . . 2

**2 Theory** **3**
2.1 Polymorphism . . . 3
2.2 Solubility . . . 3
2.3 Supersaturation . . . 3
2.4 Crystal nucleation . . . 5
2.5 Primary homogeneous nucleation . . . 6
2.6 Primary heterogeneous nucleation . . . 6
2.7 Secondary nucleation . . . 7
2.7.1 Seeding . . . 7
2.8 Crystal growth . . . 8
2.8.1 Spherulitic growth . . . 8
2.8.2 Agglomeration . . . 9
2.9 Scaling . . . 9
2.10 Reaction crystallization . . . 9
2.11 Filtration . . . 10

**3 Experimental overview** **11**
3.1 Governing parameters . . . 11
3.2 Experimental procedure . . . 14
3.3 Chemicals . . . 18

**4 Results and discussion** **19**
4.1 Seed characteristics . . . 19
4.2 Reproducibility of experiments . . . 23
4.2.1 In terms of filterability . . . 23
4.2.2 In terms of chord length measurements . . . 24
4.3 Seeding material and seeding ratio . . . 28
4.3.1 Implementation of seeding . . . 28
4.3.2 Untreated seeding . . . 30
4.3.3 Wet-milled seeding . . . 34
4.3.4 Dry-milled seeding . . . 37
4.3.5 Filterability at varying seeding ratios . . . 40
4.4 Nature of dry-milled seeds . . . 43
4.4.1 Filterability . . . 45

4.5 Total surface area of seeds . . . 47
4.6 Degree of supersaturation at seeding . . . 49
4.6.1 Partial neutralization . . . 49
4.6.2 100 % neutralization . . . 53
4.6.3 Filterability . . . 56
4.7 Crystallization from a process solution . . . 57
4.7.1 Untreated seeding . . . 57
4.7.2 Dry-milled seeding . . . 59
4.7.3 Filterability . . . 61

**5 Summary and conclusions** **63**

**6 Recommendations for further work** **64**

**Bibliography** **65**

**A Experiment data** **I**

**B Filtration data** **II**

**C Maximum increase of particle diameter** **III**

**D Calculation of composition** **V**

**E Calculation of required mass of HCl** **VI**
E.1 Neutralization of excess NaOH . . . VI
E.2 Reaching the saturation point . . . VII
E.3 100 % neutralization . . . VIII

**F Linearity factor for calculation of concentration** **IX**

**G Tables of composition and distribution** **X**
G.1 Composition of basis solution . . . X
G.2 Composition of synthetic solution . . . X
G.3 Diluted NaOH-solution . . . XI
G.4 Diluted HCl-solution . . . XI

**H Physical data** **XII**

# List of Figures


2.1 Solubility-supersolubility diagram . . . . . 5
2.2 Nucleation mechanisms . . . . . 5
3.1 Batch reactor set-up . . . . . 15
3.2 Elimination of scaling in CLD . . . . . 16
4.1 SEM, seed characteristics . . . . . 19
4.2 CLD, seed characteristics, standard conditions . . . . . 20
4.3 CLD, seed characteristics, dispersed . . . . . 21
4.4 Filtrate volume vs. time for five parallels . . . . . 23
4.5 Filtrate volume per time vs. filtrate volume for five parallels . . . . . 24
4.6 Chord lengths vs. time for four parallels . . . . . 25
4.7 Coefficient of variation vs. time for four parallels . . . . . 25
4.8 CLD for four parallels, total and relative . . . . . 27
4.9 SEM, implementation of seeding, seeding ratios . . . . . 28
4.10 CLD, implementation of seeding, seeding ratios . . . . . 29
4.11 SEM, untreated seeding, seeding ratios . . . . . 30
4.12 CLD, untreated seeding, seeding ratios . . . . . 32
4.13 $C_{AA}$ vs. time, untreated seeding, seeding ratios . . . . . 32
4.14 SEM, wet-milled seeding, seeding ratios . . . . . 34
4.15 CLD, wet-milled seeding, seeding ratios . . . . . 36
4.16 $C_{AA}$ vs. time, wet-milled seeding, seeding ratios . . . . . 36
4.17 SEM, dry-milled seeding, seeding ratios . . . . . 37
4.18 CLD, dry-milled seeding, seeding ratios . . . . . 39
4.19 $C_{AA}$ vs. time, dry-milled seeding, seeding ratios . . . . . 40
4.20 Average specific cake resistance vs. seeding ratio . . . . . 40
4.21 SEM, untreated seeding, filter cake . . . . . 41
4.22 SEM, untreated vs. wet-milled seeding, filter cakes . . . . . 42
4.23 SEM, dry-milled seeding, slurry . . . . . 43
4.24 CLD, dry-milled seeding, slurry . . . . . 44
4.25 $C_{AA}$ vs. time, dry-milled seeding, slurry . . . . . 45
4.26 Average specific cake resistance vs. total BET surface area . . . . . 47
4.27 SEM, untreated seeding, degree of S, partial neutralization . . . . . 50
4.28 Chord lengths vs. time (long), untreated, degree of S, partial neutr. . 51
4.29 Chord lengths vs. time (short), untreated, degree of S, partial neutr. . 51
4.30 CLD, untreated seeding, degree of S, partial neutralization . . . . . 52
4.31 SEM, untreated seeding, degree of S, 100 % neutralization . . . . . 53
4.32 CLD, untreated seeding, degree of S, 100 % neutralization . . . . . 54
4.33 $C_{AA}$ vs. time, untreated seeding, degree of S, 100 % neutralization . . 55
4.34 SEM, untreated seeding, process solution . . . . . 57
4.35 CLD, untreated seeding, process solution . . . . . 58
4.36 $C_{AA}$ vs. time, untreated seeding, process solution . . . . . 59
4.37 SEM, dry-milled seeding, process solution . . . . . 59
4.38 CLD, dry-milled seeding, process solution . . . . . 60
4.39 $C_{AA}$ vs. time, dry-milled seeding, process solution . . . . . 61
F.1 Linearity factor for calculations of $C_{AA}$ . . . . . IX

# List of Tables


3.1 List of chemicals . . . . . 18
4.1 Average particle diameter of seeding materials . . . . . 21
4.2 Specific BET surface area of seeding materials . . . . . 22
4.3 Calculations of average specific cake resistance . . . . . 24
4.4 Extent of crystal growth, untreated seeding, seeding ratios . . . . . 31
4.5 Estimated diameters of nuclei, untreated seeding, seeding ratios . . . 31
4.6 Estimated diameters of nuclei, wet-milled seeding, seeding ratios . . . 35
4.7 Extent of crystal growth, dry-milled seeding, seeding ratios . . . . . 38
4.8 Estimated diameters of small crystals, dry-milled seeding, seeding ratios 39
4.9 Extent of crystal growth, dry-milled seeding, slurry . . . . . 44
4.10 Estimated diameters of small crystals, dry-milled seeding, slurry . . . 44
4.11 Average specific cake resistance, dry-milled seeding, slurry . . . . . 45
4.12 Extent of crystal growth, untreated seeding, degree of S . . . . . 54
4.13 Estimated diameters of nuclei, untreated seeding, degree of S . . . . . 54
4.14 Estimated time periods of reduction, untreated seeding, degree of S . 55
4.15 Average specific cake resistance, untreated seeding, degree of S . . . . 56
4.16 Extent of crystal growth, untreated seeding, process solution . . . . . 57
4.17 Estimated diameters of nuclei, untreated seeding, process solution . . 58
4.18 Extent of crystal growth, dry-milled seeding, process solution . . . . . 60
4.19 Estimated diameters of small crystals, dry-milled seeding, process solution . . . . . 60
4.20 Average specific cake resistance, dry-milled seeding, process solution . 61
A.1 List of performed experiments . . . . . I
B.1 List of filtration data . . . . . II
G.1 Composition of basis solution . . . . . X
G.2 Composition of synthetic solution . . . . . X
G.3 Distribution of HCl at varying degrees of S . . . . . X
G.4 Required HCl in order to reach saturation . . . . . XI
H.1 Physical data . . . . . XII
H.2 Filtration data, supplementary . . . . . XII
H.3 Other data . . . . . XII

# 1 Introduction

Crystallization is a predominantly applied unit operation in pharmaceutical industry, due to its ability to achieve products of high purity. A high quality solid-liquid separation relies on control of important crystallization properties, which in turn determine the efficiency of downstream processes such as filtration, washing and drying. Some of the crucial parameters that have to be controlled are size, size distribution and morphology of the crystals. As high filtration times typically are associated with smaller crystals and presence of fines (Togkalidou et al., 2001), achieving large particle sizes and a high degree of uniformity can improve filterability significantly.

A *supersaturated* solution, a solution containing more solute than the solubility concentration of the same compound, is required for crystallization to initiate. A commonly applied strategy that is used to control crystallization is called *seeding*, where small crystals are added to a supersaturated solution. Correct seeding leads crystallization to start at a desired supersaturation level, and provides sufficient surface area to ensure consumption of supersaturation in a controlled way.

GE Healthcare Lindesnes, a manufacturer of X-ray and MR contrast agents, is an example of a pharmaceutical industry that heavily relies on batch crystallization as a separation technique. One of the intermediates in their production, an aromatic amine derivative, exists as an anion prior to the crystallization. Supersaturation with respect to the aromatic amine derivative is generated through a reaction with a strong acid. This compound, commonly referred to as *aromatic amine*, is typically crystallized with a roughly spherical shape.

One of the major bottle necks in the production at Lindesnes is the filtration step where aromatic amine crystals are separated from the mother liquor. Based on recent experience in the production, awareness has been raised concerning variations in seeding parameters and their significant impact on crystallization behaviour and filtration abilities. In order to achieve a high filterability, it has traditionally been of interest to achieve as large crystals and with as narrow size distribution as possible. This corresponds to a high crystal growth rate and a limited rate of nucleation.

Parameters of seeding and their impact on crystallization, however, is still not a thoroughly understood subject. Seeding in crystallization of the aromatic amine has traditionally been performed on an empirical basis, and it is of high interest to establish a more *quantitative* description of seeding; such as the significance of seed size, surface area, size distribution and the level of supersaturation at which seeds are added to the solution.

## 1.1 Objective

The scope of this study is to investigate essential parameters related to seeding of a supersaturated solution of an aromatic amine and how they affect the crystallization behaviour. This study is also an attempt to connect properties of crystallization to filtration abilities. All experimental work is based on a collaboration with GE Healthcare Lindesnes and NTNU.

The main focus of this study is to examine changes occurring from *seeds* to *final* particles at the stage of filtration tests. Final particles imply achieved particles after all anionic AA is neutralized and cooled to room temperature. In order to fully understand crystallization mechanisms, a short analysis of intermediate crystals at *partial* neutralization only will also be performed.

Different types of seeding materials have been applied in industry, where the main differences involve varying degrees of milling as a pretreatment for the seeds. This study will therefore involve an examination of different types of *seeding material* and their effect on morphology, size, size distribution and filterability of the final crystals. This also includes a short analysis of how *preactivation* of seeds through a slurry addition instead of a dry addition affects the final outcome. Another objective is to look at how *total surface area* of the seeds affects crystallization properties and filtration abilities.

As crystallization mechanisms such as secondary nucleation depends strongly on magma density, the mass *ratio* of seeds to final crystals is of high importance. However, as the number of seeds initially present also affects supersaturation; rate of crystal growth is also a mechanism that must be taken into account. It is therefore of interest to study how the ratio of seed mass to the mass of final crystals affects morphology, size and size distribution. This study also includes a connection to filtration tests, where the scope is to find an optimal seeding ratio at which filterability of final crystals is the highest.

Seeds are always added at a certain *degree of supersaturation*, and the effect of varying the supersaturation level at which seeding is performed, is another important objective in this study. The primary goal is to look at variations of crystallization properties and filterability at different supersaturations, corresponding to varying initial additions of acid prior to seeding.

The final objective is to look at how essentials of crystallization change when being performed in a *process solution*. A process solution contains a certain amount of by-products from previous process stages. As experiments generally will be performed in a synthetic solution based on the real composition at Lindesnes, but with less contamination from by-products, the objective is to analyze whether the same trends can be observed in an actual process solution.

# 2 Theory

Crystals are solids "in which the atoms are arranged in a periodic repeating pattern that extends in three dimensions" (Schwartz and Myerson, 2002). In a geometrical sense, they can be characterized as lattices consisting of multiple unit cells with different spatial and angular properties. Due to the rigid arrangement of unit cells, crystals generally consist of a low degree of impurities.

Crystals are usually formed through a solid phase change obtained from a solution, a process commonly known as *crystallization*. In this context, the term *solution* implies a liquid solution consisting of a liquid solvent and a solid solute. From an industrial perspective, crystallization is a highly important separation and purification technique which leads to a production of a wide range of materials.

## 2.1 Polymorphism

A lot of organic and inorganic compounds have abilities to crystallize into more than one arrangement in a crystalline lattice. Different crystal arrangements of one chemical component is described by the phenomenon *polymorphism*. Compounds are generally classified into a *crystalline*, ordered, and an *amorphous*, disordered, state. The crystalline state differs from the amorphous in the sense that it has a fixed and rigid pattern, known as a lattice, in the regular arrangement of constituent molecules, atoms or ions (Hilfiker, 2006).

## 2.2 Solubility

The addition of a solid solute to a solvent, following a dissociation of the solute, results in the formation of a solution. At a given temperature, a solution is said to be *saturated* when a maximum amount of solute is dissolved in a given amount of solvent. The exact amount of solute required to reach the saturated state is defined as the *solubility* concentration, also referred to as the equilibrium concentration of a solute, denoted by $C^*$ (Schwartz and Myerson, 2002).

## 2.3 Supersaturation

The driving force for nucleation and growth of one-component crystals in liquid solutions is defined as *supersaturation* (Kashchiev and van Rosmalen, 2003). A supersaturated solution has a higher solute concentration than the solubility of the solute at a given temperature (Schwartz and Myerson, 2002). In terms of chemical potential, it can be described as the difference between the potential of a solute in solution, $\mu_s$, and the potential of a solute in the bulk of the crystal phase, $\mu_c$.

$$\Delta\mu = \mu_s - \mu_c \tag{2.1}$$

A positive difference, $\Delta\mu > 0$, describes a supersaturated solution and is the requirement for nucleation and/or growth of crystals to occur. A difference in chemical potential of $\Delta\mu = 0$ and $\Delta\mu < 0$ marks a saturated and undersaturated solution respectively. In dimensionless form, this difference can be expressed as:

$$\frac{\Delta\mu}{RT} = \ln\frac{a}{a^*} = \ln\frac{C\,\gamma_c}{C^*\,\gamma_c^*} = \ln S \tag{2.2}$$

where $a$ is activity, $C$ is concentration, $\gamma_c$ is activity coefficient and $^*$ denotes the property at saturated conditions (Schwartz and Myerson, 2002). $S$ is defined as *degree of supersaturation*. For sufficiently low concentrations, the activity coefficient can generally be assumed to equal unity, which allows the use of supersaturation expressed directly in terms of concentration.

$$S \approx \frac{C}{C^*} \tag{2.3}$$

In solutions characterized by a high degree of non-ideality, activity coefficients differ from unity and have to be included. However, assuming low concentrations and with a limited availability of thermodynamical data, it is common practice to ignore activity coefficients and use concentration-based expressions of supersaturation exclusively.

This simplification allows for further definitions of terms related to supersaturation. One of the most common ways of quantifying supersaturation is through *relative* supersaturation, denoted by $\sigma$.

$$\sigma = \frac{C - C^*}{C^*} = S - 1 \tag{2.4}$$

Nucleation and growth of crystals occurs in supersaturated solutions. As the solubility of a compound changes with temperature, a concentration-temperature-diagram can be used to illustrate the fundamentals of supersaturation.

In Figure 2.1, all concentrations under the solubility line are in the *stable* region, where concentration is too low for crystallization to occur. The *metastable zone* is the region above the solubility line, where only crystal nucleation induced by *seeding* will occur (Wojciech, 2014). Seeding, further described in Section 2.7.1, is a technique for induction of crystallization commonly applied in industry. Spontaneous nucleation starts in the *labile* zone, divided from the metastable zone by a less well defined supersolubility line.

Figure 2.1 also illustrates different methods for obtaining a supersaturated solution. The horizontal arrow ABC shows how spontaneous crystallization will occur to the

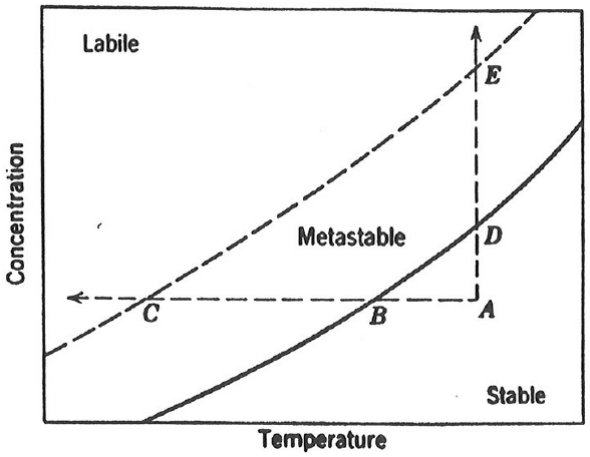


**Figure 2.1:** Solubility-supersolubility diagram showing how crystallization can be obtained (Andreassen, 2015).

left of point C after *cooling* the solution. The vertical arrow ADE shows how crystals start forming above point E after *evaporating* solvent and by that increasing the concentration of the solute.

Another method for generating supersaturation is modification of the solvent composition, generally by adding another solvent to the system in order to create a mixed solvent system where the solubility of the solute is significantly decreased. Supersaturation by chemical reaction, usually in the context of precipitation, involves an addition of two soluble materials in a solution where the two react to form a product with a low solubility (Schwartz and Myerson, 2002).

## 2.4 Crystal nucleation

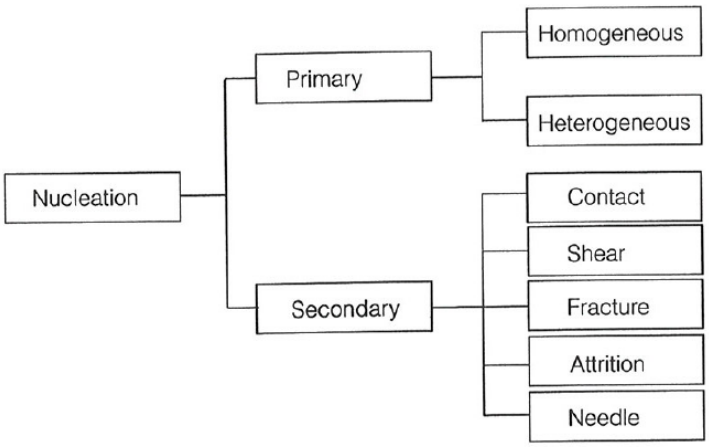


**Figure 2.2:** Different kinds of nucleation mechanisms (Andreassen, 2015).

The formation of a new crystal nucleus, often regarded as the birth of a new crystal, is described by the term *nucleation*. The condition of supersaturation is not sufficient

for a system to begin crystallizing. Before crystals can grow, new crystallization centres have to exist in the solution. The formation of a solid phase in the liquid phase involves an overcoming of a free energy barrier, which defines the process of nucleation (Garside, 1982). Categories of nucleation are shown in Figure 2.2, where the main difference between primary and secondary nucleation is the presence of crystalline particles in the latter.

## 2.5 Primary homogeneous nucleation

Nuclei formed in perfectly clean solutions in the absence of any foreign particles or surfaces, describes the mechanism of homogeneous nucleation, often referred to as *spontaneous* nucleation (Garside, 1982). This is a phenomenon that rarely occurs in practice, but it still forms the basis for several nucleation theories.

The classical theory of nucleation is based on an assumption that clusters are formed in a supersaturated solution according to a sequence of bimolecular additions (Myerson, 2002). A cluster is initially unstable, and further additions to it give rise to nucleation and growth only when it exceeds a critical size. This construction process occurs at a high rate and in local regions of very high supersaturations.

The rate of nucleus formation according to a homogeneous nucleation mechanism is given by an Arrhenius type of expression. This, in combination with a thermodynamical foundation developed by Gibbs (1928), Volmer (1939) and others, yields the following rate expression (Myerson, 2002) assuming a spherical nucleus being formed:

$$J = A \exp \frac{-16\pi\gamma^3 v^2}{3k^3T^3(\ln S)^2} \tag{2.5}$$

where $A$ is a preexponential factor, $k$ is the Boltzmann constant, $\gamma$ is the interfacial tension and $v$ is the molecular volume.

## 2.6 Primary heterogeneous nucleation

Primary heterogeneous nucleation is characterized by nucleation with the nucleus at a surface. A foreign substance being present in a supersaturated solution is generally known to reduce the critical energy required for nucleation. A lower free energy barrier indicates that a heterogeneous system occurs at a lower supersaturation than a homogeneous system. Considering a lower energy barrier for the onset of nucleation, the nucleation rate expression for the heterogeneous nucleation mechanism can also be described by (2.5) with a *reduced* pre-exponential factor $A$ (Beck, 2009).

After supersaturation has been generated, there is a certain time lag before crystals can be detected in the system. This is referred to as *induction time*, and consists of time required for the system to reach steady-state, $t_r$, nucleation time, $t_n$ and time

required for the nucleus to grow to a detectable size, $t_g$. For systems where detection of the induction period is hard to measure, an additional term called latent time, $t_l$, is introduced. A significant change such as massive nucleation marks the end of the latent time.

$$t_{ind} = t_r + t_n + t_g \ (+ t_l) \tag{2.6}$$

## 2.7 Secondary nucleation

Secondary nucleation is induced by the presence of crystals in a supersaturated solution. Parent crystals act in the same way as foreign substances in primary *heterogeneous* nucleation by reducing the supersaturation level needed for spontaneous nucleation. However, the two mechanisms have proved to be profoundly different, despite a far less thorough understanding of the mechanisms behind secondary nucleation (Myerson, 2002).

Several theories have been proposed to explain secondary nucleation. The first main category has its focus on the origin of the secondary nuclei to the parent crystal, including the concepts *initial* breeding, *needle* breeding and *collision* breeding (Mullin, 2001). The second main category focuses on the origin of the secondary nuclei from the solute in the liquid phase, involving impurity concentration gradient nucleation and nucleation due to fluid shear (Myerson, 2002).

One of the models aiming to describe the rate of secondary nucleation is written as following:

$$B = k_N \sigma^b \epsilon^k M_T^j \tag{2.7}$$

The secondary nucleation rate constant $k_N$ depends on factors such as temperature, rate of agitation and presence of impurities (Rousseau, 2009). Equation 2.7 shows that secondary nucleation rate most importantly increases with magma density of the present solids ($M_T$), agitator speed ($\epsilon$) and supersaturation (and consequently *growth rate*, see Section 2.8). Collision energy is denoted by $k$, crystal-crystal (or crystal-impeller/crystal-wall) interactions by $j$ and dependency on supersaturation by $b$ (Mullin, 2001).

### 2.7.1 Seeding

Addition of small particles intended to act as templates for growth and/or secondary nucleation in a supersaturated solution, is a commonly applied technique for induction of crystallization. This technique is referred to as *seeding*, and it is common practice in industry in order to gain control over particle size and particle size distribution. Seeds normally contain the same material as is to be crystallized, however, seeds containing other substances can also induce crystallization (Mullin, 2001).

Parameters such as seed crystal size is believed to have a significant impact on secondary nucleation. Although not thoroughly described in the literature, one theory is that as a result of higher contact probabilities and collision energy, large seeds generate more secondary nuclei than do small seeds (Mullin, 2001). However, as contact probability and collision energy also increase with total surface area of the seeds, a correlation between this parameter and generation of secondary nuclei can not be excluded.

## 2.8 Crystal growth

After the generation of a stable nucleus over a certain critical size, $r_c$, in a supersaturated system, crystals start to grow into a visible size. Crystal growth is defined as an increase in size due to addition of growth units (atoms, ions or polymers) to the crystal lattice, and is the mechanism following nucleation (Mullin, 2001).

There are many proposed mechanisms aiming to explain crystal growth. The surface energy theory is based on the postulation that the shape of the growing crystal is the one with the minimum surface energy. The diffusion theory presumes a continuous deposit of mass on the crystal surface, following a rate determined by the concentration difference between the deposit surface and the bulk of the solution. The adsorption theory assumes a discontinuous addition, layer by layer, of growth units on the crystal surface. Crystal growth rate, in linear dimensions, can generally be written as:

$$G = \frac{dL}{dt} = k_g \sigma^g \tag{2.8}$$

The characteristic length, $L$, changes to $r$ for the assumption of spherical particles. The growth rate constant $k_g$ depends on temperature, and $g$ denotes dependency on relative supersaturation, $\sigma$, usually in the range between 1 and 2.

### 2.8.1 Spherulitic growth

Most examples of crystal growth involve a primary nucleus growing into a crystallite with a discrete crystallographic orientation, which in turn develops as a single crystal until it collides with other crystals or surfaces. In some systems, however, primary nuclei induce the formation of less radially symmetric *polycrystalline* aggregates (Keith and Padden Jr, 1963). This is commonly known as *spherulitic growth*.

Spherulites initially consist of fibers or fibrils separated from one another by layers of uncrystallized melt. After a period of radial growth is completed, several layers of melt will crystallize slowly and eventually fill in the overall structure. This further crystallization is characterized by slow lateral growth (coarsening) of the existing fibers, as well as formation of new branches. The spherical shape can be explained by a high degree of branching (Bakke, 2016).

### 2.8.2 Agglomeration

Small particles have a high probability of clustering together, which is described by the term *agglomeration*. In contrast to crystal growth, where the size of one crystal increases, agglomeration involves the process where multiple crystals stick together to create a bigger crystal. This leads to the fact that the number of particles will stay constant in the case of crystal growth only, whereas the number will be reduced in the case of agglomeration (Mullin, 2001).

## 2.9 Scaling

Scaling is described by a crystalline solid layer being formed on solid surfaces such as reactor walls or probes. In the literature, it is typically distinguished between two types of scaling; *mechanical* and *chemical* scaling. Mechanical scaling occurs when small particles attach to a solid surface induced by physical forces, where a surface layer is formed because of an agglomeration of particles. Chemical scaling is a result of nucleation and growth of particles on a solid surface induced by supersaturation, where heterogeneous nucleation is the most predominant mechanism (Söhnel and Garside, 1992).

## 2.10 Reaction crystallization

The aromatic amine, denoted as AA, is a solid that acts as an intermediate in the production of contrast agents at GE Healthcare Lindesnes site. Since a neutral aromatic amine molecule has a relatively low solubility in water compared to an aromatic amine anion, a strong base is added in order to achieve high concentrations of solute aromatic amine (Bakke, 2016).

The aromatic amine anion is crystallized through a reaction with a strong acid. Supersaturation of the aromatic amine is formed when the concentration of the aromatic amine exceeds the solubility (Smith, 2006):

$$AA^{-}\left(aq\right) + H^{+} \rightarrow AA\left(aq\right) \rightarrow AA\left(s\right) \tag{2.9}$$

In industry, the aromatic amine exists in a solution containing water, sodium acetate and methanol. NaOH is commonly used as the strong base and HCl as the strong acid (Håland, 2017). Previous studies show that the aromatic amine commonly crystallizes as a spherulitic polymorph, as described in Section 2.8.1 (Smith, 2006).

## 2.11 Filtration

Solid-liquid separation is based on a separation of a solid and liquid phase from a suspension. Filters are usually applied to fulfill the separation task, and one of the most frequently used models to describe filtration performance is called *cake filtration* (Beck, 2009).

This model is based on the assumption that solids are deposited on a filter medium as a homogeneous porous layer with a constant permeability. As soon as the first cake layer is formed, filtration occurs on the top of the cake such that the medium only provides a supporting function.

Filtration experiments performed at constant pressure are normally based on the general filtration equation applied to the filter medium and filter cake (Beck, 2009):

$$\frac{t}{V} = \alpha_{ave}\frac{\eta\, c_s}{2A^2\Delta p}V + \frac{\eta\,\beta}{A\Delta p} \tag{2.10}$$

where $t$ is time, $V$ is the filtrate volume, $\eta$ is dynamic viscosity of the liquid phase, $c_s$ is the effective solids concentration, $A$ is the filter area, $\Delta p$ is the applied pressure difference and $\beta$ is the filter medium resistance. Average specific cake resistance, $\alpha_{ave}$, is calculated based on experimental data, leading to a quantitative comparison of suspension filterability. If the pressure is constant during the filtration, a plot based on (2.10) should give a straight line, where $\alpha_{ave}$ is found through the slope.

Filter cakes are to some extent compressible, leading to a structural dependency on the applied pressure difference. An increase of pressure leads to a lower porosity and consequently a higher resistance towards throughput of the mother liquor. As the mechanical stress exerted on the particles of the cake is highest close to the filter medium, local cake resistance may also vary through the depth of the cake at constant pressure difference (Beck, 2009).

Effective solids concentration, $c_s$, is calculated as (Wakeman and Tarleton, 1999):

$$c_s = \frac{\rho_l}{\dfrac{m_{susp}}{m_{sol}} - \left(1 + \dfrac{\rho_l}{\rho_s}\dfrac{\varepsilon}{1-\varepsilon}\right)} \tag{2.11}$$

where $m_{susp}$ is the mass of filtered suspension, $m_{sol}$ is the mass of solids (corresponding to a dry filter cake), $\rho_l$ and $\rho_s$ are filtrate and particle density respectively and $\varepsilon$ is the average porosity of the cake. The latter is calculated by the following equation:

$$\varepsilon = \frac{Ah - \dfrac{m_{sol}}{\rho_s}}{Ah} \tag{2.12}$$

where $h$ is the height of the filter cake.

# 3 Experimental overview

## 3.1 Governing parameters

The objective of this research is to investigate crystallization of AA at a temperature based on the operation at GE Healthcare Lindesnes. All experiments were therefore carried out at 60 °C during the interval of acid addition. After all acid was added, corresponding to 100 % neutralization of anionic AA, the suspension was slowly cooled to 22 °C.

Aromatic amine was dissolved in a solution based on the industrial crystallization process, which from now on is referred to as a *synthetic solution*. The same composition of synthetic solution was used for all experiments as given in Appendix G. In order to demonstrate the degree of resemblance, two additional experiments were performed with the real *process solution* sent directly from Lindesnes site.

In general only seeded experiments were performed, with the exception of one *unseeded* experiment. This was performed in order to demonstrate absence of seeding and its effect on crystallization and filtration of AA. Three different types of seeding materials were applied, further described in Section 4.1.

### Particle diameter estimation

In order to quantify an average particle size of a sample, SEM pictures give valuable information. The particle diameter estimation method is based on measuring diameters of 20 crystals *in the category of interest* in a SEM picture. As an example, diameters of 20 crystal with evidences of growth are selected as randomly as possible. A mean and a standard error of the mean is then calculated from the 20 measurements, thus representing an average estimated diameter and a quantified variation of crystals with observed evidences of growth. Diameters are estimated in ImageJ (Image processing and analysis in Java).

### Extent of crystal growth

One of the motives of this study is to obtain an enhanced understanding of mechanisms occurring after seeding of an AA crystallization process. This can be achieved by calculating the *extent of crystal growth* on a single seed particle.

Maximum achievable increase in diameter for a single seed particle to a final particle, $\Delta D_{max}$, can be calculated as described in Appendix C. Real increase in diameter, $\Delta D_{real}$, can be estimated using the particle diameter estimation method. Extent of crystal growth is thus defined as the ratio between the two quantities:

$$\xi = \frac{\Delta D_{real}}{\Delta D_{max}} = \frac{D_{f,\,real} - D_{s,\,real}}{\Delta D_{max}} \tag{3.1}$$

where $D_{f,\,real}$ and $D_{s,\,real}$ are the estimated diameters of an average final crystal and seed particle respectively based on SEM pictures. Table 4.1 lists estimated diameters of all categories of seed particles. Results will be analyzed in terms of $\xi$ only when clear evidences of growth are visible in SEM pictures.

### Seeding ratio

Seeding ratio is defined as the ratio of seed mass to the final crystal mass of aromatic amine when all anionic AA has been neutralized. Seeding ratio can be calculated by the following equation:

$$\phi = \frac{m_{AA,\,s}}{m_{AA,\,s} + m_{AA,\,tot}} \tag{3.2}$$

where $m_{AA,\,s}$ is total mass of AA seeds and $m_{AA,\,tot}$ is total mass of initially dissolved AA. As applied $\phi$ normally is in the range of 0.5 to 1 % in industry (Håland, 2017), two of the chosen seeding ratios for the experimental outline are outside this interval as a lower and upper bound. In addition, a seeding ratio of approximately 10 times the lowest $\phi$ is chosen as an extreme. In summary, this results in the following tested seeding ratios for the experimental set-up:

1. $\phi = 0.3$ %
2. $\phi = 1.7$ %
3. $\phi = 3.3$ %

### Total surface area of seeds

Specific BET surface area, $a_{\mathrm{BET}}$, can be found as described in Section 3.2 for each characteristic seeding material. Combined with the seeding ratio, this information can be used in order to calculate total surface area of seeds added for each experiment. Total BET surface area, $A_{\mathrm{BET}}$, is thus calculated as:

$$A_{\mathrm{BET},\,j} = a_{\mathrm{BET},\,i}\left(\frac{m_{AA,\,s,\,j}}{m_{AA,\,s,\,j} + m_{AA,\,tot}}\right) \cdot 100 = a_{\mathrm{BET},\,i}\,\phi_j \cdot 100 \tag{3.3}$$

where $i$ is the seeding material and $j$ is the number of experiment. $A_{\mathrm{BET}}$ is given in units of $\mathrm{m}^2$ seeds/100 g final crystals.

### Degree of supersaturation at seeding

Timing of seeding can in this context be interpreted as the degree of supersaturation at which seeds are added. As AA is crystallized through a reaction with HCl, this corresponds to the fraction of total required HCl for 100 % neutralization already added at the point of seeding. Fraction of total required HCl added in the initial portion is hereby denoted by $\omega$:

$$\omega = \frac{m^{(0)}_{HCl,\,dil}}{m^{tot}_{HCl,\,dil}} \tag{3.4}$$

where $m^{(0)}_{HCl,\,dil}$ is the mass of initially added diluted HCl, and $m^{tot}_{HCl,\,dil}$ is the total mass of diluted HCl required to achieve 100 % neutralization of anionic AA. Note that diluted HCl for simplicity reasons is referred to as HCl in the following sections. For exact weight fraction of HCl in the solution ($\chi_{HCl}$), see Appendix G.4.

As illustrated in Figure 2.1, seeding is typically performed after entering the metastable zone. The minimum fraction of initially added HCl should therefore correspond to the solubility concentration of aromatic amine at 60 °C, in other words where AA is at the *saturation point*.

The saturation point marks the standard amount of HCl added before seeding in the experimental outline. Crystallization experiments with seeds added at supersaturations *exceeding* the saturation point were also performed. In summary, the three different applied initial fractions of HCl at seeding are the following:

1. $\omega = 27$ %. Calculated as the required amount of HCl needed to reach the solubility concentration of AA. Referred to as the *saturation point*.
2. $\omega = 40$ %. The approximate amount of HCl added at GE Healthcare Lindesnes before seeding. Corresponds to a supersaturation.
3. $\omega = 53$ %. Calculated as twice the amount of HCl needed at the saturation point, but still under the point of possible spontaneous nucleation based on FBRM data for the unseeded experiment. Corresponds to a supersaturation.

For calculations of required mass of HCl needed to reach the theoretical solubility, see Appendix E. In general, experiments are performed with 100 % neutralization of anionic AA. The initial portion is added instantaneously, whereas the remaining HCl is added continuously at a constant rate by a pump.

A minimum addition time of 1 hour for the applied total mass of HCl is recommended in order to avoid an excessively high supersaturation (Linga, 2016). An addition time of 1 hour after seeding at $\omega = 27$ % was therefore set as a basis, corresponding to an addition rate of ∼0.64 g/min for all experiments. A constant rate of acid addition implies lower addition times in experiments with a higher $\omega$. Experiments related to varying degrees of supersaturation at seeding were also performed at *partial* neutralization, without further addition of HCl.

## 3.2 Experimental procedure

All experiments were carried out at 60 °C during the time interval of acid addition in a 1 L batch reactor, with a stirring speed of 500 rpm. An FBRM-probe was inserted in order to monitor a dynamical chord length distribution throughout all experiments. In general, samples were taken out regularly during the experiment in order to determine concentration of aromatic amine in the liquid phase as a function of time. This was made possible by dilutions of the samples followed by absorbance measurements through UV spectrophotometry.

An initial portion of HCl was added instantaneously at the start of each experiment ($t = 0$). Seeding was performed at $t \approx 1.5$ min. The remaining acid conditions can be classified into two series of experiments, A and B:

**A**: 100 % neutralization. All remaining HCl was added at a constant rate of ∼0.64 g/min starting at $t \approx 3.5$ min.

**B**: Partial neutralization only. No HCl added after the initial portion.

Samples of final crystals of AA for SEM analysis were withdrawn (and filtered, washed, and dried) as following:

**A**: After cooling to 22 °C at $t \approx 2$ h 40 min.

**B**: After a solubility concentration of AA in the liquid phase was assumed achieved at 60 °C. Based on previous studies at GE Healthcare, this was set to $t = 3$ h 30 min (Håland, 2017).

Filtration tests were performed for series A only. After all acid was added, typically after ∼65 minutes, the system was cooled to 22 °C for approximately 90 minutes. Suspension was withdrawn from the reactor at $t \approx 2$ h 40 min under constant agitation, and was used for a Nutsche filtration test. A solid sample was taken from the filter cake after filtration, and was dried for Scanning Electron Microscopy (SEM) analysis.

In the following sections, crystals withdrawn at the time of suspension withdrawal for filtration tests ($t \approx 2$ h 40 min) are referred to as *final crystals*. All performed experiments are listed in Table A.1.

### Batch Reactor Set-Up

All experiments were performed batch-wise in a 1 L thermostated glass reactor as shown in Figure 3.1. Stirring was performed using a three-bladed propeller connected to a reactor top, additionally equipped with two baffles.

A condenser was installed in order to prevent evaporation of water and MeOH. For series A of experiments, a plastic tube connected to a pump (Gilson Minipuls 3) was vertically oriented through a hole in the lid for continuous addition of acid. One hole was used for sample outtake and was sealed with a small cap when not in use.

A set-up of the reactor including distance measurements is shown in the following figure.

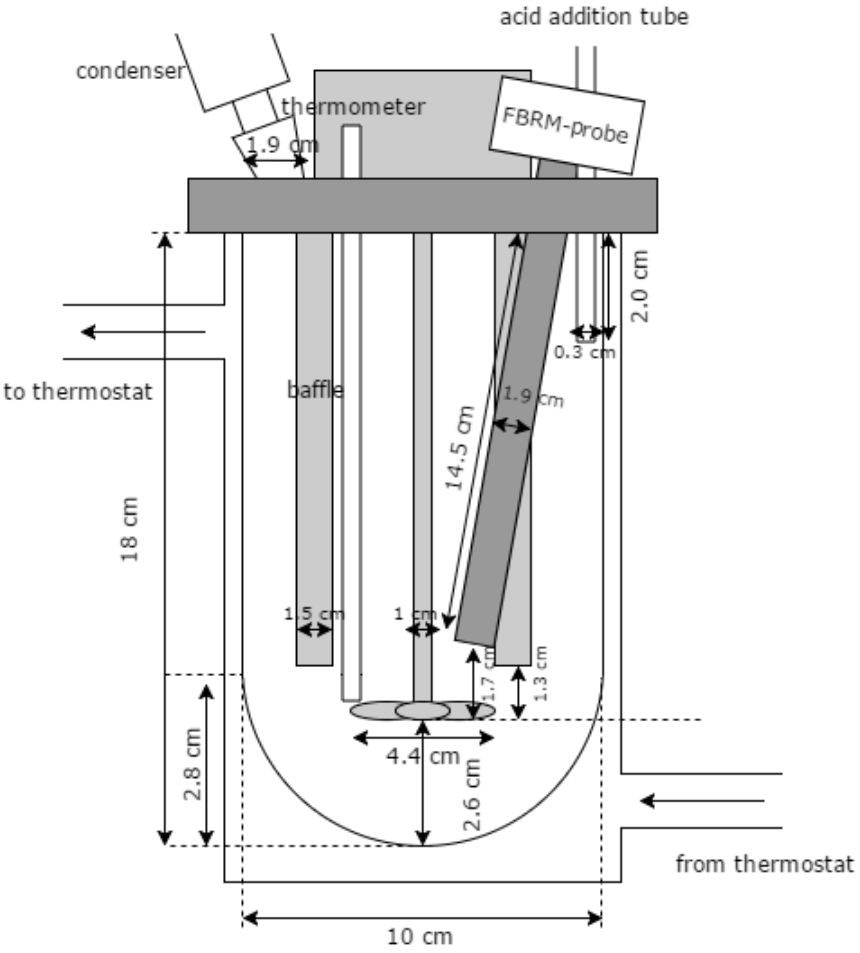


**Figure 3.1:** Batch reactor set-up for all crystallization experiments. Note that the acid addition tube is installed for series A of experiments only.

### Chord Length Measurements

Focused Beam Reflectance Measurement (FBRM) is an online technique allowing for in-situ measurements of concentrated suspensions. An FBRM-probe (Mettler Toledo, Lasentec D600L) was used during all experiments, providing a chord length distribution rather than an actual particle size distribution. Chord lengths were recorded every 5 second in a *fine* operation mode, at a laser rotation velocity of 2 m/s. All measurements were monitored by using the software iC FBRM.

A common problem of FBRM-measurements is the formation of a thin layer of small particles on the probe and the probe window, commonly referred to as *scaling* (see Section 2.9). This may lead to a disproportionately high number of smaller chord

lengths in the chord length distribution. An instantaneous and excessively high formation of particles of the smallest chord length interval in the dynamical FBRM software, gives an indication of scaling. Removal of the probe for 1 minute and washing of the probe window was therefore performed accordingly during each experiment.

Since the probe had to be withdrawn multiple times from the reactor during every experiment, the chord lengths of the time region surrounding the withdrawal can be considered invalid. For better representation of the chord length measurements, invalid counts are eliminated in figures showing chord lengths vs. time as presented in the following example.

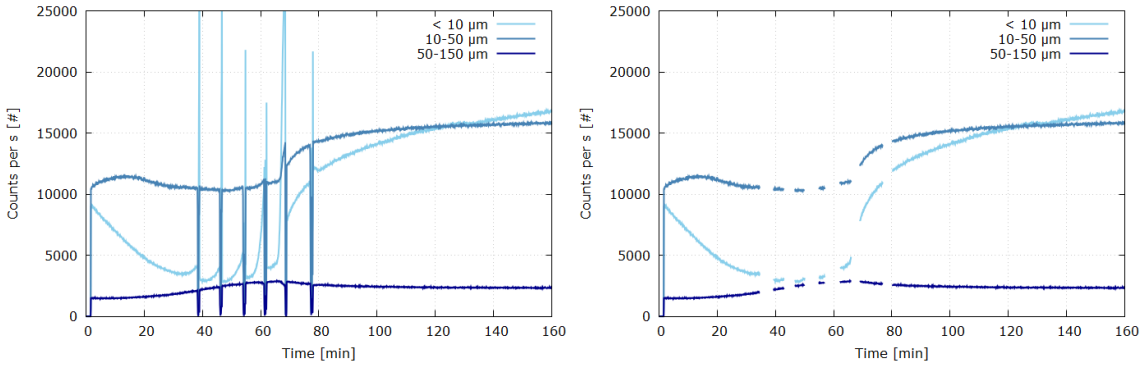


**(a)** Scaling included.

**(b)** Scaling removed.

**Figure 3.2:** Example of (number weighted) chord length counts vs. time, where invalid data regions due to scaling are eliminated.

### Concentration Measurements of Liquid Phase

Liquid samples from the reactor were collected approximately every 6 minute during the first 65 minutes; the interval where acid was added. At low concentrations of solids, a syringe coupled with a Millex GS 0.22 µm filter unit was used to withdraw samples of 4-5 mL. At higher solid concentrations, samples of 8-10 mL were withdrawn with a syringe and filtered through a Büchner funnel.

Concentration of AA in the liquid phase was determined through absorbance measurements in UV spectrophotometry (Thermo Helio $\gamma$) at a wavelength of 241 nm. Two dilutions with distilled water of each sample were required prior to the measurements in order to reach sufficiently low, thus stable, absorbance values. A 4 mL plastic cuvette was washed three times with diluted sample before each measurement. The cuvette was also washed with distilled water followed by a calibration between each measurement. The absorbance value was displayed with three digits.

As the UV spectrophotometer does not distinguish between the neutral aromatic amine molecule and the anion, concentration of AA should hereby be interpreted as the sum of $AA^-$ (aq) and AA (aq). As all outtakes were based on *weight* of sample

and water, each concentration of AA ($C_{AA}$) was calculated as a weight percentage. This was achieved using a linearity factor based on standard concentrations of AA, as explained in Appendix F. Concentration of aromatic amine in the liquid phase was hence calculated by:

$$C_{AA} = 0.00261 \cdot A \cdot DF_1 \cdot DF_2 \tag{3.5}$$

where $A$ is measured absorbance value and $DF_1$ and $DF_2$ denotes dilution factor 1 and 2 respectively. Each dilution factor was calculated as following:

$$DF_i = \frac{m_{total,i}}{m_{sample,i}} \tag{3.6}$$

where $i = \{1, 2\}$ denotes total mass and sample mass of the first and second dilution respectively. $DF_2$ is adjusted according to $DF_1$ as a minimum dilution factor product ($DF_1 \cdot DF_2$) of 5000 was required in general.

Five samples were collected before the initial addition of HCl in each experiment, in order to quantify the uncertainty of dilutions *and* UV measurements. A mean and a standard error of the mean was calculated based on the five initial concentration values. For simplicity, it was assumed that the same standard error, one for each experiment, was applicable for all measurements after this point. Error bars in all following plots of $C_{AA}$ show 1 standard error.

### Nutsche Filtration

*Nutsche* filtration is a batch filtration process where, in this case, pressure is applied in a closed vessel (Mayo, 2017). A BHS column connected to a nitrogen gas tank was used, operated with a pressure of 1 barG into the column.

A crystal suspension of 200 mL was filtered after each experiment at 22 °C. An additional back-up test was collected for most experiments. A filter (FDA PP 1050 SK25) with a pore size of 25 µm was used in all filtrations. The filter was washed in NaOH and distilled water between each filtration.

Mass of filtrate, $m$, and filtration time, $t$, were recorded continuously by a scale connected to a data collection program. Mass was converted to filtrate volume, V, through density of the filtrate, $\rho_l$. Recording was stopped after air was blown through the filter cake or dripping of filtrate ended. Due to the risk of crack formation in the filter cake, hence leading to an incomplete washing of the cake, *washing* of the filter cake was omitted.

### Scanning Electron Microscopy

A further study of the morphology and size of the final crystals and filter cake was performed through Scanning Electron Microscopy, SEM (Hitachi S TM3030 Plus).

A 1 mL sample was generally withdrawn from the suspension after cooling to 22 °C, followed by washing with distilled water and methanol. An additional solid sample was taken from the filter cake after filtration. Both samples were dried at 40 °C for 24 hours. In order to enable imaging of the samples, gold coating of the samples was required prior to the analysis.

#### Specific Surface Area

In order to determine surface area per unit mass of seeding material, BET/$N_2$ adsorption analysis was applied for the three main types of seeding material. Approximately 100 mg sample was used in a Micromeritics TriStar II 3020 Surface Area and Porosity Analyzer.

## 3.3 Chemicals

Aromatic amine was generally dissolved in a synthetic solvent based on the composition at GE Healthcare Lindesnes site, containing water, methanol and sodium acetate. Diluted sodium hydroxide (20.0 wt.%) was chosen as the strong base required to bring AA to anionic form, added with a molar excess ratio of $R = 1.22$ with respect to AA.

Two additional experiments were performed with the real process solution containing anionic aromatic amine, brought directly from the relevant stage in the process at GE Healthcare Lindesnes. Solute AA was crystallized through addition of diluted hydrochloric acid (17.5 wt.%). As a preparation for SEM, all crystal samples were washed with distilled water and methanol.

**Table 3.1:** List of all chemicals used in the experimental work.

| Chemical | Formula | Manufacturer | Purity |
|---|---|---|---|
| Distilled water | $H_2O$ | NTNU | ∼100 % |
| Methanol | $CH_3OH$ | Merck KGaA, EMPARTA® | ≥ 99.8 % |
| Hydrochloric acid, fuming | HCl | Merck KGaA, EMSURE® | 17.5 wt.% |
| Sodium acetate, anhydrous | $NaC_2H_3O_2$ | S-d-s | ∼99 % |
| Sodium hydroxide | NaOH | VWR AnalaR, NORMAPUR® | 20.0 wt.% |
| Aromatic amine | - | GE Healthcare, Lindesnes site | - |
| Process solution | - | GE Healthcare, Lindesnes site | - |

# 4 Results and discussion

## 4.1 Seed characteristics

Typical seed characteristics that may vary are structure and roughness of the surface, size and size distribution. Recent experiments in industry also involve prewetting of the seeds before addition, generally referred to as a slurry addition. Seeds in its most basic form are AA crystals from the production that are filtered, washed and dried. Other seeds may have been treated with varying degrees of milling afterwards. The current technique in industry is dry-milling (Håland, 2017), whereas recent experiments also involve wet-milling of seeds in a slurry. Based on traditional and possible future pretreatment techniques for seeds, three types of seeding material form the basis for this study as presented:

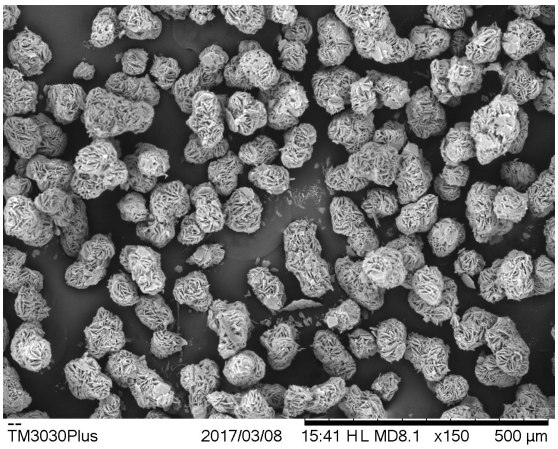


**(1)** Untreated seeds

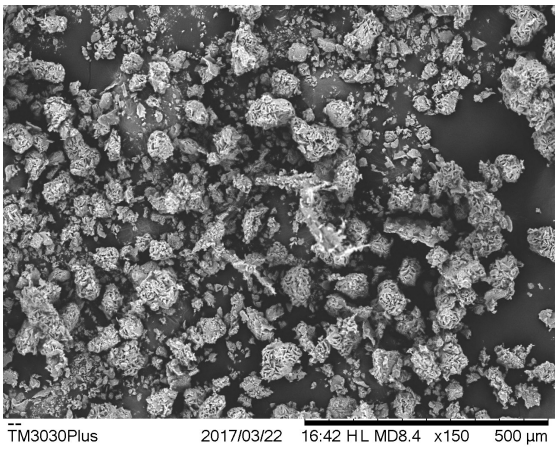


**(2)** Wet-milled seeds

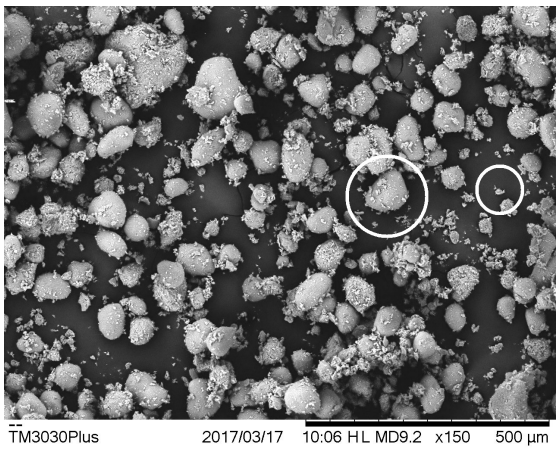


**(3)** Dry-milled seeds

**Figure 4.1:** Three types of seeding materials. The total scale bar shows a realistic length of 500 µm.

1. **Untreated seeds**. AA crystals directly from the process at Lindesnes after filtration, washing and drying without any kind of milling. No treatment at NTNU lab. Added as a premade slurry composed of 30 wt.% seeds and 70 wt.% saturated AA solution.
2. **Wet-milled seeds**. AA crystals directly from the process at Lindesnes after filtration, washing and drying without any kind of milling. Crushed by wet-milling for 48 hours at 350 rpm with a magnetic stirrer at NTNU lab. Added as a premade slurry composed of 30 wt.% seeds and 70 wt.% saturated AA solution.
3. **Dry-milled seeds**. AA crystals directly from the process at Lindesnes after filtration, washing, drying and dry-milling. No additional treatment at NTNU lab. Traditionally added as dry seeds.

Untreated seeds were prepared as a slurry by magnetic stirring in a solution for a maximum of 5 minutes in order to avoid milling. A new slurry was prepared for each experiment. Wet-milled seeds were stored in a solution with no agitation between each experiment. In order to minimize the time period of wet storage, all experiments involving wet-milled seeding were run consecutively and with a total storage time of ∼48 hours after ended wet-milling.

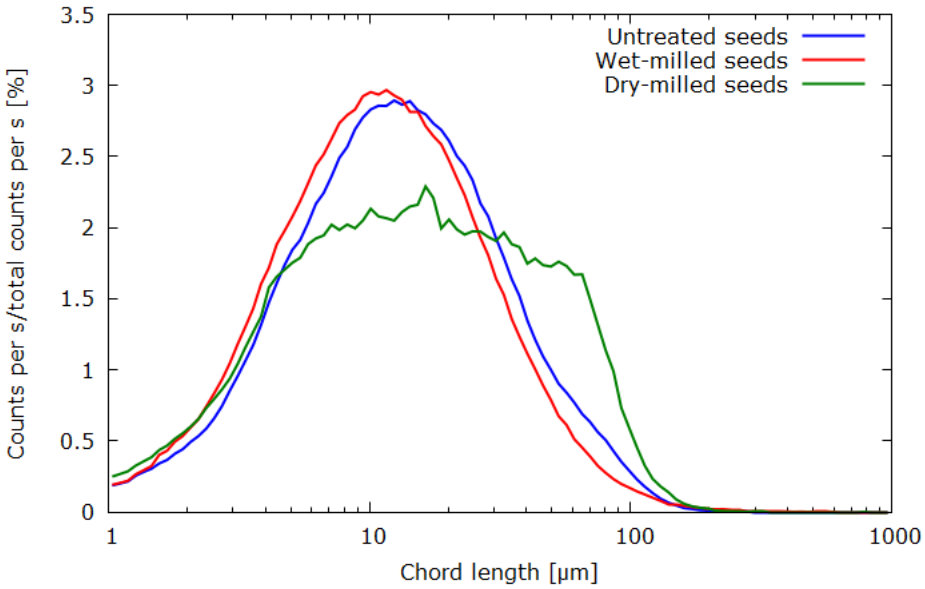


**Figure 4.2:** Relative chord length distributions for three seeding materials at standard conditions.

As seeds are added to a solution containing no solids, chord length distributions monitored immediately after seeding represent the chord length distribution of the seeds solely. Figure 4.2 shows the average of all chord length distributions involving untreated, wet-milled and dry-milled seeds at *standard conditions*.

Standard conditions, based on common practice in industry, implies that untreated and wet-milled seeds are added as a slurry, whereas dry-milled seeds are added dry. As one experiment was performed using slurry-based dry-milled seeds (see Section 4.4), Figure 4.3 gives a better representation of *dispersed* seeds only.

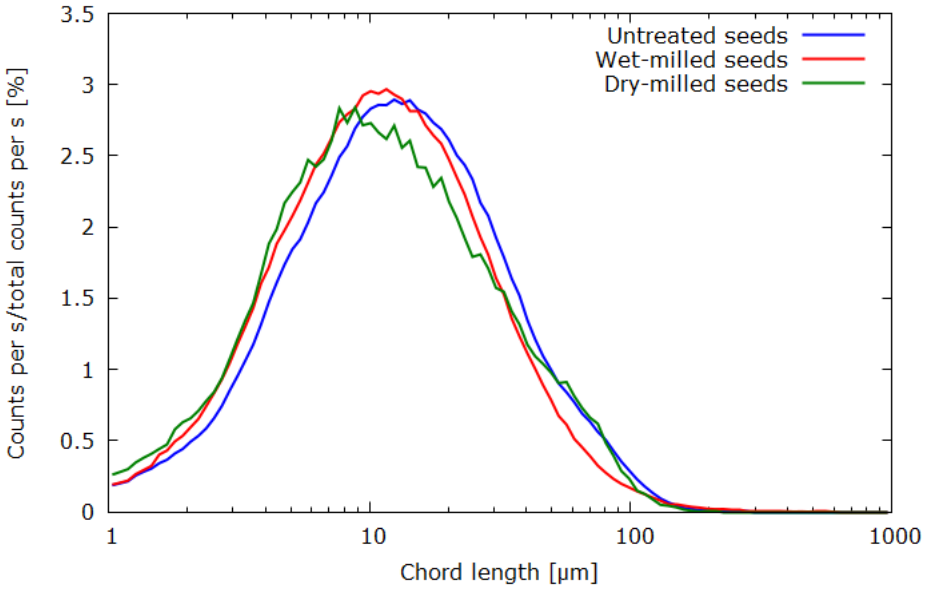


**Figure 4.3:** Relative chord length distributions for the three categories of seeding materials. Slurry addition only.

The broadest chord length distribution is seen for dry-milled seeds, even after being dispersed. Wet-milling of untreated seeds results in a small shift to the left, corresponding to a reduction of mean chord length.

### Size and surface area estimations

The particle diameter estimation method has been used for Figure 4.1. Table 4.1 lists estimates of an average particle diameter, $D_{s,\,real}$, for each seeding material.

**Table 4.1:** Average particle diameter estimated for three types of seeding material.

| **Seed characteristics** | $\mathbf{D_{s,\,real}}$ [µm] |
|---|---|
| Untreated | $82 \pm 2$ |
| Wet-milled | $53 \pm 4$ |
| Dry-milled, large | $57 \pm 2$ |
| Dry-milled, fine | $11 \pm 1$ |

Two white circles in Figure 4.1 (3) indicate two characteristic particles for dry-milled seeds. The large circle marks large, spherical particles with a smooth surface. The small circle indicates fine particles. As the sizes are clearly different, the two categories are separated into *large* and *fine* in Table 4.1 in order to provide representative estimates. A general distinction between various wet-milled seed particles has not been made.

Specific BET surface area, denoted by $a_{\mathrm{BET}}$, has been measured for each of the three types of seeding material:

**Table 4.2:** BET surface area per unit mass of seeding material for three types of seeding materials. Measured by $N_2$ adsorption analysis.

| **Seed characteristics** | $\mathbf{a_{BET}}$ $\mathbf{[m^2/g]}$ |
|---|---|
| Untreated | 1.4245 |
| Wet-milled | 2.4667 |
| Dry-milled | 1.8514 |

## 4.2 Reproducibility of experiments

When analyzing trends at varying seeding conditions, it is of high interest to know if the same results can be achieved when repeating an experiment multiple times. The degree of reproducibility of one experiment has been analyzed both in terms of filterability and chord length measurements in this section.

### 4.2.1 In terms of filterability

In order to quantify the reproducibility of one crystallization experiment, the standard error of average specific cake resistance, $\alpha_{ave}$, provides valuable information. This is achieved by performing the same crystallization experiment multiple times, followed by a filtration test. A mean of $\alpha_{ave}$ for all parallels is then calculated, in addition to a standard error of the mean. This procedure can potentially be repeated for each experiment that is subject to a change of an important parameter. However, in order to minimize the number of experiments, it is hereby assumed that the same standard error is applicable for each unique experiment.

A standard experiment has been chosen as a basis for this research; 1.7 % untreated seeds in slurry, added at the saturation point in a synthetic solution. The same crystallization experiment has been repeated four times, resulting in a total of five unique parallels. Approximately 200 mL suspension is withdrawn after each performed parallel, followed by a Nutsche filtration test with an applied pressure of 1 barG. Accumulated filtrate volume as a function of time, converted from mass by density of filtrate, is presented in the following figure for the five parallels.

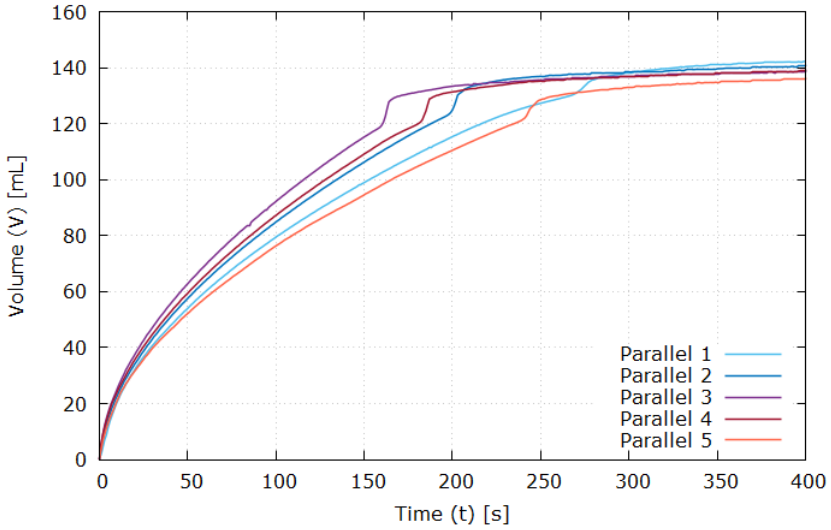


**Figure 4.4:** Accumulated filtrate volume as a function of time for five unique crystallization experiments (Experiment A4 and A18-21): 1.7 % untreated seeds in slurry, added at the saturation point, synthetic solution. The point where the slope increases rapidly before levelling off marks the end of filtration.

The information from Figure 4.4 can be used together with the general equation for cake filtration, Equation 2.10, by calculating $t/V$ for all data of $V$ for each parallel. By performing a linear regression of the data points, the slope of the regression equation combined with parameters of (2.10) yields an approximation of $\alpha_{ave}$ for all five parallels.

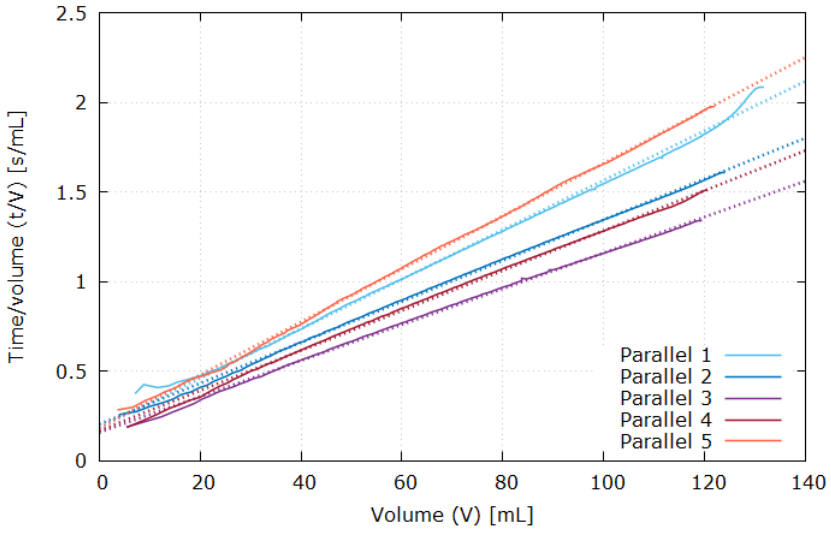


**Figure 4.5:** Time per accumulated filtrate volume as a function of volume for the five parallels. $\alpha_{ave}$ is found through the slope of the linear regression as marked by the dotted lines.

**Table 4.3:** Parameters of the linear regression equations for the five parallels as presented in Figure 4.5, written as $y = ax + b$. Average specific cake resistance calculated for each specific parallel.

| **Parallel [#]** | **a [s/cm$^6$]** | **b [s/cm$^3$]** | **R$^2$ [-]** | $\alpha_{ave}$ **[cm/g]** |
|---|---|---|---|---|
| 1 | 0.0138 | 0.1835 | 0.9953 | $2.71 \cdot 10^9$ |
| 2 | 0.0114 | 0.2037 | 0.9994 | $2.01 \cdot 10^9$ |
| 3 | 0.0100 | 0.1572 | 0.9989 | $1.53 \cdot 10^9$ |
| 4 | 0.0112 | 0.1678 | 0.9987 | $1.99 \cdot 10^9$ |
| 5 | 0.0148 | 0.1834 | 0.9996 | $2.15 \cdot 10^9$ |

Average specific cake resistance for all parallels, $\overline{\alpha}_{ave}$, is calculated to $2.08 \cdot 10^9$ cm/g. Standard error is calculated to $\mathbf{1.90 \cdot 10^8}$ cm/g. Supplementary filtration data for Parallel 1-5 are given for Experiment A4 and A18-21 respectively in Table B.1.

### 4.2.2 In terms of chord length measurements

The same parallels as described previously, with the exception of Experiment A4, also include valid measurements of chord lengths vs. time. A figure including the overlap between the four parallels divided into three chord length intervals, depicts the reproducibility of a single experiment in terms of chord lengths vs. time.

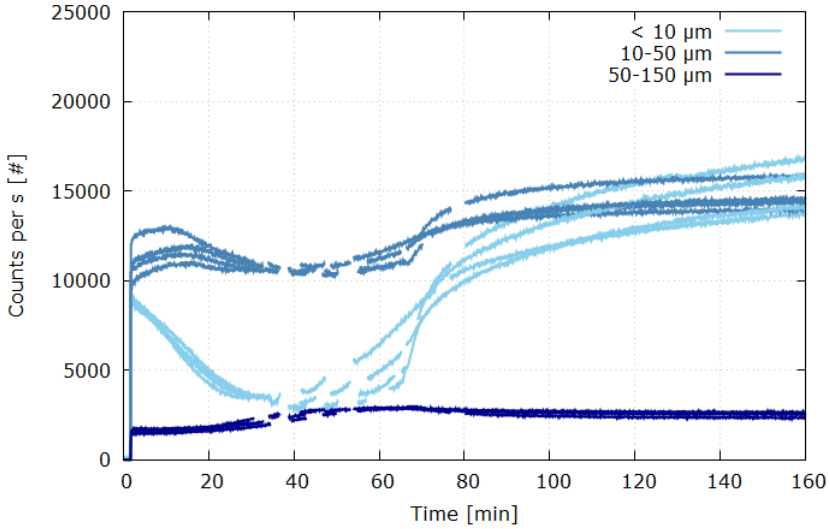


**Figure 4.6:** Chord lengths divided into three intervals as a function of time for four unique crystallization experiments (Experiment A18-21): 1.7 % untreated seeds in slurry, added at the saturation point, synthetic solution.

At t = 1.5 min in Figure 4.6, the solution contains seeds only and no growth/nucleation has taken place yet. It can easily be seen that the chord lengths of 10-50 µm have a significantly higher variation between the parallels than do the smallest chord lengths (<10 µm) at this point. At the endpoint (t = 160 min), where suspension is withdrawn for filtration tests, the smallest chord lengths now experience the *largest* variation. These observations are further illustrated by looking at the coefficient of variation between the four parallels divided into three chord length intervals.

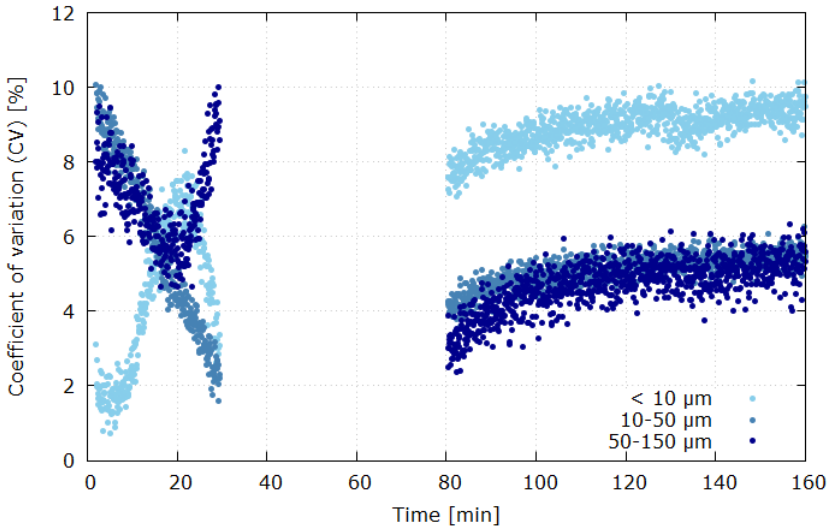


**Figure 4.7:** Coefficient of variation vs. time of four unique experiments divided into three chord length intervals (Experiment A18-21): 1.7 % untreated seeds in slurry, added at the saturation point, synthetic solution. Note that the time interval characterized by scaling (t = 30 min to t = 80 min) is removed entirely.

Whereas the coefficient of variation, CV, of <10 µm is by far the lowest at the point of seeding, Figure 4.7 shows that CV has increased by a factor of ∼5 at the point of suspension withdrawal. The coefficient of variation of the smallest chord lengths is almost twice the CV of the two larger chord length intervals at this point.

Variations between parallels can to some extent be explained by uncertainty in measurements by the FBRM probe, but a difference within the three chord length intervals also indicates *real* variations from experiment to experiment. Figure 4.7 indicates that generation of fine particles varies more from parallel to parallel than larger chord lengths. Based on an assumption that the increase of <10 µm in Figure 4.6 is a result of nucleation only, these observations may indicate that this mechanism is less reproducible than e.g. crystal growth. However, it should be emphasized that the increase of 10-50 µm in Figure 4.6 also can be a result of nucleation.

By separating chord lengths into exact numbers and not intervals, Figure 4.8 on the following page accurately reflects variations between parallels for *seeds* and *final* crystals. As shown in the figure, chord length distributions can be presented as number weighted total counts (counts per s) and number weighted relative counts (counts per s/total counts per s).

Figure 4.8 (a) illustrates that a relative chord length distribution shows the highest degree of resemblance from parallel to parallel. Both distributions show that the most significant variations are found from chord lengths of 3-30 µm. In the following sections, relative chord length distributions will be emphasized, as these are more comparative at e.g. different seeding ratios. All presented chord length distributions are *number weighted*.

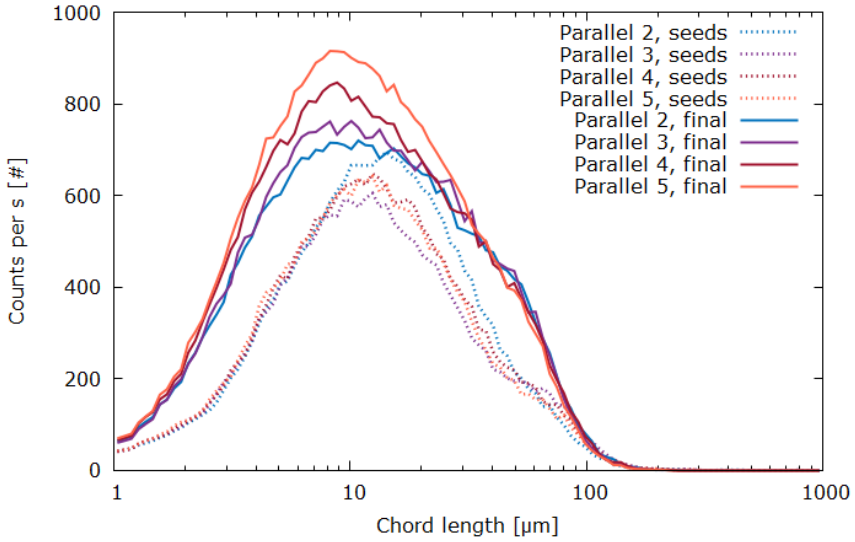


**(a)** Total chord length distribution (number weighted)

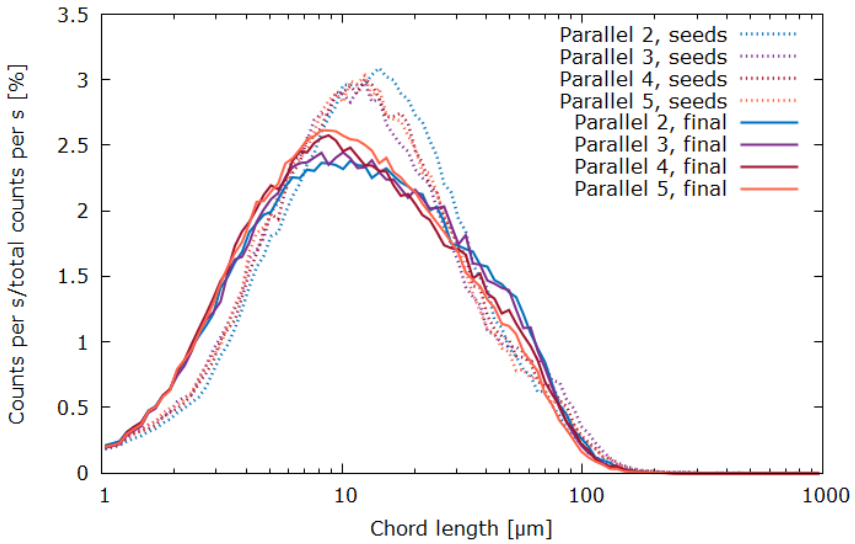


**(b)** Relative chord length distribution (number weighted)

**Figure 4.8:** Chord length distribution of solid AA for seeds (t = 1.5 min) and final crystals (t = 2 h 40 min). Four parallels included (Experiment A18-21): 1.7 % untreated seeds in slurry, added at the saturation point, synthetic solution. Note that the same parallels with respective colours are shown in Figure 4.4 and 4.5, with the exception of Parallel 1.

## 4.3 Seeding material and seeding ratio

*In this section; SEM pictures, chord length measurements and concentration data related to seeding ratio ($\phi$) for different seeding materials are presented and discussed. The section ends with results and discussion related to filtration abilities.*

Seeding is performed at the saturation point in a synthetic solution for all experiments in this section. Extent of crystal growth, $\xi$, is presented for seeded experiments where evidences of growth are observed.

### 4.3.1 Implementation of seeding

A reference experiment *without* seeding has been performed at the saturation point in a synthetic solution. In order to demonstrate the effect of introducing seeding in a crystallization process, a comparison of a seeded process with a low $\phi$ is included in the following figure. Untreated seeds (slurry) added at the saturation point in a synthetic solution has been applied in the picture on the right.

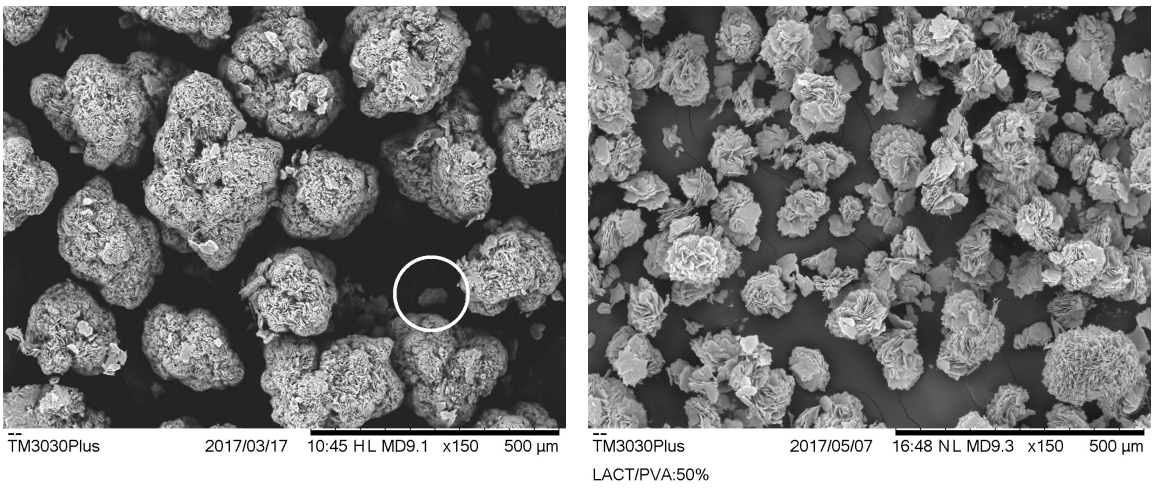


**(a)** No seeding **(b)** $\phi = 0.3$ %

**Figure 4.9:** Final crystals (Experiment A3 and A17 respectively); effect of implementing seeding in a crystallization process. The total scale bar shows a realistic length of 500 µm.

The figure shows that even a small increase in seeding ratio ($\Delta\phi = 0.3$ %) yields a significant difference in the outcome both with respect to surface characteristics and size. Whereas the final crystals of the unseeded process appear as relatively large (up to 200 µm) and spherical, the seeded process shows a higher number of crystals with smaller, plate-like characteristics down to ∼20 µm.

However, small particles below 40 µm can be observed also in the unseeded case, as indicated by the white circle in (a). Although less evident based on the SEM pictures, the relative chord length distributions of the final crystals indicate a similar formation of fines for both the unseeded and seeded process.

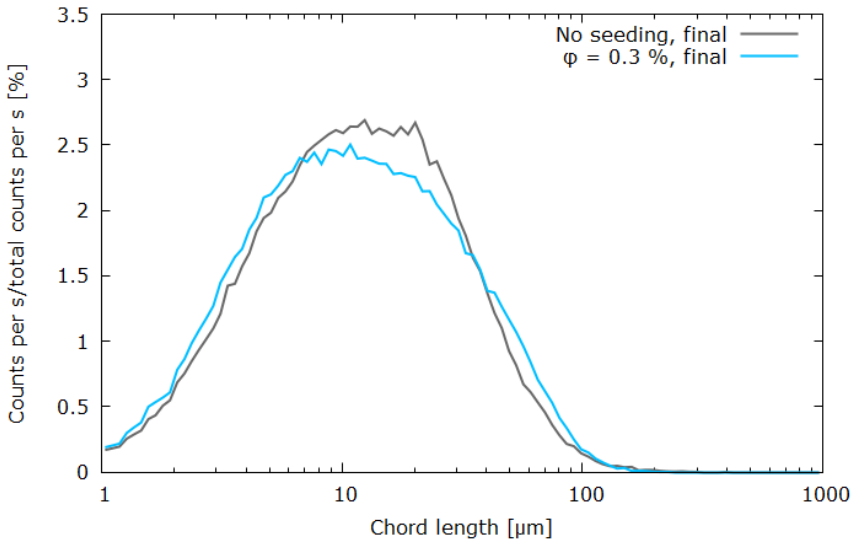


**Figure 4.10:** Chord length distribution of solid AA for final crystals (t = 2 h 40 min). No seeding compared to untreated seeds in slurry.

The figure indicates a slightly narrower chord length distribution for the unseeded process, but the characteristics of Figure 4.9 are not clearly reflected. The figure illustrates that chord length distributions should be used *with reservation* in the case of an unseeded process, as the relatively large observed particle sizes are not translated into large chord lengths. This can be a result of FBRM monitoring in a *fine* instead of a *coarse* operation mode, apparently not picking up chord lengths up to 200 µm. However, as all seeded experiments include only crystals at significantly smaller sizes, this problem should be less evident in the following cases.

A concentration profile of AA in the liquid phase for an unseeded process is not included in this section, but instead given as a reference for each of the seeding materials at varying seeding ratios.

### 4.3.2 Untreated seeding

The following figure shows the characteristics of untreated seeds and final crystals after cooling to 22 °C as seeding ratio, $\phi$, is increased for untreated seeding; slurry addition. Seeding is performed at the saturation point in a synthetic solution.

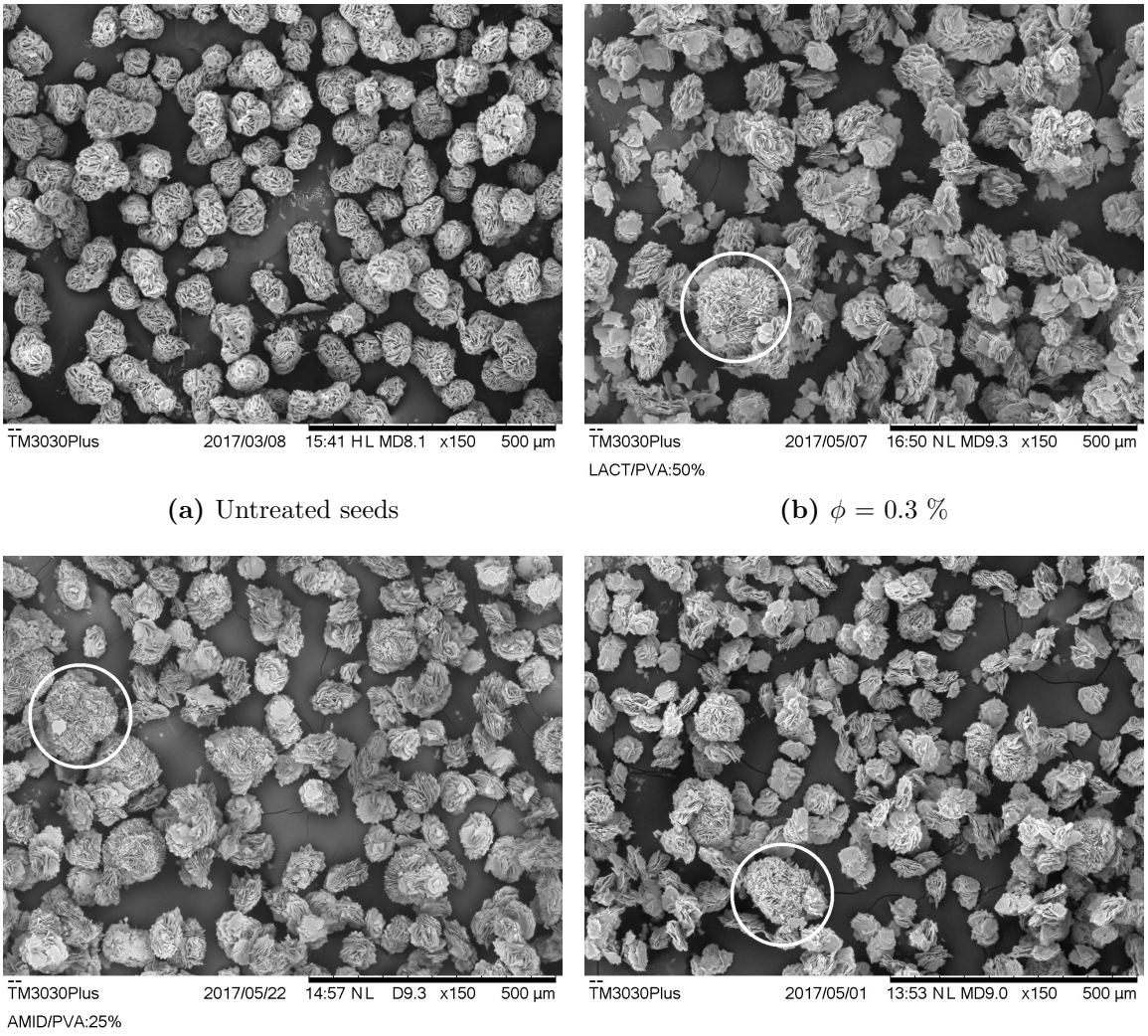


**(a)** Untreated seeds **(b)** $\phi = 0.3$ %

**(c)** $\phi = 1.7$ % **(d)** $\phi = 3.3$ %

**Figure 4.11:** Untreated seeds and final crystals at increasing seeding ratios, $\phi = \{0.3, 1.7, 3.3\}$ %: Experiment A17, A19 and A14 respectively. The total scale bar shows a realistic length of 500 µm.

Figure 4.11 shows two main categories of crystals for all seeding ratios: Large, spherical crystals, as indicated by the white circles, and significantly smaller crystals with plate-like characteristics. As the large, spherical crystals are probable evidences of growth on seed particles, the white circles also represent typical estimated final particle sizes caused by growth. Including only crystals larger in size than the untreated seed particles, extent of crystal growth has been calculated as presented in the following table based on the particle diameter estimation method.

**Table 4.4:** Estimated real final particle size, $D_{f,\,real}$, and extent of crystal growth, $\xi$, calculated at varying seeding ratios. Only crystals in Figure 4.11 *larger* than the untreated seed particles are included.

| $\phi$ [%] | $D_{f,\,real}$ | $\Delta D_{real}$ [µm] | $\Delta D_{max}$ [µm] | $\xi$ [%] |
|---|---|---|---|---|
| 0.3 | 164 ± 5 | 82 ± 7 | 479 ± 12 | 17 |
| 1.7 | 125 ± 3 | 43 ± 5 | 237 ± 6 | 18 |
| 3.3 | 107 ± 6 | 25 ± 8 | 173 ± 4 | 14 |

Based on Table 4.4, the highest extent of crystal growth is found at $\phi = 1.7$ %. However, no major differences are found in terms of $\xi$ for any of the seeding ratios. With a peak of $\xi = 18$ %, it can safely be assumed that crystal growth is not the only present mechanism in the crystallization process of AA.

As the smaller, plate-like final crystals are smaller in size than any of the original seed particles, these can not be explained by crystal growth. The smaller final crystals can be classified as either:

- New crystals generated by nucleation. As seeding ratio is increased, so is magma density ($M_T$), and the probability of a *secondary* nucleation increases.
- Fragments of original seed particles as a result of mechanical breakage by agitation.

Assuming that the smaller crystals are results of nucleation, they can be referred to as *nuclei*. The following table lists average particle diameter of assumed nuclei, thus excluding all observed crystals above seed particle size.

**Table 4.5:** Estimated average particle diameter of assumed nuclei, $D_{nuclei}$, corresponding to all particles *smaller* than the seed particles in Figure 4.11.

| $\phi$ [%] | $D_{nuclei}$ [µm] |
|---|---|
| 0.3 | 63 ± 6 |
| 1.7 | 72 ± 2 |
| 3.3 | 67 ± 2 |

As seen by the low average and high standard error at $\phi = 0.3$ %, there is a significantly larger domination of fine particles at this seeding ratio. Although some plate-like particles of ∼100 µm in Figure 4.11 (b) can be observed, there is also a significant presence of fine particles of ∼20 µm. As seen by (c) and (d) combined with the standard error in Table 4.5, uniformity with respect to particle size increases significantly for nuclei at $\phi = 1.7$ and 3.3 %.

As the rate of secondary nucleation increases with magma density, corresponding to seeding ratio, there is a possibility that some *primary* heterogeneous nucleation is present at lower seeding ratios. A significant presence of fines at $\phi = 0.3$ % indicates nuclei generated by this mechanism. However, size uniformity at $\phi = 1.7$ and 3.3 % indicates a predominant *secondary* nucleation.

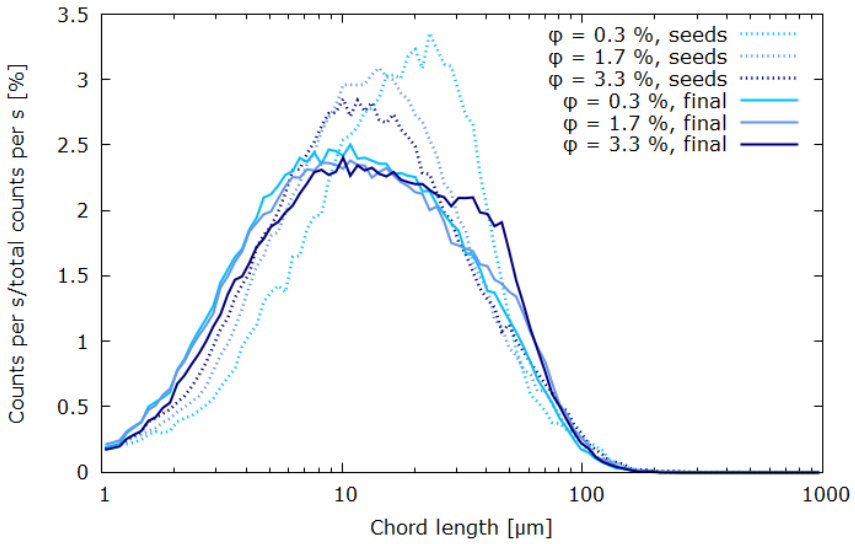


**Figure 4.12:** Relative chord length distribution of solid AA for seeds (t = 1.5 min) and final crystals (t = 2 h 40 min). Untreated seeds in slurry at increasing seeding ratios.

Differences at varying seeding ratios are less evident in terms of relative chord length distributions. A general trend is that the distribution is wider for final crystals compared to the seeds. However, an assumed increase of size uniformity at higher seeding ratios is not confirmed. A shift to the right from seed to product crystals, indicating increase in final chord lengths, is most evident for $\phi = 3.3\,\%$. The largest dominance of fine particles is found for $\phi = 0.3\,\%$ and $\phi = 1.7\,\%$.

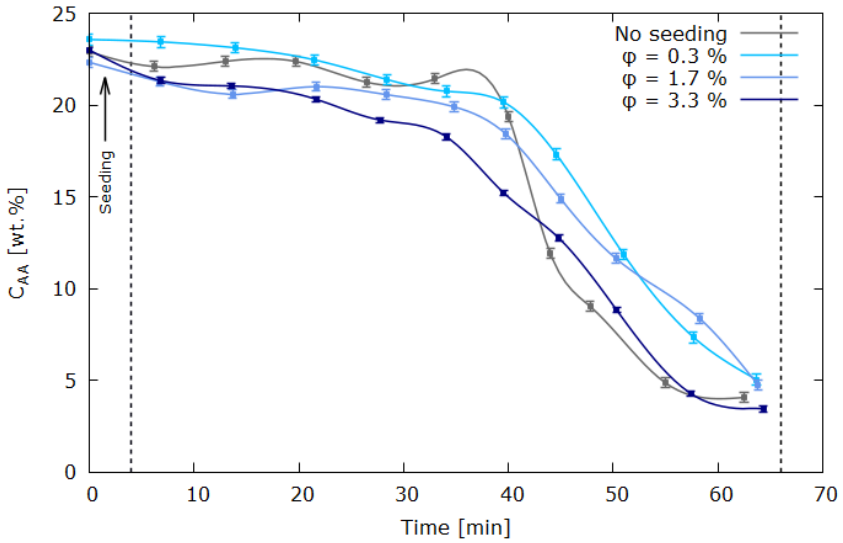


**Figure 4.13:** Concentration of AA in the liquid phase during the first 70 minutes. Untreated seeds in slurry at increasing seeding ratios. Note that the time region of continuous acid addition is marked with vertical dotted lines.

Figure 4.13 shows that concentration of AA in the liquid phase drops *earlier* as seeding ratio is increased. Concentration starts to drop significantly at around 40, 30 and 20 minutes for $\phi = 0.3$, 1.7 and 3.3 % respectively. A general trend is that the reductions are far smoother than for the unseeded case.

As seeding ratio is increased, it can be assumed that major nucleation occurs at a lower supersaturation. Whereas the unseeded process is dominated by primary nucleation, the more slowly proceeding *secondary* nucleation is a more probable mechanism for seeded experiments as $\phi$ is increased. However, as previously mentioned, fine particle formation at $\phi = 0.3$ % indicates a certain primary nucleation. The fact that $C_{AA}$ has the steepest and latest reduction at $\phi = 0.3$ % compared to $\phi = 1.7$ and 3.3 %, supports this theory. A late reduction corresponds to nucleation at a high supersaturation. Combined with a *fast* reduction, this indicates primary nucleation, as demonstrated by the unseeded process.

An analysis of the expression describing secondary nucleation, Equation 2.7, gives valuable information. It can be assumed that supersaturation, $\sigma$, decreases at the same time as magma density (corresponding to number of seeds present in the solution), $M_T$, increases. Based on a larger number of crystals present at $\phi = 3.3\,\%$ in Figure 4.11, the rate of secondary nucleation is expected to be higher at increased seeding ratios, whereas extent of crystal growth does not increase similarly. The latter was further illustrated by the calculated values of $\xi$ as presented in Table 4.4.

### 4.3.3 Wet-milled seeding

The following figure shows the characteristics of wet-milled seeds and final crystals after cooling to 22 °C as seeding ratio, $\phi$, is increased for wet-milled seeding; slurry addition. Seeding is performed at the saturation point in a synthetic solution.

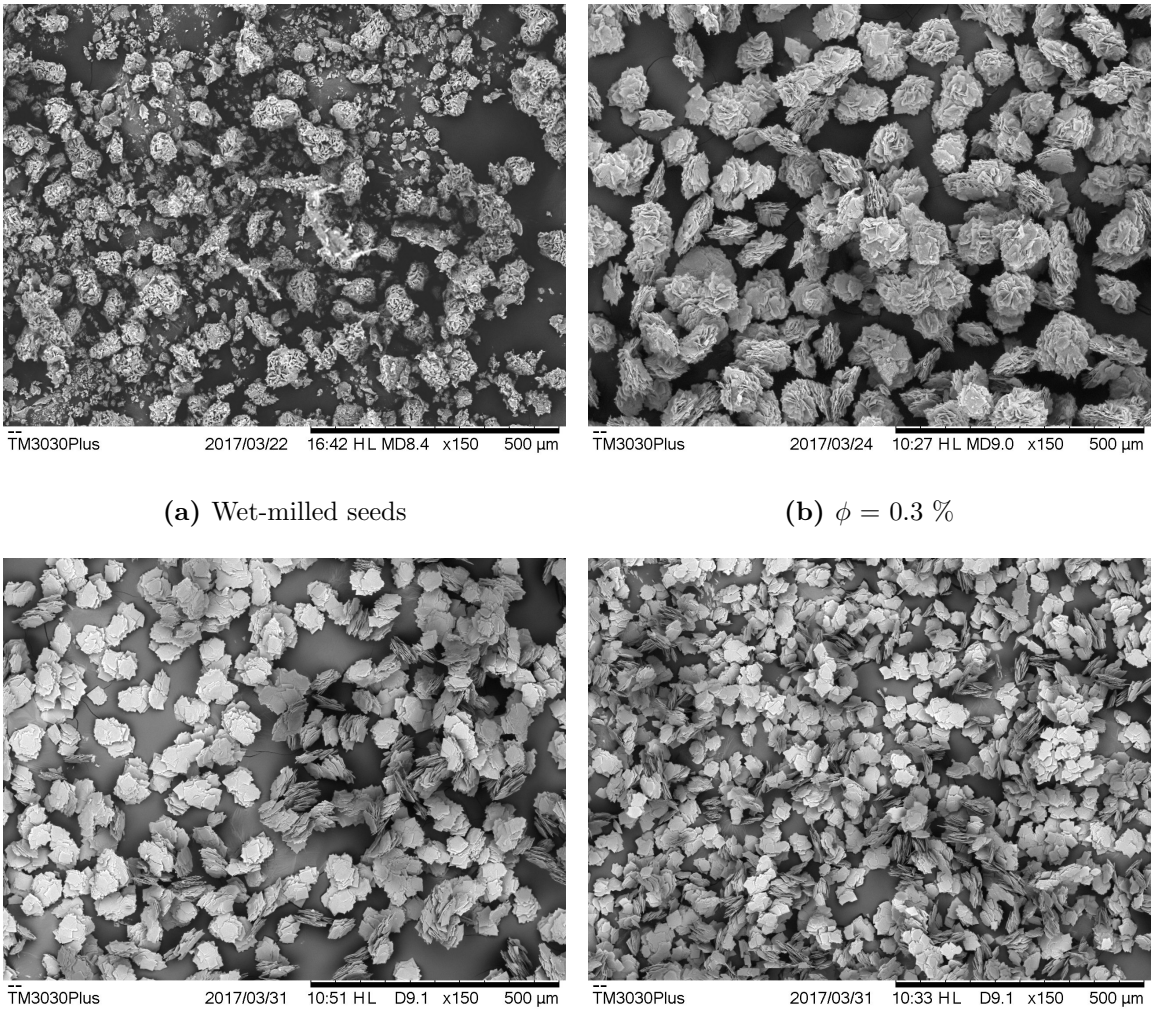


**(a)** Wet-milled seeds

**(b)** $\phi = 0.3$ %

**(c)** $\phi = 1.7$ %

**(d)** $\phi = 3.3$ %

**Figure 4.14:** Wet-milled seeds and final crystals at increasing seeding ratios, $\phi = \{0.3, 1.7, 3.3\}$ %: Experiment A5, A6 and A7 respectively. The total scale bar shows a realistic length of 500 µm.

Explicit evidences of crystal growth, as marked by the white circles in Figure 4.11, can not be observed at any seeding ratios for wet-milled seeding. As wet-milled seeds, shown in (a), are a lot less uniform with respect to size compared to untreated seeds, growth is harder to characterize in this case. As a result of this, calculations of $\xi$ do not provide valid information and are therefore *not* presented for wet-milled seeding.

Only one category of crystals is roughly observed at each seeding ratio. At $\phi = 0.3$ %, the final crystals have classical rose-shaped characteristics resembling the assumed *nuclei* for untreated seeding. However, a significant change in shape occurs at $\phi =$ 1.7 %, where final crystals show strong plate-layer characteristics solely. The same characteristics can be observed at $\phi = 3.3$ %, where the only difference is a significant reduction in average particle size.

Based on the simplification that *all* final crystals are results of nucleation, average estimated particle diameter of assumed nuclei is presented in the following table.

**Table 4.6:** Estimated average particle diameter of assumed nuclei, $D_{nuclei}$, corresponding to all particles in Figure 4.14.

| $\phi$ [%] | $D_{nuclei}$ [µm] |
|---|---|
| 0.3 | 103 ± 3 |
| 1.7 | 68 ± 2 |
| 3.3 | 43 ± 1 |

As seen by Figure 4.14 and standard errors in Table 4.6, final crystals at all seeding ratios show a high degree of uniformity with respect to size. Whereas untreated seeding at $\phi = 0.3$ % yields particles down to ∼20 µm, almost no particles below 40 µm can be observed for wet-milled seeding. Despite a reduction in average particle size at increasing $\phi$, standard errors indicate that uniformity *increases*.

As previously indicated, it can be assumed that nucleation is by far the most predominant mechanism at wet-milled seeding. Because of the high degree of uniformity, no clear evidences of fine particle formation and consequently *primary* nucleation can be found. Equation 2.7 reveals that rate of secondary nucleation is proportional to crystal-crystal-collisions, $j$, and magma density, $M_T$, which in turn are interrelated. A larger number of smaller plates for $\phi = 3.3$ % can be explained by a a higher number of crystal-crystal collisions leading to a higher secondary nucleation rate and a lower average size.

Although not observed based on the SEM pictures, crystal growth can not be ruled out completely as a present mechanism. As seen by Figure 4.14 (a), wet-milled seeds contain a significant amount of fine particles ($< 10$ µm), and some of the final crystals *may* have grown on them, although not clearly represented in the sample.

The general uniformity with respect to size is further proven by the narrow relative chord length distribution given in Figure 4.15. As for the SEM pictures, a leap is indicated from $\phi = 0.3$ % to 1.7 %. Whereas the product crystals have a wider distribution than the seeds for 0.3 % seeding, the two higher ratios result in a clear shift to the right from seeds to final crystals. The tightest distribution is the one at 3.3 % seeding, although the peak can be seen at a lower chord length.

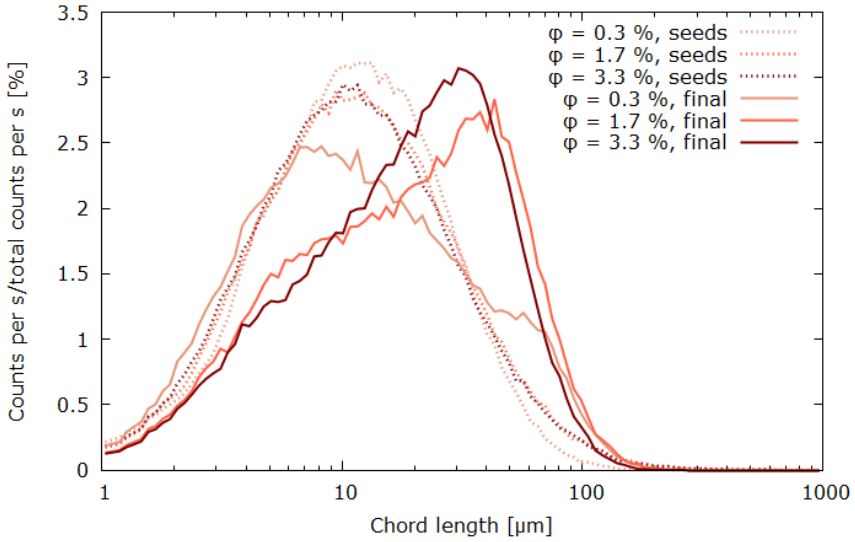


**Figure 4.15:** Relative chord length distribution of solid AA for seeds (t = 1.5 min) and final crystals (t = 2 h 40 min). Wet-milled seeding in slurry at increasing seeding ratios.

The same trends as for untreated seeding are found in concentration of AA in the liquid phase. As $\phi$ is increased, a significant reduction of $C_{AA}$ occurs earlier. At $\phi$ = 3.3 %, concentration drops noticeably already at ∼18 minutes.

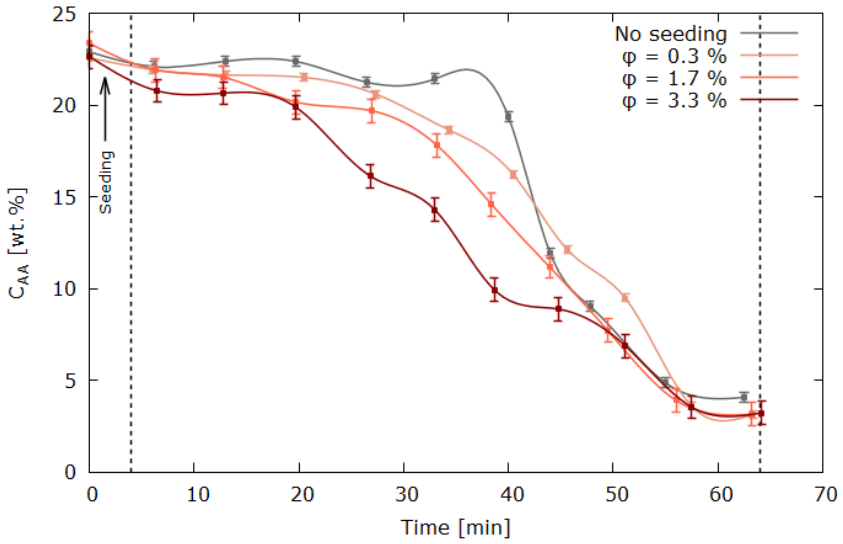


**Figure 4.16:** Concentration of AA in the liquid phase during the first 70 minutes. Wet-milled seeds in slurry at increasing seeding ratios. Note that the time region of continuous acid addition is marked with vertical dotted lines.

As seeding ratio is increased, supersaturation is exposed to a higher total surface area, which again makes the reduction of supersaturation proceed faster. However, this argumentation does still not distinguish further between growth and secondary nucleation. The narrow size distribution of $\phi$ = 1.7 % and 3.3 % is still the clearest evidence of a predominant secondary nucleation.

### 4.3.4 Dry-milled seeding

The following figure shows the characteristics of dry-milled seeds and final crystals after cooling to 22 °C as seeding ratio, $\phi$, is increased for dry-milled seeding; dry addition. For the effect of a *slurry* addition of dry-milled seeds, see Section 4.4. Seeding is performed at the saturation point in a synthetic solution.

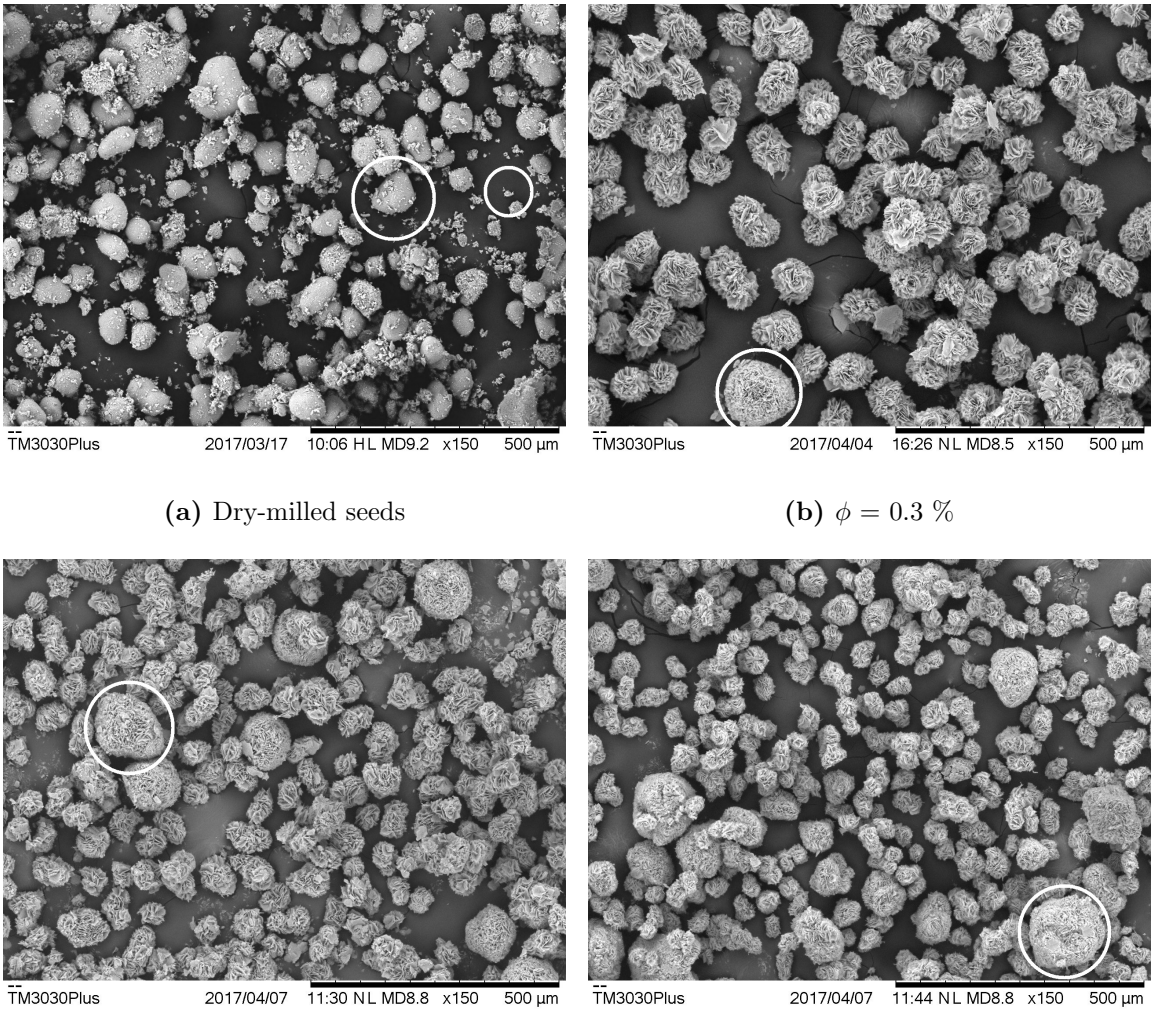


**(a)** Dry-milled seeds

**(b)** $\phi = 0.3$ %

**(c)** $\phi = 1.7$ %

**(d)** $\phi = 3.3$ %

**Figure 4.17:** Dry-milled seeds and final crystals at increasing seeding ratios, $\phi = \{0.3, 1.7, 3.3\}$ %: Experiment A8, A9 and A10 respectively. The total scale bar shows a realistic length of 500 µm.

Two categories of crystals can roughly be observed for dry-milled seeding:

1. Large, almost perfectly spherical particles as indicated by the white circles in (b)-(d).
2. Smaller, more open-structured spherical particles surrounding the large crystals.

As for untreated seeding, there are clear indications that the large, spherical particles are results of crystal growth on the large seed particles with a smooth surface (as indicated by the large white circle in Figure 4.17 (a)). However, the second category of crystals is harder to classify. In order to gain an understanding of the mechanisms creating this category of particles, two extremes can be launched as hypotheses:

- The smaller crystals are all results of nucleation, mainly secondary, in the same way as for untreated seeding.
- The smaller crystals are all results of crystal growth on fine seed particles as indicated by the small white circle in Figure 4.17 (a).

Extent of crystal growth is calculated and presented in the following table in the same way as for untreated seeding. The calculations are based on the assumption that growth occurs on large particles with a smooth surface only, thus neglecting fine particles of dry-milled seeds.

**Table 4.7:** Estimated real final particle size, $D_{f,\,real}$, and extent of crystal growth, $\xi$, calculated at varying seeding ratios. Only crystals in Figure 4.17 (b)-(d) larger than the large dry-milled seed particles are included. Fine seed particles are neglected.

| $\phi$ [%] | $D_{f,\,real}$ | $\Delta D_{real}$ [µm] | $\Delta D_{max}$ [µm] | $\xi$ [%] |
|---|---|---|---|---|
| 0.3 | 143 ± 4 | 86 ± 6 | 327 ± 11 | 26 |
| 1.7 | 122 ± 3 | 65 ± 5 | 164 ± 6 | 40 |
| 3.3 | 117 ± 5 | 60 ± 7 | 120 ± 4 | 50 |

Calculated values of $\xi$ for dry-milled seeding are significantly higher than all calculated values of $\xi$ for untreated seeding. This illustrates that growth is more predominant on large particles of dry-milled seeds than on untreated seeds. Extent of growth also seems to increase at increasing values of $\phi$. However, considering a maximum $\xi$ of 50 %, a significant amount of crystallizing mass still results in nuclei or growth on fine particles of dry-milled seeds.

In contrast to untreated seeds, dry-milled seeds consist of many fine particles, which makes growth and nucleation harder to distinguish. However, as no fine particles are observed for the final crystals, *secondary* nucleation can be considered as a more probable mechanism than a primary nucleation.

The fact that no fine particles originating from the seeds (<10 µm) can be observed for the final crystals, indicates that a certain growth on fine particles has occurred. In fact, hardly any particles below 50 µm are observed at all values of $\phi$. The final crystals also have noticeably spherical characteristics, as opposed to the plate-like nuclei at untreated seeding, which can be explained by a spherulitic growth.

In summary, crystal growth on fine particles is an evident mechanism. However, as secondary nucleation rate in turn is proportional to growth rate, it can be assumed that secondary nucleation also occurs to some extent. In the following table, estimated diameters of the smaller final crystals are presented.

**Table 4.8:** Estimated average particle diameter of the smaller crystals, $D_{small}$, based on final crystals in Figure 4.17 *not* indicated by the white circles.

| $\phi$ [%] | $D_{small}$ [µm] |
|---|---|
| 0.3 | 89 ± 2 |
| 1.7 | 67 ± 2 |
| 3.3 | 50 ± 2 |

Average size for the smaller final crystals is reduced as $\phi$ is increased, which can be explained by a higher frequency of crystal-crystal collisions and a higher magma density. Based on the standard errors in Table 4.8, size uniformity is stable as $\phi$ increases.

All seeding ratios yield a narrower chord length distribution from seeds to final crystals, as shown in Figure 4.18. The large, spherical particles are not detected for any of the experiments. Chord length distributions indicate that uniformity increases slightly at higher seeding ratios, and a small shift to the left indicates a reduction of average size at higher values of $\phi$.

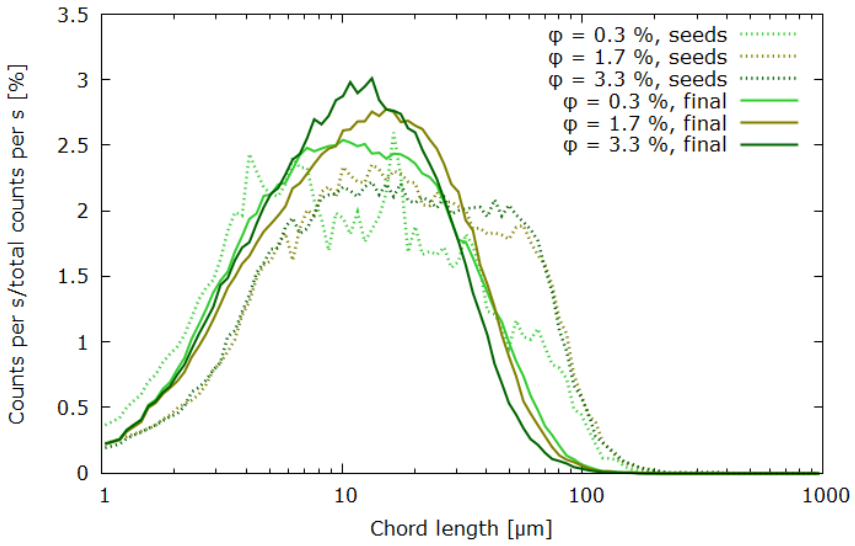


**Figure 4.18:** Relative chord length distribution of solid AA for seeds (t = 1.5 min) and final crystals at suspension withdrawal (t = 2 h 40 min). Dry-milled seeds, dry, at increasing seeding ratios.

The clear correlation between reduced concentration and increased seeding ratios that could be observed for untreated and wet-milled seeding, is not seen in Figure 4.19. The reduction proceeds slowly, especially compared to an unseeded process, but only a modest reduction from $\phi$ = 0.3 to 3.3 % is indicated. Assuming growth is the dominating mechanism, concentration of AA vs. time does not confirm that higher seeding ratios favour higher growth rates.

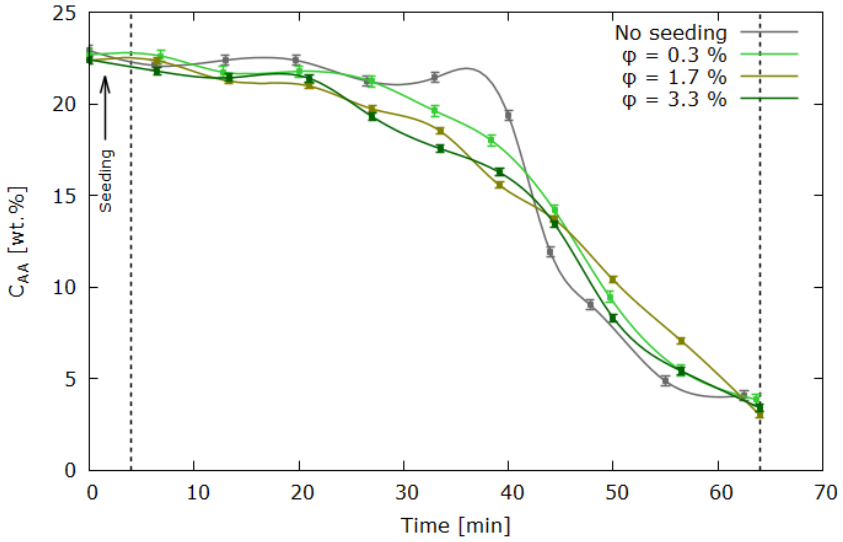


**Figure 4.19:** Concentration of AA in the liquid phase during the first 70 minutes. Dry-milled seeds, dry, at increasing seeding ratios. Note that the time region of continuous acid addition is marked with vertical dotted lines.

### 4.3.5 Filterability at varying seeding ratios

Nutsche filtration tests have been performed for suspensions at t = 2 h 40 min seeded by the three types of seeding material at $\phi = \{0.3, 1.7, 3.3\}$ %. The following figure presents average specific cake resistance, $\alpha_{ave}$, vs. exact seeding ratio, $\phi$, for all previously listed experiments in Section 4.3. All error bars of $\alpha_{ave}$ show 1 standard error, based on calculations described in Section 4.2.1.

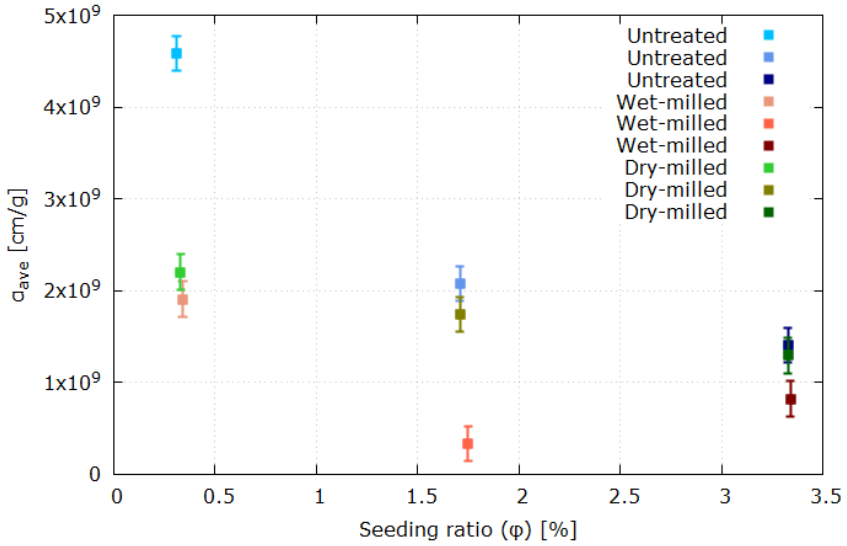


**Figure 4.20:** Average specific cake resistance, $\alpha_{ave}$, vs. seeding ratio, $\phi$, for three types of seeding material.

Table B.1, listing filtration data and values of $\alpha_{ave}$ for all experiments, reveals that the *unseeded* experiment yields an average specific cake resistance of $\mathbf{1.96 \cdot 10^{10}}$ cm/g; more than 4 times higher than the highest $\alpha_{ave}$-value presented in Figure 4.20. In order to be able to distinguish differences at varying seeding ratios, this value is left out of the figure.

However, this clearly states the effect of implementing seeding in a crystallization process of aromatic amine. Despite a higher estimated average size, Figure 4.21 illustrates that the final crystals of the unseeded experiment, as seen by Figure 4.9 (a), show a high degree of compressibility during filtration, corresponding to a low filterability.

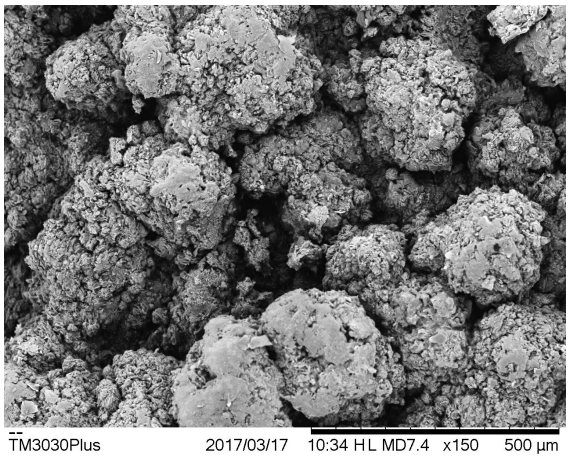


**Figure 4.21:** Sample of filter cake from the unseeded experiment (Experiment A3). The total scale bar shows a realistic length of 500 µm.

For all types of seeding material, the lowest seeding ratio, $\phi = 0.3$ %, causes the worst filtration performance. The effect of increasing seeding ratio is clear in the case of untreated and dry-milled seeding. An increase of $\phi$ yields an $\alpha_{ave}$ *under* the standard error of the preceding $\alpha_{ave}$ (at the lower $\phi$), thus corresponding to a *better* filtration performance. Although specific cake resistance for wet-milled seeding is reduced significantly from $\phi = 0.3$ % to 1.7 %, the latter still yields a better performance than $\phi = 3.3$ %.

By comparing the three types of seeding material, the clearest difference is observed between untreated and wet-milled seeding, where the latter leads to better performance for all values of $\phi$. Despite a lower average particle size and an assumed higher secondary nucleation rate in the case of wet-milled seeding, this still results in a lower $\alpha_{ave}$-value. The following figure shows different characteristics of filter cakes at untreated and wet-milled seeding for $\phi = 1.7$ %.

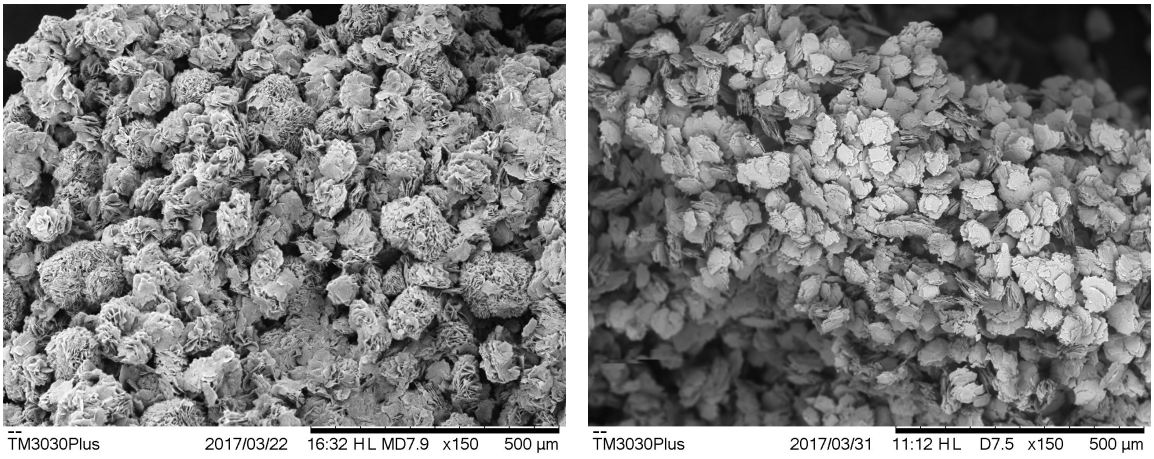


**(1)** Untreated seeding, $\phi = 1.7$ %

**(2)** Wet-milled seeding, $\phi = 1.7$ %

**Figure 4.22:** Sample of filter cakes from experiments with untreated and wet-milled seeding (Experiment A4 and A6 respectively). The total scale bar shows a realistic length of 500 µm.

Figure 4.22 illustrates clear differences in how the final crystals pack together as a filter cake. Although average particle size is lower in the case of wet-milled seeding, the cake is still noticeably less compressed than for untreated seeding. The uniformity of the particles at wet-milled seeding can help explaining this phenomenon. As the final crystals here contain almost no particles below 66 µm in diameter, no fines are present acting as *gap fillers* between the plates. The final crystals of untreated seeding, however, has a lower degree of uniformity and a higher presence of small particles; presumably resulting in a higher density.

The visual characteristics of final crystals at wet-milled seeding, $\phi = 1.7$ % and 3.3 % are relatively similar, as shown in Figure 4.14 (c) and (d), also with respect to uniformity. The higher filtration performance of $\phi = 1.7$ % can be explained by a higher average particle size - the filter cakes of both cases have the same structure, except that the void is more dominating as the plates are larger.

Wet-milled seeding generally yields significantly better filterability than dry-milled seeding, except at $\phi = 0.3$ % where the error bars overlap. At $\phi = 1.7$ and 3.3 %, this also applies to untreated and dry-milled seeding, as the standard errors are within the same region.

## 4.4 Nature of dry-milled seeds

*This section includes a presentation and discussion of SEM pictures, chord length measurements, concentration data and filtration tests related to the nature of dry-milled seeds; dry vs. slurry addition.*

As mentioned in Section 4.1, dry-milled seeds are traditionally added dry in industry. This research has therefore primarily been based on a dry addition, but the potential effects of a *slurry* addition of dry-milled seeds have to be taken into account as well. Preparing seeds in a slurry under a short period of agitation implies that potential lumps of dry seeds can be dispersed before entering the solution. In addition, a slurry addition of seeds may also imply that the surface of the seeds is further *activated*, possibly inducing a higher crystal growth rate.

A similar experiment as described in Section 4.3.4 was performed; dry-milled seeds added at the saturation point, $\phi = 1.7$ %, but this time with *slurry* seeding. The premade slurry is composed of 30 wt.% dry-milled seeds and 70 wt.% saturated AA solution.

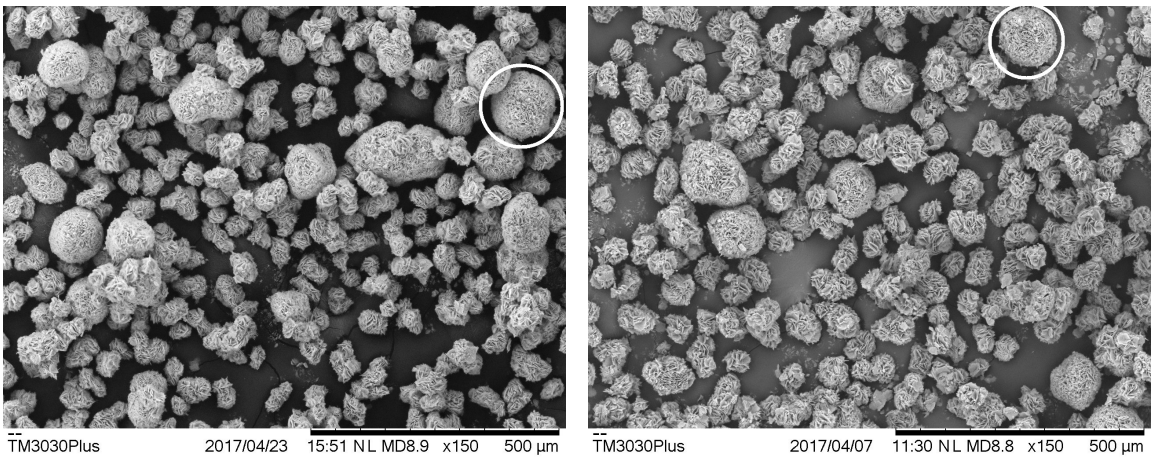


**(a)** Slurry seeding **(b)** Dry seeding

**Figure 4.23:** Final crystals from slurry vs. dry addition of dry-milled seeds ($\phi = 1.7$ %): Experiment A11 and A9 respectively. The total scale bar shows a realistic length of 500 µm.

A distinction between small, roughly spherical crystals and larger, perfectly spherical crystals is observed also for slurry seeding. Crystal growth is evident for the large final crystals as indicated by the white circles. Assuming growth occurs on large particles with a smooth surface only, extent of crystal growth can be calculated as presented in the following table.

**Table 4.9:** Estimated real final particle size, $D_{f,\,real}$, and extent of crystal growth, $\xi$, calculated for dry-milled seeding; slurry and dry addition. Only crystals in Figure 4.23 larger than large dry-milled seed particles are included. Fine seed particles are neglected.

| **Dry/slurry** | $D_{f,\,real}$ | $\Delta D_{real}$ [µm] | $\Delta D_{max}$ [µm] | $\xi$ [%] |
|---|---|---|---|---|
| Slurry | 124 ± 4 | 67 ± 6 | 164 ± 6 | 41 |
| Dry | 122 ± 3 | 65 ± 5 | 164 ± 6 | 40 |

As shown by Table 4.9, approximately the same extent of crystal growth is calculated for the two cases. This implies that the same mechanism is present for slurry seeding as for dry seeding. In order to obtain a comparison of the smaller, roughly spherical particles, estimated diameters are presented in the following table.

**Table 4.10:** Estimated average particle diameter of the smaller crystals, $D_{small}$, based on Figure 4.23.

| **Dry/slurry** | $D_{small}$ [µm] |
|---|---|
| Slurry | 60 ± 2 |
| Dry | 67 ± 2 |

The smaller crystals have a slightly lower average size for slurry seeding compared to dry seeding. Although less distinguishable than growth, a certain rate of secondary nucleation is expected. A possible explanation of the reduced size is a more predominant secondary nucleation for slurry seeding. As suggested in Section 4.2.2, nucleation can be assumed less reproducible than crystal growth.

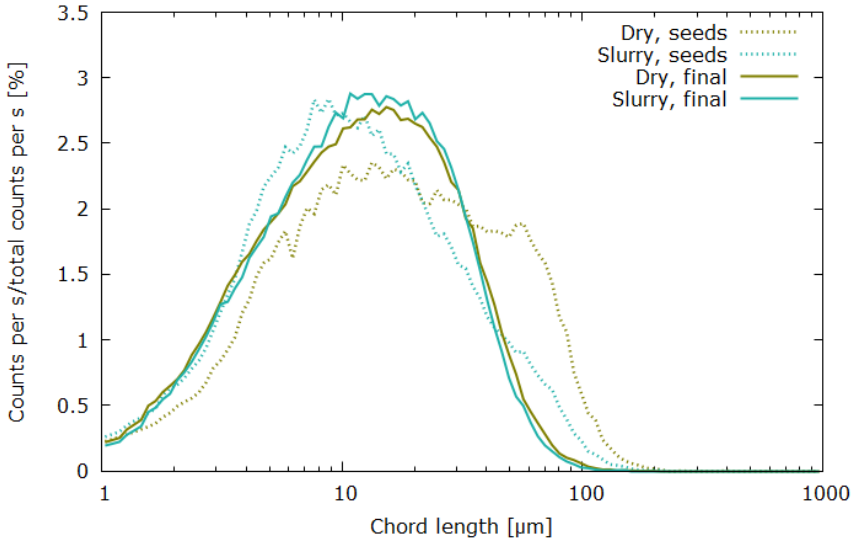


**Figure 4.24:** Relative chord length distribution of solid AA for seeds (t = 1.5 min) and final crystals (t = 2 h 40 min). Dry-milled seeding, slurry vs. dry.

Figure 4.24 is of particular interest, as it shows clear differences in relative chord length distribution of the seeds. Slurry addition of seeds leads to a narrower distribution and a clear shift to the left. This is an indication of seed dispersion, implying

that big lumps of seeds have been separated into smaller particles. However, slurry and dry seeding practically yield the same distributions for final crystals.

$C_{AA}$ for slurry seeding vs. dry seeding follows almost the exact same trendlines until $t \approx 45$ min, where concentration for slurry seeding drops noticeably faster. A faster concentration drop is typically an indication of nucleation, and as no fines are present, a *secondary* nucleation is the most probable. A smoother drop for dry seeding indicates that growth has been dominating for a longer period. A higher rate of secondary nucleation coincides with Table 4.10, where slurry seeding yielded smaller particle sizes for the smaller category of final crystals.

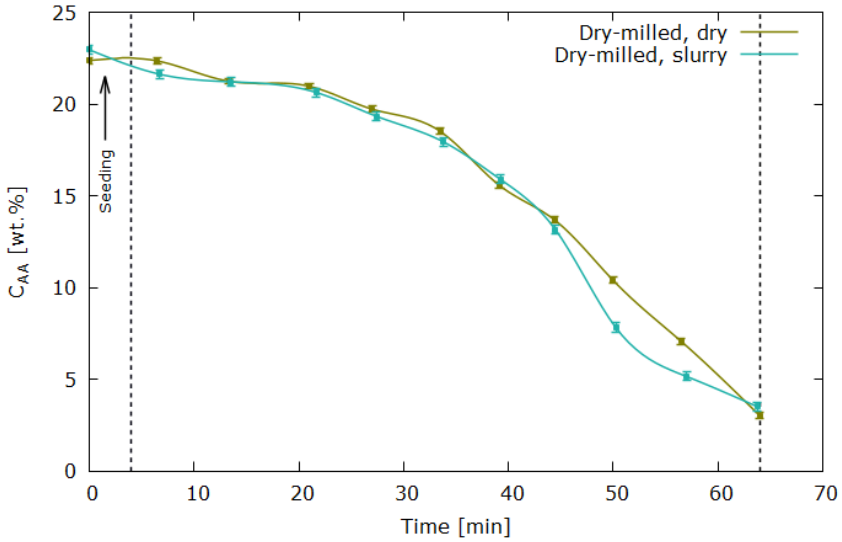


**Figure 4.25:** Concentration of AA in the liquid phase during the first 70 minutes. Dry-milled seeding, slurry vs. dry. Note that the time region of continuous acid addition is marked with vertical dotted lines.

### 4.4.1 Filterability

**Table 4.11:** Average specific cake resistance for slurry seeding, $\alpha_{ave,\,slurry}$, and dry seeding, $\alpha_{ave,\,dry}$. Dry-milled seeds applied, A11 and A9 respectively in Table B.1.

| **Seed characteristics** | $\alpha_{ave,\,slurry}$ **[cm/g]** | $\alpha_{ave,\,dry}$ **[cm/g]** | $\frac{\alpha_{ave,\,slurry}}{\alpha_{ave,\,dry}}$ [%] |
|---|---|---|---|
| Dry-milled | $1.11 \cdot 10^9 \pm 0.19 \cdot 10^9$ | $1.74 \cdot 10^9 \pm 0.19 \cdot 10^9$ | 64 |

Although visual characteristics, extent of growth and chord length distributions of the final crystals do not differ significantly for slurry and dry seeding, Table 4.11 indicates a slightly better filtration performance in the case of slurry seeding. Based on the listed values, a transition from dry to slurry seeding yields a reduction of 36 % in terms of average specific cake resistance.

Table 4.10 and Figure 4.25 indicate a more predominant secondary nucleation for slurry seeding. Although traditionally connecting high filterability to a high growth rate, Section 4.3.5 showed that final crystals of wet-milled seeding, being strongly affected by secondary nucleation, yielded the best filtration performances of all tests. Assuming a higher rate of secondary nucleation for slurry seeding, this can explain the small reduction of average specific cake resistance.

However, it should be noted that only *one* filtration test has been performed for both experiments. Multiple repetitions of the two experiments, in the same way as described in Section 4.2.1, could potentially have resulted in convergence to an average specific cake resistance within *the same standard error*. All discussions related to filterability are based on the assumption of the same standard error of $\alpha_{ave}$ for all experiments.

## 4.5 Total surface area of seeds

*This section comprises total surface area of seeds and its effect on filterability. The same experiments as presented in Section 4.3 will be analyzed, thus involving seeds added at the saturation point in a synthetic solution.*

Section 4.3, where seeding materials and seeding ratios were compared, can also be interpreted in terms of total surface area of seeds, $A_{\mathrm{BET}}$, added in each specific experiment. This can be calculated by Equation 3.3 where $a_{\mathrm{BET}}$ is found for each characteristic seeding material in Table 4.2. In terms of total surface area of seeds added, average specific cake resistance of each experiment, $\alpha_{ave}$, can be presented as given in the following figure. All error bars of $\alpha_{ave}$ show 1 standard error, based on calculations described in Section 4.2.1.

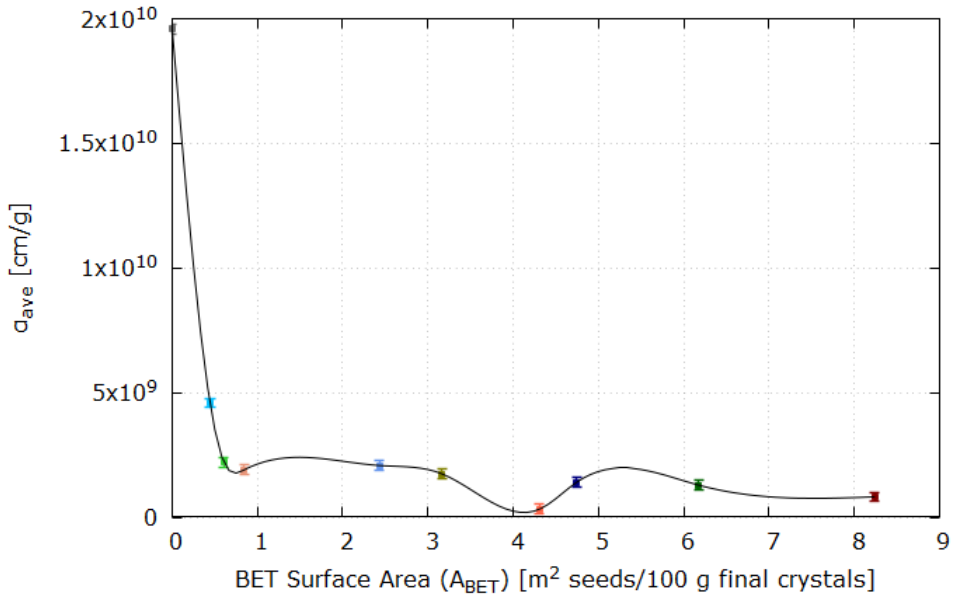


**Figure 4.26:** Average specific cake resistance, $\alpha_{ave}$, vs. total BET surface area per final crystal mass, $\mathrm{A_{BET}}$, for the three categories of seeding material. All values of $\alpha_{ave}$ are specified with the same colours as previously.

Unlike Figure 4.20, the unseeded experiment is included in Figure 4.26. The most significant change in filtration performance occurs before $\sim$1 $\mathrm{m^2}$/100 g, where average cake resistance is reduced by a factor of more than 10. The change after this point is less noticeable, with a minimum being indicated at $\sim$4 $\mathrm{m^2}$/100 g.

It is still a possibility that a lower value of $\alpha_{ave}$ would occur at an $A_{\mathrm{BET}}$ exceeding 8.2 $\mathrm{m^2}$/100 g. However, as extremely high total surface areas of seeds would yield high collision frequencies and consequently high secondary nucleation rates, average particle size would be expected to decrease; hence resulting in a high specific cake resistance. The interpolation curve would therefore presumably increase at some point if higher values of $A_{\mathrm{BET}}$ were tested.

Figure 4.26 mainly gives an indication that a minimum surface area of approximately 1 $m^2$/100 g is required to achieve an acceptable filtration performance. However, isolating surface area as a parameter of seeding excludes the fact that *surface characteristics* of the seeds also can have a certain impact. As seen in Section 4.1, smooth surfaces of dry-milled seeds differ a lot to the open-structured untreated seeds, which in turn causes differences in the visual outcome of the final crystals. The significance of other parameters than total surface area alone can therefore not be excluded when choosing a proper method of seeding.

## 4.6 Degree of supersaturation at seeding

*This section includes a presentation and discussion of SEM pictures, chord length measurements, concentration data and filtration tests related to degree of supersaturation at the point of seeding.*

A fixed seeding material was required in order to isolate $\omega$, fraction of HCl added initially, as a parameter. As *untreated* seeds are the most uniform particles with respect to size, Section 4.3.2 shows that this material makes it easier to distinguish growth on original seed particles from new-born crystals. Untreated seeds in slurry ($\phi = 1.7$ %, synthetic solution) was consequently chosen as the seeding material for all experiments described in this section. Extent of crystal growth has only been calculated for 100 % neutralization experiments.

### 4.6.1 Partial neutralization

No further increase of supersaturation after the initial portion of HCl, gives a better insight into crystallization mechanisms. Thus, experiments without addition of HCl after the initial portion have been performed. Supersaturation is hence reduced at a faster rate than for 100 % neutralization, but the system needs time for all supersaturation to be consumed by the seeds. Based on tests performed at Lindesnes, a concentration sufficiently close to the solubility of AA is reached at t = 3 h 30 min (Håland, 2017).

Figure 4.27 on the following page shows the characteristics of crystals withdrawn at 60 °C at t = 3 h 30 min as fraction of HCl added initially, $\omega$, is increased. Assuming $\omega = 27$ % corresponds to the *saturation point*, there should in theory be no nucleation or growth going on in the system when no further HCl is added. However, a small number of particles can be observed in between the original seeds in Figure 4.27 (a). This can be a result of two factors:

- The calculated saturation point deviates slightly from the real saturation point, implying that it really is a *supersaturation* point. In that case, small observed particles can be a result of a modest nucleation.
- Fragments of seed particles have been torn off under agitation. Considering agitation has been going on for 3 h 30 min, a certain degree of mechanical breakage is inevitable.

Whereas only a few small fragments could be observed in (a), nuclei formation is far more predominant in (b). Considering seeding now occurs at a theoretical supersaturation, thus *exceeding* the saturation point, this is a clear evidence of an initiated secondary nucleation. The smaller, plate-like crystals show a high degree of uniformity, with an estimated average diameter of ∼20 µm. Larger, more spherical crystals observed in (b) have an estimated average diameter of ∼130 µm, corresponding to an increase of ∼40 µm compared to the original seed particles. This observation is a clear indication of crystal growth.

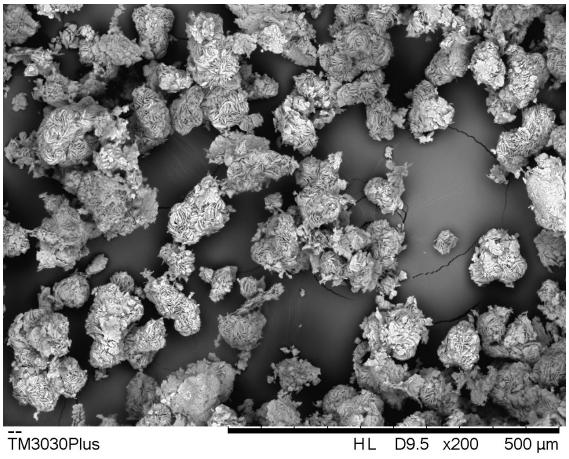


**(a)** $\omega = 27$ %

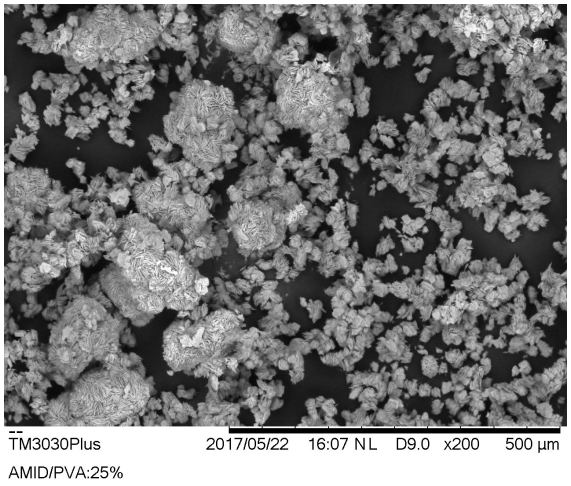


**(b)** $\omega = 40$ %

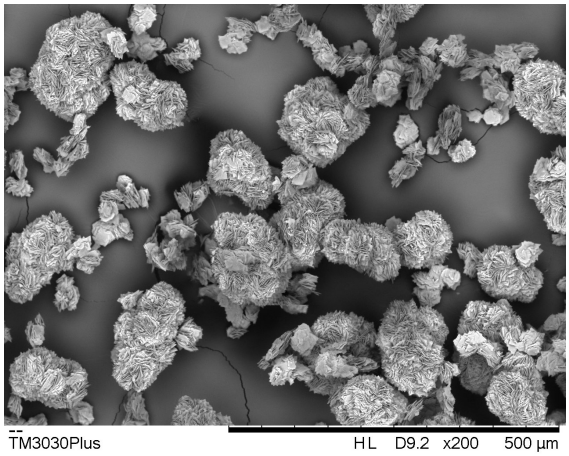


**(c)** $\omega = 53$ %

**Figure 4.27:** Crystals after partial neutralization at increasing fractions of HCl added initially, $\omega = \{27, 40, 53\}$ %: Experiment B1, B2 and B3 respectively. The total scale bar shows a realistic length of 500 µm.

Large, spherical crystals in (c) have approximately the same estimated diameter as in (b), possibly indicating that growth merely on original seed particles reaches a maximum before $\omega = 53$ %. However, plate-like crystals of ∼50 µm are by far the most predominant particles at this supersaturation. As they have the same characteristics as the smaller crystals of (b), but a twofold increase in diameter, it can be assumed that crystal growth has occurred on these particles.

Based on the fact that rate of secondary nucleation is proportional to growth rate, a presence of newly formed nuclei would be expected for $\omega = 53$ % as well. In spite of this, no presence of particles at ∼20 µm can be observed in (c). As SEM pictures do not represent 100 % of the generated crystals, a certain formation of nuclei at $\omega = 53$ % can still not be excluded.

A further distinction between mechanisms occurring throughout the experiments at varying $\omega$, can be obtained by analyzing chord lengths vs. time.

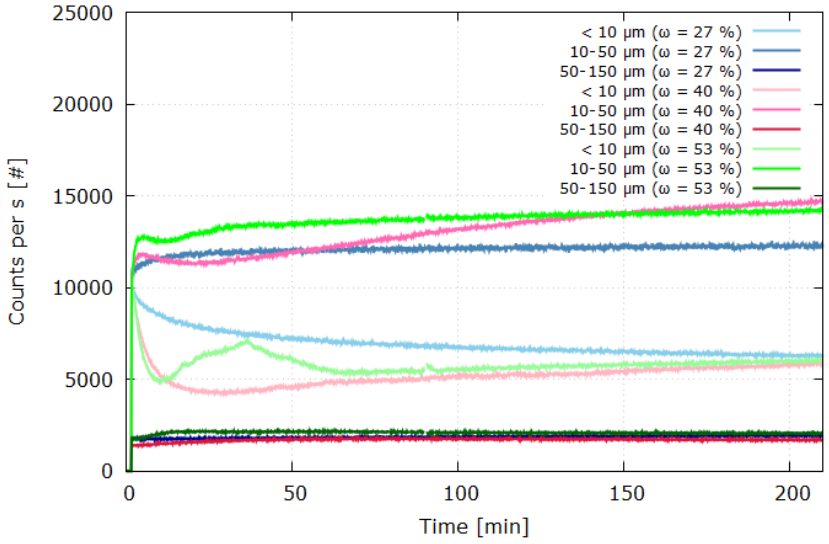


**Figure 4.28:** Chord length distribution separated into three intervals vs. time for $\omega = \{27, 40, 53\}$ %.

A significant difference at varying $\omega$ can be observed during *the first 10 minutes* after seeding, as shown in the following figure.

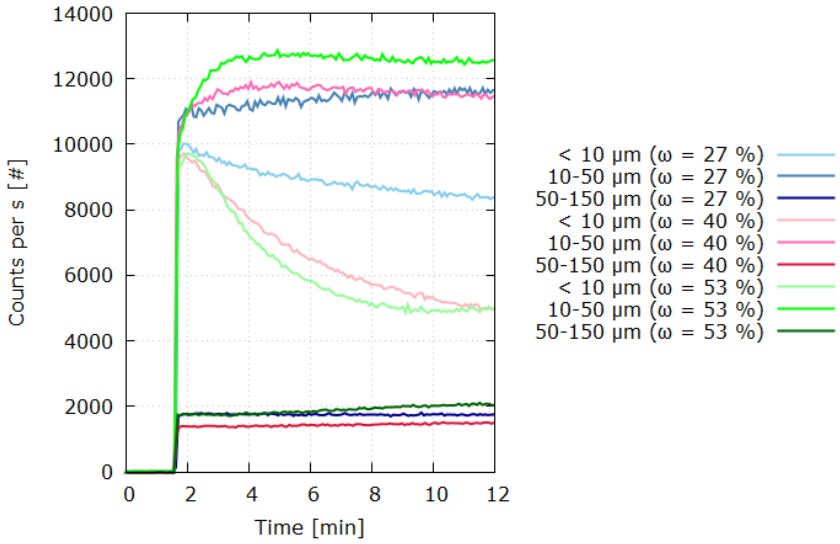


**Figure 4.29:** Chord length distribution separated into three intervals vs. time for $\omega = \{27, 40, 53\}$ %, limited to $\Delta t \approx 10$ min after seeding.

Figure 4.28 shows a significant increase over time in chord lengths of 10-50 µm at $\omega = 40$ %, possibly explaining a high rate of secondary nucleation as observed in the SEM pictures. Figure 4.29 shows that the number of fine particles (<10 µm) are reduced faster at increasing $\omega$. Chord lengths of 10-50 µm simultaneously *increase* at higher

values of $\omega$. This can imply a higher rate of secondary nucleation as $\omega$ is increased. Based on the SEM pictures, it could also imply a subsequent growth on the nuclei within the same chord length interval. In this case, the figure also indicates a higher growth rate as $\omega$ is increased.

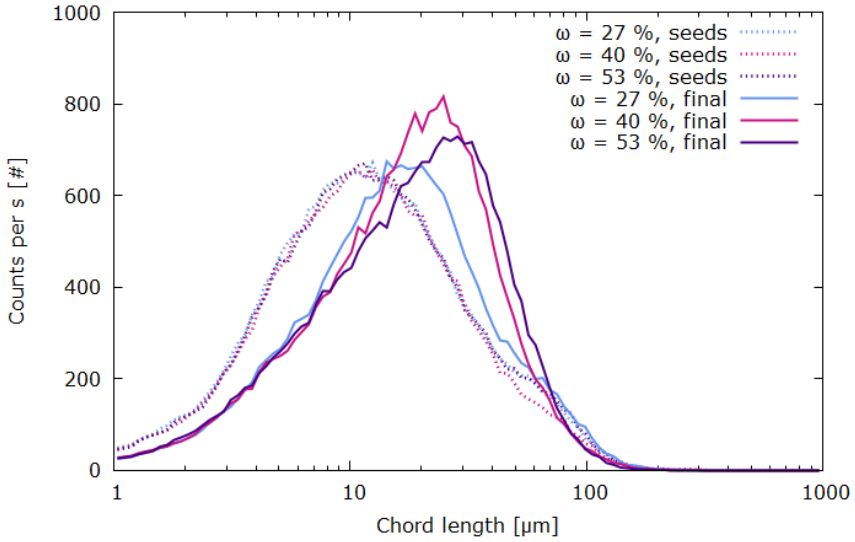


**Figure 4.30:** Total chord length distribution of solid AA for seeds (t = 1.5 min) and assumed solubility concentration (final, t = 3 h 30 min). Partial neutralization only; no HCl added after initial portion. Note that counts per s are total and not relative, because yield of total crystal mass differs as the degree of neutralization varies.

A further examination of changes occurring from seeds to final crystals, as presented in Figure 4.30, reveals a shift to the right for all chord length distributions for the final crystals. The peak of $\omega$ = 40 % is found within the interval of 15-25 µm, whereas the peak of $\omega$ = 53 % is found within 25-35 µm. This is an indication of the twofold increase that was observed in Figure 4.27 from $\omega$ = 40 % to 53 % for assumed nuclei.

### 4.6.2 100 % neutralization

The following figure shows the characteristics of final crystals after cooling to 22 °C as $\omega$ is increased for untreated seeds in slurry, $\phi = 1.7$ %, synthetic solution.

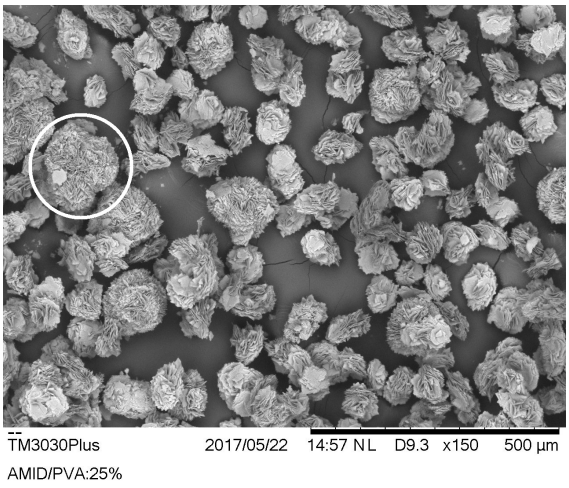


**(a)** $\omega = 27$ %

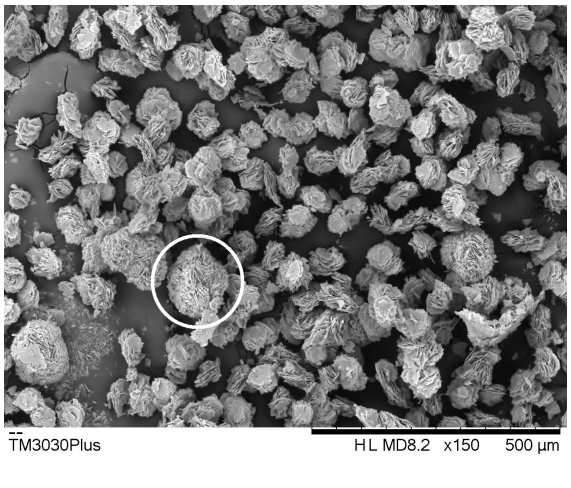


**(b)** $\omega = 40$ %

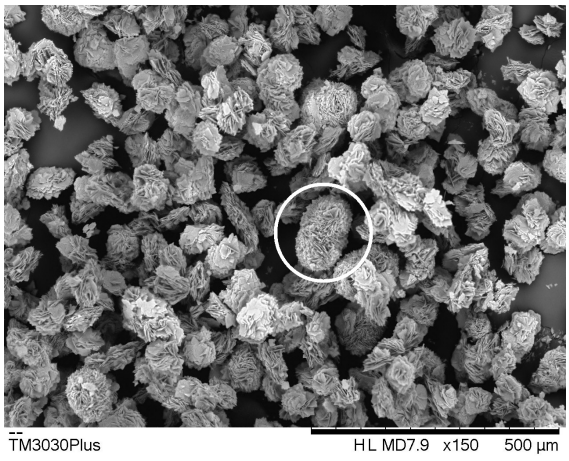


**(c)** $\omega = 53$ %

**Figure 4.31:** Final crystals at increasing fractions of HCl added initially, $\omega = \{27, 40, 53\}$ %: Experiment A19, A12 and A13 respectively. The total scale bar shows a realistic length of 500 µm.

Large, spherical crystals are marked by white circles in Figure 4.31. As they indicate growth on original seed particles, extent of crystal growth is calculated as presented in Table 4.12 based on the particle diameter estimation method. Only crystals larger than the seeds are included in the calculations.

**Table 4.12:** Estimated real final particle size, $D_{f,\,real}$, and extent of crystal growth, $\xi$, calculated at varying fractions of initially added HCl. Only crystals in Figure 4.31 larger than the untreated seed particles are included.

| $\omega$ [%] | $D_{f,\,real}$ | $\Delta D_{real}$ [µm] | $\Delta D_{max}$ [µm] | $\xi$ [%] |
|---|---|---|---|---|
| 27 | 125 ± 3 | 43 ± 5 | 237 ± 6 | 18 |
| 40 | 117 ± 3 | 35 ± 5 | 237 ± 6 | 15 |
| 53 | 121 ± 3 | 39 ± 5 | 237 ± 6 | 16 |

Table 4.12 reveals a low extent of growth for all $\omega$. Assuming the smaller crystals are results of nucleation, the following table lists average particle diameter of nuclei. This implies that only crystals without growth characteristics are included.

**Table 4.13:** Estimated average particle diameter of assumed nuclei, $D_{nuclei}$, corresponding to all particles in Figure 4.31 *smaller* than the seed particles.

| $\omega$ [%] | $D_{nuclei}$ [µm] |
|---|---|
| 27 | 72 ± 2 |
| 40 | 68 ± 3 |
| 53 | 72 ± 2 |

Despite a slightly higher extent of crystal growth at $\omega$ = 27 %, no clear differences can be observed neither in terms of $\xi$ nor $D_{nuclei}$. Differences at varying $\omega$ are small, as shown both by average sizes and standard errors. This observation is further confirmed by analyzing the chord length distributions of the seeds and final crystals. Figure 4.32 indicates formation of both smaller and larger chord lengths compared to the seeds, but no clear differences between the varying fractions of initially added HCl.

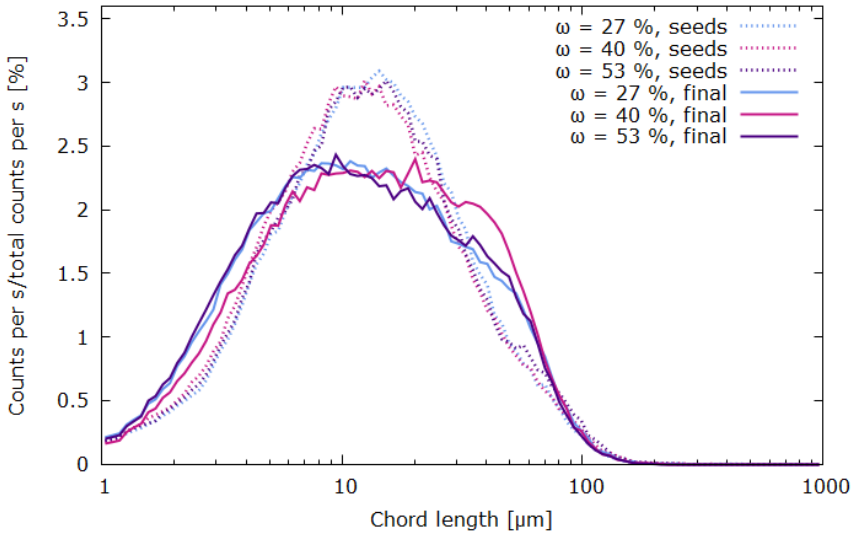


**Figure 4.32:** Relative chord length distribution of solid AA for seeds (t = 1.5 min) and final crystals (t = 2 h 40 min). Untreated seeds in slurry at increasing $\omega$.

Figure 4.33 provides a comparison of concentration profiles of AA at varying $\omega$. As remaining HCl is added at the same rate for all $\omega$, a total addition time of 42, 52 and 62 minutes has been achieved for $\omega$ = 27, 40 and 53 % respectively. The figure shows that $C_{AA}$ for $\omega$ = 53 % is significantly reduced instantaneously after seeding. For $\omega$ = 40 %, concentration reduces significantly at t ≈ 6 min, whereas $C_{AA}$ for $\omega$ = 27 % does not start to drop before halfway into the acid addition regime (at t ≈ 38 min).

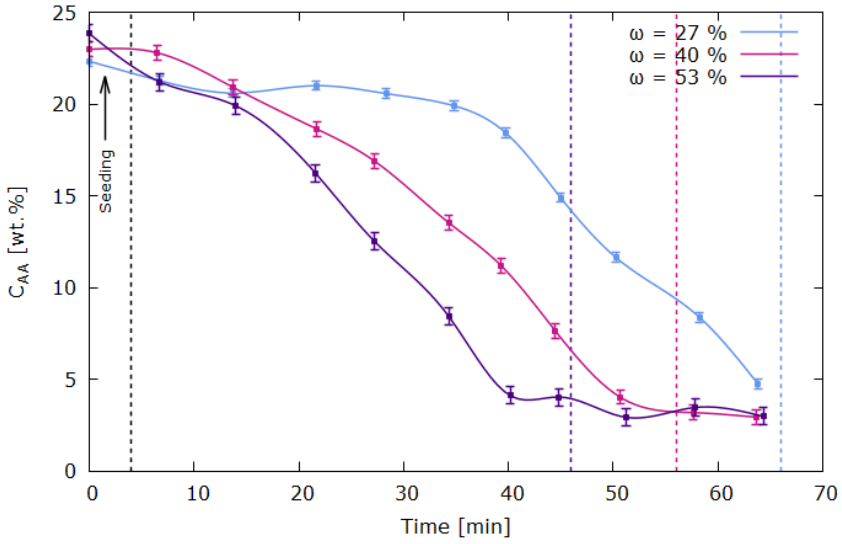


**Figure 4.33:** Concentration of AA in the liquid phase during the first 70 minutes at varying $\omega$, fraction of initially added HCl. Note that the time region of continuous acid addition is marked with vertical dotted lines. End of the region is marked with specified colours for each applied $\omega$.

**Table 4.14:** Estimated time periods from start of significant reduction of $C_{AA}$ until solubility concentration of AA is approximately reached.

| $\omega$ [%] | $\Delta t_{reduction}$ [min] |
|---|---|
| 27 | ∼28 |
| 40 | ∼45 |
| 53 | ∼40 |

Table 4.14 reveals a noticeably shorter reduction period for $\omega$ = 27 % than the other two. Based on this observation only, indications of a predominant (secondary) nucleation is strongest in the case of $\omega$ = 27 %.

### 4.6.3 Filterability

**Table 4.15:** Average specific cake resistance, $\alpha_{ave}$, for $\omega = 27$ %: average of A4 and A18-21, $\omega = 40$ %: A12 and $\omega = 53$ %: A13 in Table B.1.

| $\omega$ [%] | $\alpha_{ave}$ [cm/g] |
|---|---|
| 27 | $2.08 \cdot 10^9 \pm 0.19 \cdot 10^9$ |
| 40 | $1.56 \cdot 10^9 \pm 0.19 \cdot 10^9$ |
| 53 | $1.95 \cdot 10^9 \pm 0.19 \cdot 10^9$ |

Despite a slightly smaller estimated average particle size for $\omega = 40$ %, this is the initial fraction of HCl that yields the *lowest* $\alpha_{ave}$. For $\omega = 53$ %, the resulting $\alpha_{ave}$ is within the lower bound (1 standard error) of $\alpha_{ave}$ for $\omega = 27$ %.

It should be noted that the latter is calculated as an average of 5 parallels ($\overline{\alpha}_{ave}$), as described in Section 4.2.1. Parallel 3 (Experiment A19) yields an average specific cake resistance of $1.53 \cdot 10^9$ cm/g; slightly lower than for $\omega = 40$ %. Consequently, the same argumentation as in Section 4.4 follows. If multiple parallel tests had been performed for $\omega = 40$ % and 53 % as well, $\overline{\alpha}_{ave}$ for all three cases could have ended up within the same standard error.

Based on the SEM pictures given in Figure 4.31 solely, variations of $\alpha_{ave}$ at different $\omega$ are expected to be small.

## 4.7 Crystallization from a process solution

*This section includes a presentation and discussion of SEM pictures, chord length measurements, concentration data and filtration tests related to crystallization of AA from a process solution compared to crystallization from a synthetic solution.*

In order to look at differences between crystallization from a synthetic solution and a real process solution, two characteristic seeding materials were chosen. As they are the most reproducible seeding materials, experiments with untreated seeds (slurry) and dry-milled seeds (dry) were performed. A seeding ratio of $\phi = 1.7$ % was chosen for all experiments, and seeds were added at the saturation point, $\omega = 27$ %.

### 4.7.1 Untreated seeding

The following figure shows the characteristics of final crystals after cooling to 22 °C for crystallization from a process and a synthetic solution with *untreated* seeding.

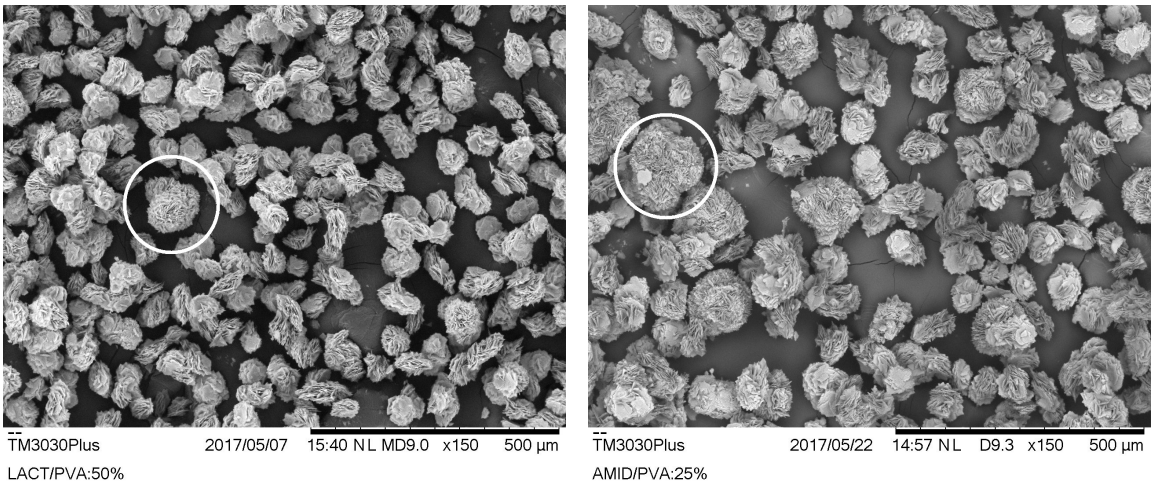


**(a)** Process solution **(b)** Synthetic solution

**Figure 4.34:** Final crystals after crystallization in a process vs. synthetic solution (untreated seeding, slurry, $\phi = 1.7$ %): Experiment A15 and A19 respectively. The total scale bar shows a realistic length of 500 µm.

**Table 4.16:** Estimated real final particle size, $D_{f,\,real}$, and extent of crystal growth, $\xi$, calculated for process vs. synthetic solution.

| **Solution** | $D_{f,\,real}$ | $\Delta D_{real}$ [µm] | $\Delta D_{max}$ [µm] | $\xi$ [%] |
|---|---|---|---|---|
| Process | 103 ± 2 | 21 ± 4 | 237 ± 6 | 9 |
| Synthetic | 125 ± 3 | 43 ± 5 | 237 ± 6 | 18 |

Calculations of $\xi$ in Table 4.16 are based on crystals larger in size than untreated seed particles, as indicated by the white circles in Figure 4.34.

Assuming the smaller crystals are all results of nucleation, the following table lists average particle diameter of nuclei. This implies that only crystals without growth characteristics are included (final crystals below seed particle size).

**Table 4.17:** Estimated average particle diameter of assumed nuclei, $D_{nuclei}$, corresponding to all particles in Figure 4.34 *smaller* than untreated seed particles.

| **Solution** | $D_{nuclei}$ [µm] |
|---|---|
| Process | 66 ± 2 |
| Synthetic | 72 ± 2 |

Although final crystals of a process vs. a synthetic solution have the same visual characteristics, Figure 4.34 and Table 4.16 reveal a smaller extent of growth for the process solution. The smaller category of final crystals is also estimated to be smaller in the case of a process solution, although the difference is less significant. Based on listed standard errors, uniformity is relatively similar for the two cases.

On the other hand, relative chord length distributions as given in Figure 4.35 do not indicate a more predominant growth in the case of a synthetic solution. Unlike the SEM pictures, a small shift is indicated to the *right* for the transition from a synthetic to a process solution, but the difference can be considered as insignificant.

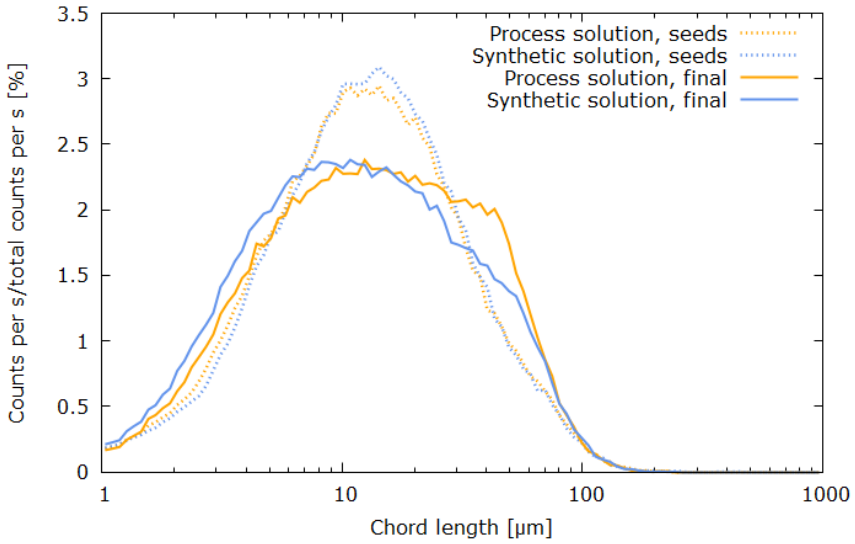


**Figure 4.35:** Relative chord length distribution of solid AA for seeds (t = 1.5 min) and final crystals (t = 2 h 40 min). Crystallization from process vs. synthetic solution by untreated seeding.

Figure 4.36 shows that concentration of aromatic amine in the process solution starts to drop already at t = 20 min, whereas a significant reduction of $C_{AA}$ in the synthetic solution starts around t = 38 min. This implies major nucleation starting at a *higher* supersaturation for a synthetic solution. According to theory, this should result in a higher dominance of small particles among the final crystals, which is a contradiction to the SEM pictures in Figure 4.34.

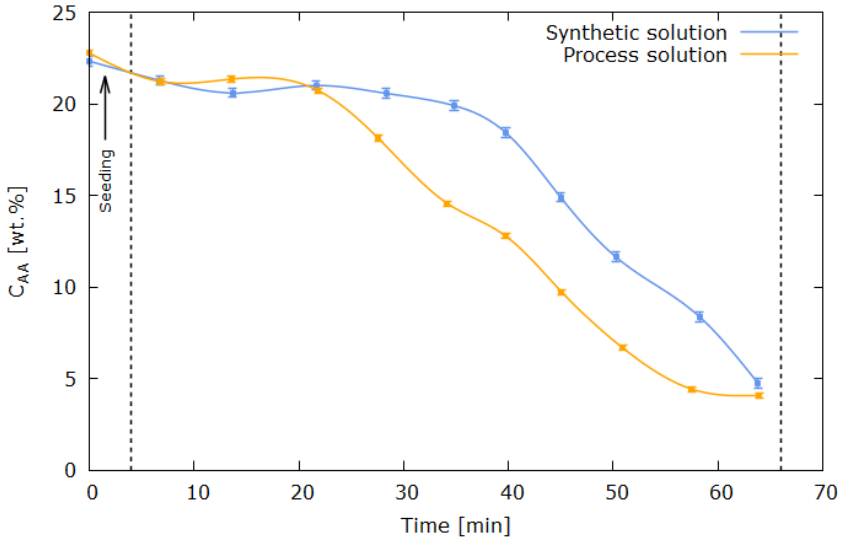


**Figure 4.36:** Concentration of AA in the liquid phase during the first 70 minutes. Untreated seeding in a process solution vs. synthetic solution. Note that the time region of continuous acid addition is marked with vertical dotted lines.

### 4.7.2 Dry-milled seeding

The following figure shows the characteristics of final crystals after cooling to 22 °C for crystallization from a process and a synthetic solution with *dry-milled* seeding.

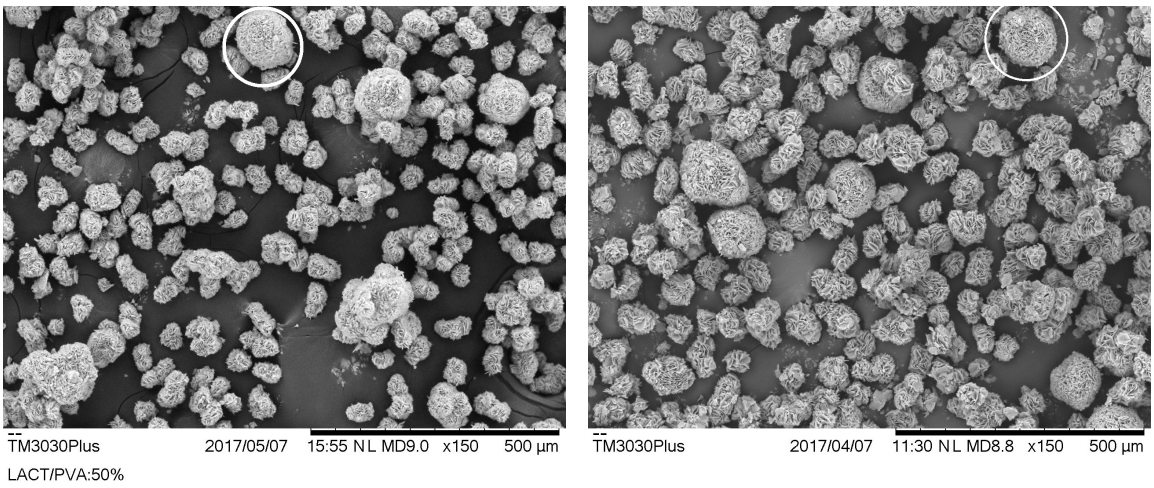


**(a)** Process solution **(b)** Synthetic solution

**Figure 4.37:** Final crystals after crystallization in a process vs. synthetic solution (dry-milled seeding, dry, $\phi = 1.7$ %): Experiment A15 and A18 respectively. The total scale bar shows a realistic length of 500 µm.

Calculations of $\xi$ are based on the assumption that growth occurs on large seed particles with a smooth surface only, thus neglecting fine seed particles. Only larger final crystals are included, as indicated by the white circles in Figure 4.37.

**Table 4.18:** Estimated real final particle size, $D_{f,\,real}$, and extent of crystal growth, $\xi$, calculated for process vs. synthetic solution. Only crystals in Figure 4.37 larger than the large dry-milled seed particles are included. Fine seed particles are neglected.

| **Solution** | $D_{f,\,real}$ | $\Delta D_{real}$ [µm] | $\Delta D_{max}$ [µm] | $\xi$ [%] |
|---|---|---|---|---|
| Process | 135 ± 4 | 78 ± 7 | 164 ± 6 | 48 |
| Synthetic | 122 ± 3 | 65 ± 5 | 164 ± 6 | 40 |

**Table 4.19:** Estimated average particle diameter of the smaller crystals, $D_{small}$, based on Figure 4.37.

| **Solution** | $D_{small}$ [µm] |
|---|---|
| Process | 66 ± 2 |
| Synthetic | 67 ± 2 |

Differences between crystallization from a process and a synthetic solution are less significant in the case of dry-milled seeding. Visual characteristics in Figure 4.37 (a) and (b) are more or less the same. However, Table 4.18 indicates a slightly more predominant growth for crystallization from a process solution. No real differences in terms of average particle diameter for the smaller crystals can be extracted from Table 4.19.

Relative chord length distributions of the final crystals, as shown in Figure 4.38, overlap to a large extent. Although crystals of the process solution show a slightly narrower distribution, the difference can be considered as negligible.

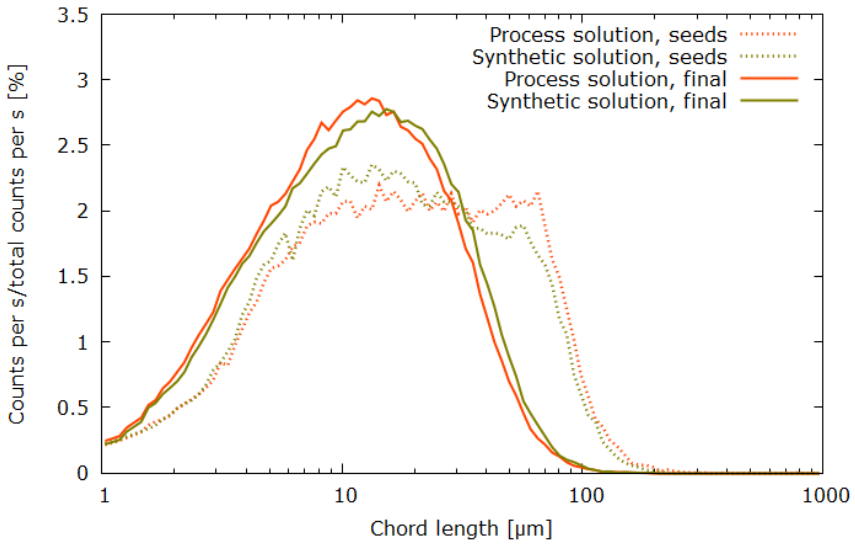


**Figure 4.38:** Relative chord length distribution of solid AA for seeds (t = 1.5 min) and final crystals at suspension withdrawal (t = 2 h 40 min). Crystallization from process vs. synthetic solution by dry-milled seeding.

Concentration of aromatic amine in the process solution generally seems to follow the same trend as for the synthetic solution. For the process solution, the significant reduction of $C_{AA}$ starts at $t \approx 25$ min, whereas $C_{AA}$ in the synthetic solution has experienced a reduction of $\sim$2 wt.% from the initial value at the same point. This could imply a more significant growth phase compared to the process solution in the same period, although this is not supported by the calculated $\xi$ in Table 4.18. After this point, however, $C_{AA}$ in the process solution drops less significantly in the very end of the acid addition interval, possibly indicating a lower rate of secondary nucleation from $t \approx 50$ min.

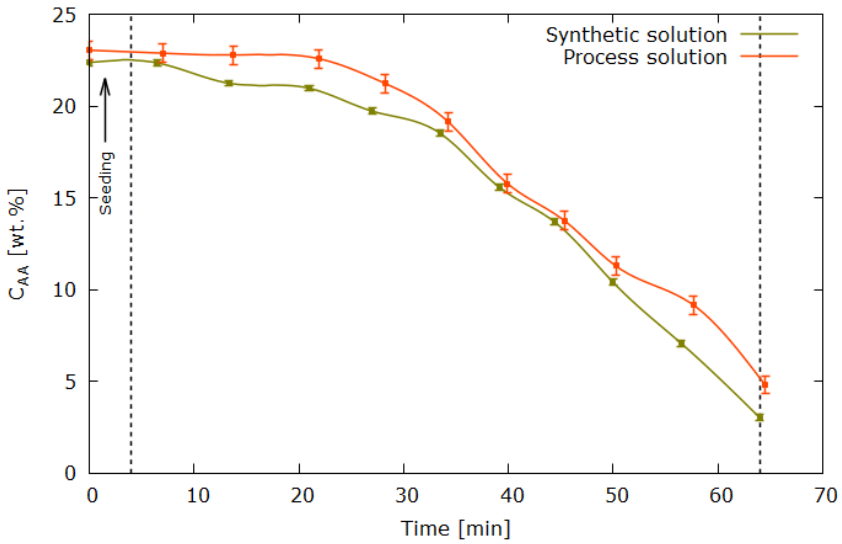


**Figure 4.39:** Concentration of AA in the liquid phase during the first 70 minutes. Dry-milled seeding in a process solution vs. synthetic solution. Note that the time region of continuous acid addition is marked with vertical dotted lines.

### 4.7.3 Filterability

Calculated average specific cake resistance, $\alpha_{ave}$, for crystallization in a process solution is presented in the following table. Ratio of $\alpha_{ave}$-values for process and synthetic solution is included.

**Table 4.20:** Average specific cake resistance for crystallization from a process solution, $\alpha_{ave,\,process}$, and a synthetic solution, $\alpha_{ave,\,synth}$. Untreated: A15, average of A4, A18-21 respectively, dry-milled: A16 and A9 respectively in Table B.1.

| **Seed characteristics** | $\alpha_{ave,\,process}$ **[cm/g]** | $\alpha_{ave,\,synth}$ **[cm/g]** | $\frac{\alpha_{ave,\,process}}{\alpha_{ave,\,synth}}$ [%] |
|---|---|---|---|
| Untreated | $1.26 \cdot 10^9 \pm 0.19 \cdot 10^9$ | $2.08 \cdot 10^9 \pm 0.19 \cdot 10^9$ | 61 |
| Dry-milled | $1.14 \cdot 10^9 \pm 0.19 \cdot 10^9$ | $1.74 \cdot 10^9 \pm 0.19 \cdot 10^9$ | 66 |

Despite strong similarities in visual characteristics and chord length distribution from a process and a synthetic solution, a general trend is that crystals from a process solution show better filtration abilities. Average specific cake resistance is reduced by 39 % and 34 % respectively in the transition from a synthetic to a process solution. This can be results of differences in extent of crystal growth and concentration profiles. It should be emphasized also here that this analysis is based on a fixed standard error for all experiments.

# 5 Summary and conclusions

Three different seed materials form the basis of this study; untreated seeds, wet-milled seeds and dry-milled seeds. Dry-milleds seeds were added dry, whereas untreated and wet-milled seeds were added in a slurry at standard conditions. Wet-milling of untreated seeds caused a lower estimated particle size and a lower mean chord length. At dispersed conditions, the broadest chord length distribution was found for dry-milled seeds. Because of large size variations, two categories of dry-milled seed particles were classified; *large* and *fine*.

Reproducibility of experiments was quantified in terms of filterability. Five experiments were performed at fixed seeding conditions followed by a filtration test, and standard error of the mean was calculated to $1.90 \cdot 10^8$ cm/g based on the five values of $\alpha_{ave}$ (average specific cake resistance). For simplicity, standard error was assumed to be the same for all unique experiments. Chord length measurements of four parallel experiments revealed a higher coefficient of variation within the chord length interval of <10 µm compared to 10-50 µm and 50-150 µm, possibly indicating larger variations in nucleation rate than growth rate from parallel to parallel.

Seeding by the three categories of material was performed at varying seeding ratios on a mass basis, $\phi = \{0.3, 1.7, 3.3\}$ %. The extent of growth did not change significantly at increasing $\phi$ for untreated seeding. At a low $\phi$, formation of fine particles and a broad chord length distribution indicated a certain *primary* nucleation, whereas the rate of *secondary* nucleation was assumed proportional to $\phi$. Whereas no evidence of crystal growth could be observed for wet-milled seeding, a predominant secondary nucleation was found at higher $\phi$.

Extent of crystal growth was higher in the case of dry-milled seeding, and based on SEM pictures extent of growth was assumed proportional to $\phi$. Because of large size variations in the seed particles, no ultimate distinction between secondary nucleation and growth was made in order to explain the formation of smaller, roughly spherical crystals. However, a reduction in average particle size for the latter indicated an increased rate of secondary nucleation at higher $\phi$. A *slurry* addition of dry-milled seeds yielded a slightly better filtration performance than a *dry* addition.

Average specific cake resistance was found to be profoundly higher in the case of an *unseeded* process, corresponding to the worst filtration performance of all tests. The lowest seeding ratio, $\phi = 0.3$ %, resulted in the lowest filterability for all seeding materials. Wet-milled seeding yielded a better filtration performance than untreated seeding at all tested values of $\phi$. In terms of total surface area of seeds, a critical point was indicated at $\sim$1 m$^2$/100 g final crystals, where $\alpha_{ave}$ is reduced significantly. The lowest average specific cake resistance was indicated at $\sim$4 m$^2$/100 g final crystals.

Untreated seeding at $\phi = 1.7$ % was performed at varying fractions of initially added HCl at seeding, $\omega = \{27, 40, 53\}$ %. Experiments without further addition of HCl indicated a high rate of secondary nucleation at $\omega = 40$ %, whereas only a twofold increase in size of the newly formed crystals could be observed at $\omega = 50$ %. Ex-

periments involving 100 % neutralization of anionic AA did not yield significant differences at varying $\omega$, although a slightly lower average specific cake resistance was achieved for $\omega = 40$ %.

A comparison of crystallization from a real process solution vs. a synthetic solution was performed with untreated and dry-milled seeding at $\phi = 1.7$ % and $\omega = 27$ %. Untreated seeding of a process solution yielded a slightly lower extent of crystal growth and a smaller average particle size of generated nuclei. No major differences from a synthetic solution could be observed in the case of dry-milled seeding. A transition from a synthetic to a process solution caused slightly improved filtration performances.

# 6 Recommendations for further work

This study comprises a thorough examination of seeding parameters with respect to seeding material and seeding ratios. By testing untreated, wet-milled and dry-milled seeds, it has been demonstrated how particle size and particle size distribution of seeds affect crystallization mechanisms of the aromatic amine. It has also been demonstrated how seeding with too *low* ratio leads to a higher risk of primary nucleation, whereas an excessively *high* ratio induces a high rate of secondary nucleation. This, in turn, has been shown to have a significant impact on filterability of the crystals.

However, a more comprehensive study of seeding in terms of *total surface area* of seeds is of high interest. Controlled milling of a fixed seeding material based on a desired total surface area, would lead to an even better understanding of crystallization mechanisms. As suggested in Section 4.5, the significance of other parameters such as *surface characteristics* can not be excluded. As an example, the smooth surface of dry-milled seeds yields a higher extent of growth than the rough surfaces of the untreated seeds. In this context, an elimination of the fine dry-milled seed particles by sieving would demonstrate the effect of surface characteristics even better.

Equation 2.7, describing rate of secondary nucleation, also includes variables such as agitator speed, $\epsilon$, and collision energy, $k$. This implies that also the *mixing regime* of a seeded crystallization process is of high importance. The current crystallization process at Lindesnes is based on a batch operation. In case of a transition to a flow-reactor based crystallization process in the future, finding an optimal mixing is expected to be crucial for seeding to work properly.

All experiments in this study were carried out at a fixed temperature of 60 °C during the acid addition regime. As described in Section 2.3, supersaturation is a temperature dependent quantity. As crystallization potentially can proceed faster at higher temperatures, it is also of high interest to study how increasing *temperature* affects seeding parameters.

# References


Andreassen, J.-P. (2015). Short course in crystallization and precipitation from solution.

Aylward, G. H. and Findlay, T. J. V. (2008). *SI chemical data*. New York, Wiley.

Bakke, B. (2016). Crystallization behavior of an x-ray contrast agent intermediate at high supersaturations and temperatures. Master's thesis, Trondheim.

Beck, R. (2009). *Crystal Growth Phenomena and Filtration: Morphology and Size Effects for Selected Industrial Compounds*. PhD thesis, NTNU.

Garside, J. (1982). Nucleation. In *Biological mineralization and demineralization*, pages 23–35. Springer.

Heskestad, R. (2008). Prosjektoppgave. Krystallisasjon og faststoffseparasjon. Betydningen av krystallisasjonsparametre på krystallstørrelsesfordeling, morfologi og filtreringsegenskaper.

Hilfiker, R. (2006). *Polymorphism: in the pharmaceutical industry*. John Wiley & Sons.

Håland, T. (2017). Personal communication.

Kashchiev, D. and van Rosmalen, G. M. (2003). Review: Nucleation in solutions revisited. *Crystal Research and Technology*, 38(7-8):555–574.

Keith, H. and Padden Jr, F. (1963). A phenomenological theory of spherulitic crystallization. *Journal of Applied Physics*, 34(8):2409–2421.

Linga, (2016). Project thesis. Crystallization behaviour of an aromatic amine under varying hydrochloric acid addition conditions.

Mayo, J. (2017). Understanding the nutsche filtration and drying process.

Mullin, J. W. (2001). *Crystallization*. Butterworth-Heinemann.

Myerson, A. (2002). *Handbook of industrial crystallization*. Butterworth-Heinemann.

Rousseau, E. R. W. (2009). *Handbook of separation process technology*. John Wiley & Sons.

Schwartz, A. and Myerson, A. (2002). Solutions and solution properties. *Handbook of Industrial Crystallization*, 2.

Smith, M. B. (2006). Prosjektoppgave. Kjernedannelse og krystallvekst av et aromatisk amin ved reaksjonskrystallisasjon.

Söhnel, O. and Garside, J. (1992). Precipitation: Basic principles and industrial applications.

Togkalidou, T., Braatz, R. D., Johnson, B. K., Davidson, O., and Andrews, A. (2001). Experimental design and inferential modeling in pharmaceutical crystallization. *AIChE Journal*, 47(1):160–168.

Wakeman, R. J. and Tarleton, E. S. (1999). *Filtration: equipment selection, modelling and process simulation*.

Wojciech, B., J. W. (2014). The metastable zone of aqueous solutions.

# A Experiment data

All performed crystallization experiments can be classified into two categories:

**A**: 100 % neutralization. All remaining HCl after the initial portion is added at a constant rate of approximately 0.64 g/min.

**B**: Partial neutralization only. No HCl added after the initial portion.

**Table A.1:** List of all performed experiments and essential data.

| **Exp.** [#] | **Seeding ratio ($\phi$)** [%] | **Seed characteristics** | **Dry/ slurry** | **Initially added HCl ($\omega$)** [%] | **Solution** |
|---|---|---|---|---|---|
| A1[a,c] | 0.32 | Untreated | Slurry | 27 | Synthetic |
| A2[a,c] | 3.38 | Untreated | Slurry | 27 | Synthetic |
| A3 | - | No seeding | - | 27 | Synthetic |
| A4[b] | 1.72 | Untreated | Slurry | 27 | Synthetic |
| A5 | 0.34 | Wet-milled | Slurry | 27 | Synthetic |
| A6 | 1.75 | Wet-milled | Slurry | 27 | Synthetic |
| A7 | 3.34 | Wet-milled | Slurry | 27 | Synthetic |
| A8 | 0.33 | Dry-milled | Dry | 27 | Synthetic |
| A9 | 1.71 | Dry-milled | Dry | 27 | Synthetic |
| A10 | 3.33 | Dry-milled | Dry | 27 | Synthetic |
| A11 | 1.71 | Dry-milled | Slurry | 27 | Synthetic |
| A12 | 1.75 | Untreated | Slurry | 40 | Synthetic |
| A13 | 1.69 | Untreated | Slurry | 53 | Synthetic |
| A14 | 3.33 | Untreated | Slurry | 27 | Synthetic |
| A15 | 1.74 | Untreated | Slurry | 27 | Process |
| A16 | 1.73 | Dry-milled | Dry | 27 | Process |
| A17 | 0.31 | Untreated | Slurry | 27 | Synthetic |
| A18 | 1.69 | Untreated | Slurry | 27 | Synthetic |
| A19[c] | 1.69 | Untreated | Slurry | 27 | Synthetic |
| A20[c] | 1.71 | Untreated | Slurry | 27 | Synthetic |
| A21[c] | 1.70 | Untreated | Slurry | 27 | Synthetic |
| B1[a,c] | 1.72 | Untreated | Slurry | 27 | Synthetic |
| B2[a,c] | 1.70 | Untreated | Slurry | 40 | Synthetic |
| B3[a,c] | 1.73 | Untreated | Slurry | 53 | Synthetic |

[a]No valid filtration data.
[b]No valid FBRM data.
[c]No valid concentration data.

# B Filtration data

**Table B.1:** Essential filtration data for calculations of specific cake resistance ($\alpha_{ave}$) in experiment A3-21.

| **Exp.** [#] | **$\Delta$t** [s] | **k** [s/cm$^6$] | **m$_{susp}$** [g] | **m$_{sol}$** [g] | **h** [cm] | $\varepsilon$ [-] | **c$_s$** [g/cm$^3$] | $\alpha_{ave}$ [cm/g] |
|---|---|---|---|---|---|---|---|---|
| A3 | 1441 | 0.0810 | 230.81 | 46.70 | 1.9 | 0.46 | 0.305 | $1.96 \cdot 10^{10}$ |
| A4 | 270 | 0.0134 | 235.49 | 51.55 | 2.8 | 0.59 | 0.375 | $2.71 \cdot 10^{9}$ |
| A5 | 187 | 0.0094 | 239.43 | 50.59 | 2.9 | 0.61 | 0.364 | $1.91 \cdot 10^{9}$ |
| A6 | 68 | 0.0017 | 241.58 | 50.16 | 3.3 | 0.66 | 0.383 | $3.28 \cdot 10^{8}$ |
| A7 | 78 | 0.0042 | 238.49 | 49.79 | 3.2 | 0.65 | 0.378 | $8.19 \cdot 10^{8}$ |
| A8 | 213 | 0.0116 | 241.91 | 53.76 | 2.9 | 0.59 | 0.389 | $2.20 \cdot 10^{9}$ |
| A9 | 159 | 0.0111 | 240.90 | 56.53 | 3.6 | 0.65 | 0.470 | $1.74 \cdot 10^{9}$ |
| A10 | 147 | 0.0097 | 240.37 | 63.57 | 3.8 | 0.62 | 0.476 | $1.29 \cdot 10^{9}$ |
| A11 | 110 | 0.0072 | 231.92 | 56.00 | 3.6 | 0.65 | 0.480 | $1.11 \cdot 10^{9}$ |
| A12 | 149 | 0.0088 | 234.48 | 52.61 | 3.3 | 0.65 | 0.417 | $1.56 \cdot 10^{9}$ |
| A13 | 170 | 0.0120 | 226.60 | 52.57 | 3.5 | 0.66 | 0.454 | $1.95 \cdot 10^{9}$ |
| A14 | 132 | 0.0087 | 231.66 | 54.51 | 3.5 | 0.65 | 0.456 | $1.41 \cdot 10^{9}$ |
| A15 | 126 | 0.0062 | 235.17 | 48.19 | 3.2 | 0.66 | 0.363 | $1.26 \cdot 10^{9}$ |
| A16 | 110 | 0.0062 | 239.65 | 52.17 | 3.3 | 0.65 | 0.401 | $1.14 \cdot 10^{9}$ |
| A17 | 405 | 0.0279 | 230.30 | 58.78 | 2.6 | 0.48 | 0.449 | $4.58 \cdot 10^{9}$ |
| A18 | 199 | 0.0114 | 238.32 | 55.91 | 3.2 | 0.60 | 0.419 | $2.01 \cdot 10^{9}$ |
| A19 | 160 | 0.0100 | 239.90 | 58.95 | 3.6 | 0.63 | 0.482 | $1.53 \cdot 10^{9}$ |
| A20 | 182 | 0.0112 | 242.72 | 55.59 | 3.7 | 0.66 | 0.442 | $1.99 \cdot 10^{9}$ |
| A21 | 241 | 0.0148 | 241.67 | 62.23 | 3.7 | 0.62 | 0.507 | $2.15 \cdot 10^{9}$ |

For supplementary filtration data held *constant* for all tests, see Table H.2.

# C Maximum increase of particle diameter

Assuming all neutralization of solute aromatic amine resulted in crystal growth on seed particles only, there would be no increase in total number of particles in the crystallizing system. In the hypothetical case that no nucleation occurs in the system, crystal growth only, a theoretical maximum increase in particle diameter of the seeds can be calculated.

Total number of seed particles added initially, $N_s$, can be calculated by the following equation:

$$N_s = \frac{m_s}{\rho_s V_s} \tag{C.1}$$

where $m_s$ is the total mass of seed particles added, $\rho_s$ is the density and $V_s$ is the volume of a seed particle. Assuming that a seed particle is a perfect sphere with a diameter $D_s$, seed particle volume can be calculated by:

$$V_s = \frac{\pi}{6} D_s^3 \tag{C.2}$$

Total mass of final particles at 100 % neutralization of anionic AA, $m_{f,\,tot}$, can be expressed as following:

$$m_{f,\,tot} = m_s + m_{tot} \tag{C.3}$$

where $m_{tot}$ is the total mass of initially dissolved solid crystals. Total volume of final particles can be calculated by the following equation:

$$V_{f,\,tot} = N_f V_f \tag{C.4}$$

where $N_f$ is the total number of final particles and $V_f$ is the volume of a single final particle. A requirement of crystal growth only is no increase in total number of particles:

$$N_f = N_s \tag{C.5}$$

Volume of a single final particle can thus be expressed as:

$$V_f = \frac{m_{f,\,tot}}{\rho_s N_s} \tag{C.6}$$

assuming density of final particles, $\rho_f$, equals $\rho_s$. Maximum change in diameter from seed particle to final particle can be written as:

$$\Delta D_{max} = D_f - D_s \tag{C.7}$$

where $D_f$ is defined as theoretical diameter of a single final particle if crystal growth was the only present mechanism. Assuming a perfect sphere for both, (C.7) can be expressed as following:

$$\begin{aligned} \Delta D_{max} &= \left(\frac{6}{\pi} V_f\right)^{\frac{1}{3}} - \left(\frac{6}{\pi} V_s\right)^{\frac{1}{3}} \\ &= \left(\frac{6}{\pi}\right)^{\frac{1}{3}} \left(V_f^{\frac{1}{3}} - V_s^{\frac{1}{3}}\right) \end{aligned} \tag{C.8}$$

Combined with (C.1), (C.2), (C.3) and (C.6), the final expression for maximum change in particle diameter is written as:

$$\begin{aligned} \Delta D_{max} &= D_s \left[ \left( \frac{m_s + m_{tot}}{m_s} \right)^{\frac{1}{3}} - 1 \right] \\ &= D_s \left[ \left( \frac{1}{\phi} \right)^{\frac{1}{3}} - 1 \right] \end{aligned} \tag{C.9}$$

where $\phi$ is defined as seeding ratio on mass basis. As $D_s$ is based on the particle diameter estimation method, it equals $D_{s,\,real}$ in all calculations.

# D Calculation of composition

A basis solution, $m_{tot}^{(1)}$, is initially set, consisting of the following components:

$$m_{tot}^{(1)} = m_{\mathrm{AA}} + m_{\mathrm{NaAc}} + m_{\mathrm{MeOH}} + m_{\mathrm{H_2O}} \tag{D.1}$$

$m_i$ for $i = \{\mathrm{AA}, \mathrm{MeOH}, \mathrm{NaAc}, \mathrm{H_2O}\}$ is calculated by setting a desired concentration $C_i^{(1)}$ ([wt.%]) for each component $i$. $m_i$ is then calculated as following:

$$m_i = \left(\frac{C_i^{(1)}}{100}\right) m_{tot}^{(1)} \tag{D.2}$$

The synthetic solution, here denoted by $m_{tot}^{(2)}$, is defined as the basis $m_{tot}^{(1)}$ plus required total mass of diluted NaOH, $m_{NaOH,\,dil}^{tot}$; before any HCl is added.

$$m_{tot}^{(2)} = m_{tot}^{(1)} + m_{NaOH,\,dil}^{tot} \tag{D.3}$$

As an excess of NaOH is required in order to dissolve solid AA, an excess ratio $R$ is defined as:

$$R = \frac{n_{\mathrm{NaOH}}}{n_{\mathrm{AA}}} \tag{D.4}$$

Amount of required NaOH, $n_{NaOH}$, is calculated according to Equation D.4 for the given $R$. Total mass of diluted NaOH, $m_{NaOH,\,dil}^{tot}$, is consequently calculated as:

$$m_{NaOH,\,dil}^{tot} = R\,\frac{M_{w,\,NaOH}}{M_{w,\,AA}}\,\frac{m_{AA,\,tot}}{\chi_{NaOH}} \tag{D.5}$$

where $\chi_{\mathrm{NaOH}}$ is the weight fraction of pure NaOH in the diluted NaOH-solution. All concentrations change from $m_{tot}^{(1)}$ as NaOH is included in the synthetic solution, $m_{tot}^{(2)}$. Resulting concentrations of $m_{tot}^{(2)}$, $C_j^{(2)}$, can be calculated by:

$$C_j^{(2)} = \frac{m_j}{m_{tot}^{(2)}} \cdot 100 \tag{D.6}$$

for $j = \{\mathrm{AA}, \mathrm{MeOH}, \mathrm{NaAc}, \mathrm{H_2O}, \mathrm{NaOH}\}$. Note that the composition of the synthetic solution will change slightly as HCl is added. All calculated masses and concentrations are listed in Appendix G. For physical data, see Appendix H.

# E Calculation of required mass of HCl

The exact neutralization of anionic AA required to reach the saturation point (also known as the solubility concentration) of aromatic amine, translates to a certain *mass* of diluted HCl that needs to be added.

Concentration of aromatic amine at the saturation point is the point where concentration equals solubility concentration:

$$C_{AA} = C^*_{AA} \tag{E.1}$$

Concentration of AA is at zero when excess NaOH is neutralized. Mass of diluted HCl added in order to reach the saturation point, $m^{sat}_{HCl,\,dil}$, can further be separated into two quantities:

$$m^{sat}_{HCl,\,dil} = m^{exc}_{HCl,\,dil} + m^*_{HCl,\,dil} \tag{E.2}$$

where $m^{exc}_{HCl,\,dil}$ is defined as mass of diluted HCl required to neutralize excess NaOH only, and $m^*_{HCl,\,dil}$ is the additional mass of diluted HCl needed to reach the solubility concentration of AA. The following sections show how the separate quantities are calculated.

## E.1 Neutralization of excess NaOH

Mass of diluted HCl required to neutralize excess NaOH can be calculated as following:

$$\begin{aligned} m^{exc}_{HCl,\,dil} &= \frac{m^{exc}_{HCl}}{\chi_{HCl}} \\ &= \frac{M_{w,\,HCl} n^{exc}_{HCl}}{\chi_{HCl}} \end{aligned} \tag{E.3}$$

where $M_{w,\,HCl}$ is the molar weight of HCl, $n^{exc}_{HCl}$ is the amount of HCl required to neutralize excess NaOH and $\chi_{HCl}$ is the weight fraction of pure HCl in the diluted HCl-solution. The following equation must be satisfied in order to neutralize excess NaOH:

$$\begin{aligned} n^{exc}_{HCl} &= n^{exc}_{NaOH} \\ &= \big(R-1\big) n_{AA,\,tot} \\ &= \big(R-1\big) \frac{m_{AA\,tot}}{M_{w,\,AA}} \end{aligned} \tag{E.4}$$

where $R$ is the excess ratio of NaOH to AA on a molar basis, $m_{AA,\,tot}$ is the total mass of initially dissolved AA and $M_{w,\,AA}$ is the molar weight of AA. Substituting (E.4) into (E.3) yields the final expression for $m^{exc}_{HCl,\,dil}$:

$$m^{exc}_{HCl,\,dil} = \big(R-1\big)\frac{M_{w,\,HCl}}{M_{w,\,AA}}\frac{m_{AA,\,tot}}{\chi_{HCl}} \tag{E.5}$$

## E.2 Reaching the saturation point

The additional mass of diluted HCl required to reach the saturation point, can be calculated as following:

$$\begin{aligned} m^{*}_{HCl,\,dil} &= \frac{m^{*}_{HCl}}{\chi_{HCl}} \\ &= \frac{M_{w,\,HCl}n^{*}_{HCl}}{\chi_{HCl}} \end{aligned} \tag{E.6}$$

where $M_{w,\,HCl}$ is the molar weight of HCl, $n^{*}_{HCl}$ is the amount of HCl required at the saturation point and $\chi_{HCl}$ is the weight fraction of pure HCl in the diluted HCl-solution. The following equation must be satisfied in order to reach the saturation point:

$$n^{*}_{HCl} = n^{*}_{AA} \tag{E.7}$$

where $n^{*}_{AA}$ is the amount of AA at saturation. Substituting into (E.6) gives the following:

$$\begin{aligned} m^{*}_{HCl,\,dil} &= \frac{M_{w,\,HCl}n^{*}_{AA}}{\chi_{HCl}} \\ &= \frac{M_{w,\,HCl}}{\chi_{HCl}}\frac{m^{*}_{AA}}{M_{w,\,AA}} \end{aligned} \tag{E.8}$$

The following equation shows how mass of AA at saturation can be calculated from concentration at saturation, $C^{*}_{AA}$:

$$m^{*}_{AA} = \left(\frac{C^{*}_{AA}}{100}\right)\big(m^{(2)}_{tot} + m^{exc}_{HCl,\,dil} + m^{*}_{HCl,\,dil}\big) \tag{E.9}$$

where $m^{(2)}_{tot}$ is the total mass of synthetic solution. $C^{*}_{AA}$ is defined in units of wt.%, and is therefore divided by 100. Substituting (E.9) into (E.8) results in the following equation:

$$m^*_{HCl,\,dil} = \frac{M_{w,\,HCl}}{\chi_{HCl}} \frac{\left(\frac{C^*_{AA}}{100}\right)\left(m^{(2)}_{tot} + m^{exc}_{HCl,\,dil} + m^*_{HCl,\,dil}\right)}{M_{w,\,AA}} \tag{E.10}$$

Rearranging the terms in (E.10) yields the final expression for $m^*_{HCl,\,dil}$:

$$m^*_{HCl,\,dil} = \frac{M_{w,\,HCl}\left(\frac{C^*_{AA}}{100}\right)\left(m^{(2)}_{tot} + m^{exc}_{HCl,\,dil}\right)}{M_{w,\,AA}\chi_{HCl} - M_{w,\,HCl}\left(\frac{C^*_{AA}}{100}\right)} \tag{E.11}$$

## E.3 100 % neutralization

Total mass of diluted HCl required to neutralize 100 % NaOH, $m^{tot}_{HCl,\,dil}$, can be calculated the same way as given in (E.5), with the exception that $(R-1)$ is substituted with $R$:

$$m^{tot}_{HCl,\,dil} = R\frac{M_{w,\,HCl}}{M_{w,\,AA}} \frac{m_{AA,\,tot}}{\chi_{HCl}} \tag{E.12}$$

# F Linearity factor for calculation of concentration

Six different standard samples of known concentration of the aromatic amine were prepared. The absorbance of each sample was measured through UV spectrophotometry (See 3.2). A model fit, using linear regression, was plotted together with measured data points as shown in the following figure and equation.

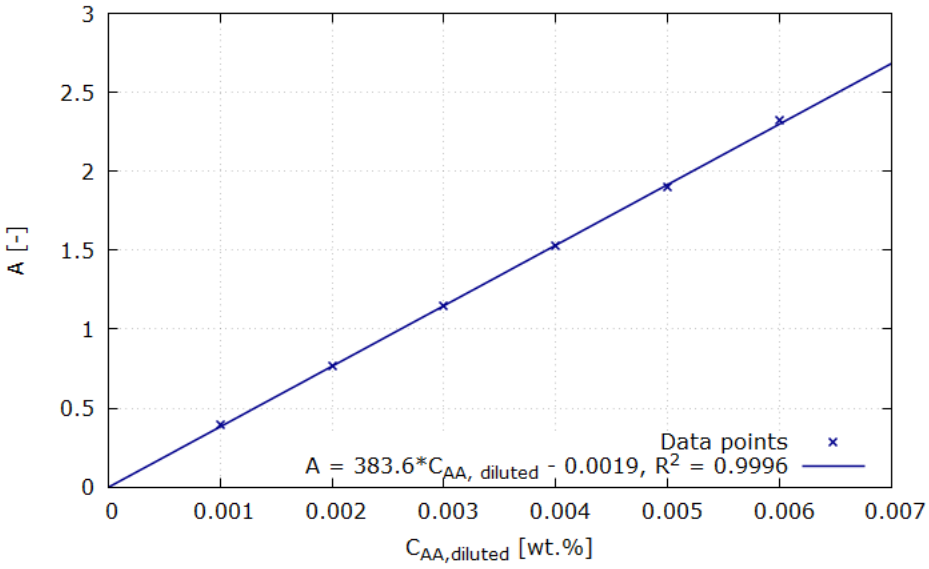


**Figure F.1:** Data points of known concentrations of aromatic amine together with an equation for the linear regression.

Since absorbance $A$ is measured in order to determine unknown concentrations, the expression for the linear regression has to be solved explicitly in terms of $C_{AA,\,\text{diluted}}$:

$$C_{AA,\,\text{diluted}} = 0.00261A \tag{F.1}$$

Defining the slope of the linear function F.1 as the *linearity factor*, it is hence calculated to 0.00261 with three significant figures. $C_{AA}$ is calculated from $C_{AA,\,\text{diluted}}$ by Equation 3.5.

# G Tables of composition and distribution

## G.1 Composition of basis solution

**Table G.1:** Composition of basis solution ($m_{tot}^{(1)}$); before addition of NaOH and HCl solution.

| $m_i$ | [g] | $C_i^{(1)}$ [wt.%] |
|---|---|---|
| $m_{\mathrm{AA}}$ | 152.78 | 23.5 |
| $m_{\mathrm{NaAc}}$ | 115.72 | 17.8 |
| $m_{\mathrm{H_2O}}$ | 269.80 | 41.5 |
| $m_{\mathrm{MeOH}}$ | 112.47 | 17.3 |
| $m_{\mathrm{tot}}^{(1)}$ | 650.76 | 100.1 |

## G.2 Composition of synthetic solution

**Table G.2:** Composition of synthetic solution ($m_{tot}^{(2)}$); including NaOH solution, before addition of HCl solution. The same composition is used for all synthetic solution experiments.

| $m_j$ | [g] | $C_j^{(2)}$ [wt.%] |
|---|---|---|
| $m_{\mathrm{AA}}$ | 152.78 | 21.8 |
| $m_{\mathrm{NaAc}}$ | 115.72 | 16.5 |
| $m_{\mathrm{H_2O}}$ | 269.80 | 38.5 |
| $m_{\mathrm{MeOH}}$ | 112.47 | 16.1 |
| $m_{\mathrm{NaOH,\,dil}}$ | 49.90 | 7.1 |
| $m_{\mathrm{tot}}^{(2)}$ | 700.01 | 100.0 |

### Distribution of HCl solution

**Table G.3:** Total masses of HCl solution at each specific fraction of initially added HCl, $\omega$. Note that $m_{\mathrm{HCl,\,dil}}^{(0)}$ is added in one instantaneous portion, whereas $m_{\mathrm{HCl,\,dil}}^{\mathrm{rest}}$ is added continuously at 100 % neutralization. In partial neutralization experiments, only $m_{\mathrm{HCl,\,dil}}^{(0)}$ is added.

| $m_{\mathrm{HCl,\,dil}}$ | $\omega = 27$ % [g] | $\omega = 40$ % [g] | $\omega = 53$ % [g] |
|---|---|---|---|
| $m_{\mathrm{HCl,\,dil}}^{(0)}$ | 13.85 | 20.78 | 27.70 |
| $m_{\mathrm{HCl,\,dil}}^{\mathrm{rest}}$ | 38.13 | 31.20 | 24.28 |
| $m_{\mathrm{HCl,\,dil}}^{\mathrm{tot}}$ | 51.98 | 51.98 | 51.98 |

**Table G.4:** Mass of diluted HCl required to neutralize excess NaOH, $m^{\text{exc}}_{\text{HCl, dil}}$, and the additional mass of HCl needed to reach solubility concentration of AA, $m^{*}_{\text{HCl, dil}}$.

| $m_{\text{HCl, dil}}$ | [g] |
|---|---|
| $m^{\text{exc}}_{\text{HCl, dil}}$ | 9.37 |
| $m^{*}_{\text{HCl, dil}}$ | 4.48 |
| $m^{(0),\,\omega=27\%}_{\text{HCl, dil}}$ | 13.85 |

## G.3 Diluted NaOH-solution

Pellets of sodium hydroxide (see Table 3.1) were dissolved in distilled water to 20.0 wt.% in order to meet process resembling conditions. Note that weight fraction of diluted NaOH is referred to as $\chi_{\text{NaOH}}$.

## G.4 Diluted HCl-solution

Hydrochloric acid, fuming (see Table 3.1) was diluted from 37 wt.% to 17.5 wt.% in order to meet process resembling conditions. Note that weight fraction of diluted HCl is referred to as $\chi_{\text{HCl}}$.

# H Physical data

**Table H.1:** Physical data used for calculations as described in D. Data are found in SI Chemical Data (Aylward and Findlay, 2008), with the exception of AA (Smith, 2006).

| **Compound** | $\mathbf{M_w}$ **[g/mol]** | $\mathbf{T_{boil}}$ [°C] |
|---|---|---|
| AA | 747.06 | – |
| NaAc | 82.03 | – |
| $H_2O$ | 18.01 | 100 |
| MeOH | 32.0 | 64.7 |
| NaOH | 40.0 | – |
| HCl | 36.46 | – |

**Table H.2:** Filtration data held constant for all experiments. Values are used in Equation 2.10 in order to calculate $\alpha_{ave}$. Supplementary data are given in Table B.1. $\rho_s$ and $\mu$ are found from relevant literature (Heskestad, 2008), (Beck, 2009).

| **Symbol** | | **Unit** |
|---|---|---|
| A | 20 | $cm^2$ |
| $\Delta p$ | $1.00 \cdot 10^8$ | mPa |
| $\rho_l$ | 1.082 | $g/cm^3$ |
| $\rho_s$ | 2.238 | $g/cm^3$ |
| $\eta$ | 1.084 | mPa · s |

**Table H.3:** Other data used for calculations. $C^*_{AA}$ is solubility of AA in a *synthetic* solution, found experimentally through UV spectrophotometry.

| **Symbol** | | **Unit** |
|---|---|---|
| $C^*_{\mathrm{AA}}$ | 2.25 | wt.% |